Identifying Druggable Sites in the Pain-Sensing TRPA1 Ion Channel

Citation

Permanent link

Terms of Use

Share Your Story

Accessibility

Dissertation Advisor: Professor Rachelle Gaudet   By: Kenneth Arthur Skinner III

Identifying druggable sites in the pain-sensing TRPA1 ion channel

Abstract

Transient receptor potential (TRP) channels, found in all eukaryotes, are a family of cation channels vital for critical physiological processes, such as mediating the sensation of unanticipated pain. Most TRP channel activities are modulated by a diverse set of exogenous and endogenous ligands, several of which are important for human life. For example, general anesthetics, which are widely used in surgical procedures, have undesired effects by activating TRPA1, which functions as a pain-sensing ion channel. Upon administration, several noxious general anesthetics stimulate peripheral sensory neurons, which transduce pain and inflammation elicited by these widely used drugs. Although evidence points to TRPA1 as the major player in this pain pathway, where propofol binds in the channel is unclear. Here I present the first photocrosslinking strategy to identify the propofol binding sites in TRPA1.

I designed synthetically expedient routes to three crosslinkable analogues of propofol, two of which are also functionalized with an alkyne affinity handle for bioorthogonal chemistry. Using mouse TRPA1 heterologously expressed in insect cells and fluorescence-based functional assays to compare propofol and the synthesized analogues, I determined that ortho-substitution, relative to the hydroxyl group, still allows for TRPA1 activation. Using the same activity assay, I conducted small molecule structure-function studies, introducing substituents replacing the phenolic hydroxyl group of propofol as well as adding or replacing substituents at the ortho and para positions. My results demonstrate the importance of hydrogen bonding in propofol activation of TRPA1 and provide evidence that halogen substitution can affect channel function. Photoaffinity labeling with a well-characterized propofol analogue, AziP*m*, which demonstrates

the same dose-dependent and bimodal TRPA1 activation profile as propofol, identified two crosslinked residues in TRPA1. Both residues lie on the S6 helix, which, together with S5, forms the channel pore and gate of TRPA1. V954 faces a pocket previously identified as the A-9607079 antagonist binding site, while E969 lies near the intracellular mouth of the pore at the junction of S6 and the "TRP-domain" α-helix, which is important for channel gating. These results provide the first direct identification of general anesthetic binding sites leading to TRPA1 activation.

Table of Contents

List of Figures

List of Tables

Page intentionally left blank

Chapter 1

Introduction: TRPA1 mediates sensation to reactive and non-electrophilic chemicals

Nociception is a fundamental sensation for all animals

Ion channels form pores in membranes, regulating ion permeability to serve as cellular messengers. Ion channels play crucial roles in many physiological processes and modifications in channel function often lead to pathological conditions (1). Although ion channels remain underexploited in the pharmaceutical industry, ~13% of marketed drugs act on ion channels, making them the second largest receptor target class (2-3). The transient receptor potential (TRP) channel superfamily is among the largest family of ion channels, consisting of at least 28 mammalian members. TRP channels, expressed by all eukaryotic organisms, are a superfamily of non-selective cation channels, implicated in all aspects of sensation, including a wide range of chemical, mechanical, and thermal stimuli (4). TRP channels are expressed in most, if not all cell types (4). The TRP subfamilies, grouped by amino acid sequence similarity, include TRPA (ankyrin), TRPC (canonical), TRPM (melastatin), TRPML, (mucolipin), TRPP (polycystin), and TRPV (vanilloid). All members of the TRP family are thought to share a tetrameric assembly in which each monomer consists of N-and C-terminal cytoplasmic domains and six transmembrane segments (S1-S6) with S1-S4 as the peripheral domain and the S5-S6 region as the pore-forming region, reminiscent of the distantly-related voltage-gated channels (**Figure 1.1**) (5,6). Non-domain-swapped transmembrane architecture is observed in channels such as hyperpolarization-activated cyclic nucleotide-regulated (HCN) and the voltage-gated K^+ channel Eag1 (7,8).

TRP channels serve as polymodal sensors that allow individual cells and whole organisms to detect and respond to potentially damaging stimuli (9). Among TRP channels, TRPA1, the sole member of the TRPA subfamily in mammals, serves as a sensor of painful stimuli by perceiving noxious chemicals and temperatures (10-13). TRPA1-expressing
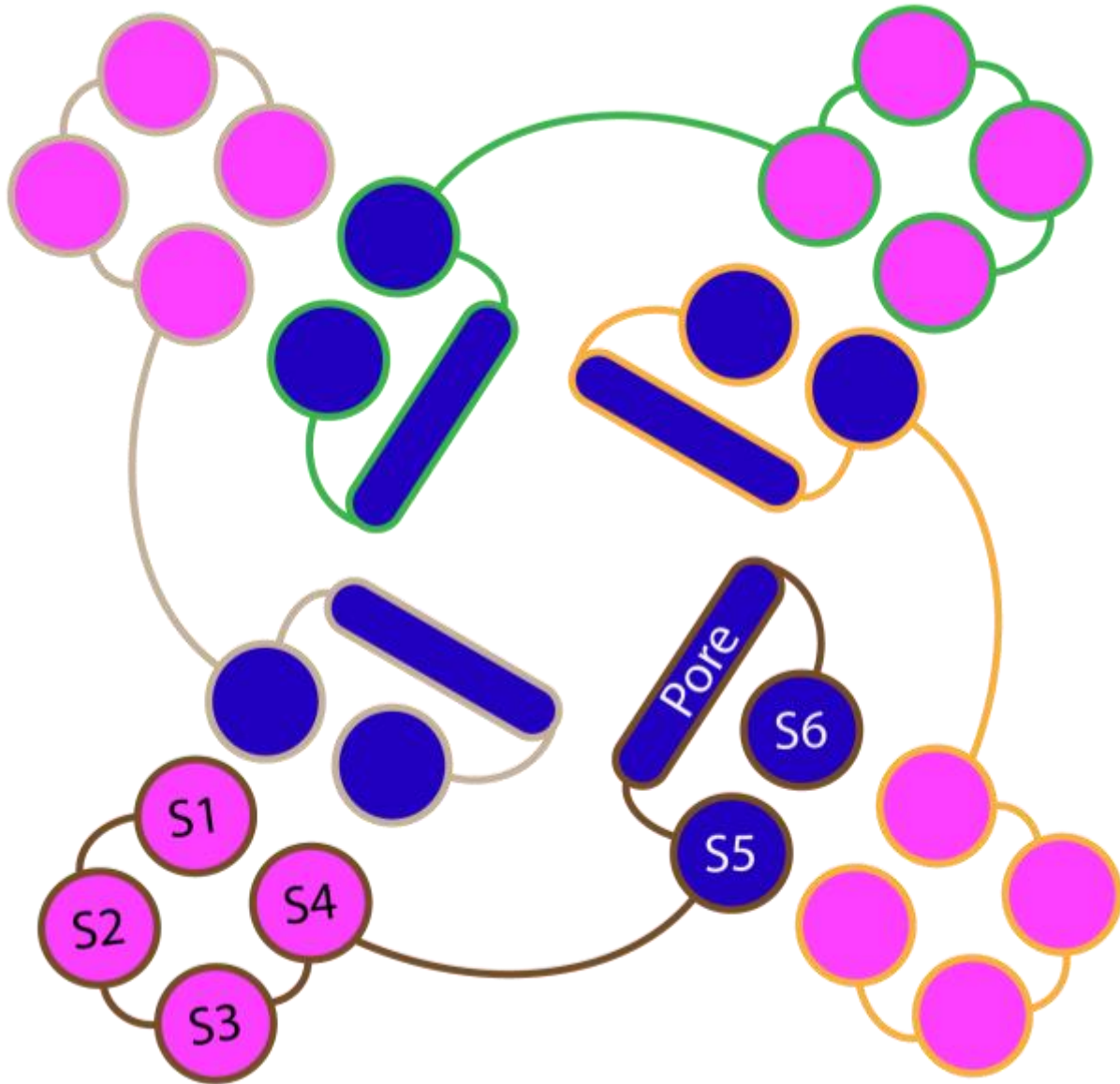
Figure 1.1 Intertwined subunit organization of most six-transmembrane (6-TM) channels

Viewed from the extracellular side**,** the S1-S4 bundles form the periphery of the channel while the S5-S6 bundles form the central ion conduction pore. The S4 helix of one subunit interacts with the S5-S6 helices on the adjacent subunit. Despite low sequence similarity between TRPs and voltage-gated ion channels (VGICs), an interlaced tetrameric assembly of the transmembrane domains is consistent with the architecture of most VGICs.

nociceptors can secrete inflammation-promoting agents locally. Thus, it is unsurprising that molecules such as 4-hydroxynonenal (HNE) and lipopolysaccharides (LPS), released during lipid peroxidation and bacterial lysis, respectively, activate TRPA1 (14,15). In sensory neurons, TRPA1 shows considerable expression overlap with TRPV1, another temperature and chemical sensor, implicating TRPA1 as a mediator of the inflammatory actions of noxious chemicals (16). TRPA1 and TRPV1 are nociceptive TRP channels that are well-established as cellular pain sensors, based upon knockout studies in pain models (17-19).

Paradoxically, individuals who cannot sense pain are unfortunate as this noxious sensation is not only a critical component of survival but also actively sought for pleasure. For example, in the case of satisfaction, humans are the only species that deliberately seek spicy foods, whereas most animals are repelled by the irritating sensation (20). While capsaicin, the active component in chili peppers, elicits a spiciness enjoyed by humans worldwide, it also serves to deter herbivores (21,22). Specific amino acids in avians, which are insensitive to the pain-producing effects of capsaicin, are thought to allow seed ingestion for wider dispersal (23-25). Similarly, TRPA1, also known as the wasabi receptor, is also activated by products of plant defense (26-28). Allyl isothiocyanate (AITC), the reactive electrophile in the wasabi delicacy, activates TRPA1, serving as an insecticide and a component of the plant defense system. Electrophiles such as AITC and acrolein (found in cigarette smoke) cause pain by covalently modifying TRPA1 (10, 29). TRPA1's ability to detect irritants goes back as far as choanoflagellates (30,31). The atomic resolution structures of TRPA1 and TRPV1 shed light on the domains important for channel gating (32-34).

Structural basis of modulation by noncovalent agonists in TRPA1

Apart from the conserved transmembrane core across TRP channels, TRPA1 exhibits distinctive features, particularly within the large cytoplasmic domains that comprise ~80% of the channel by mass (**Figure 1.2**). TRPA1 is aptly named due to the large number of N-terminal ankyrin repeats, which are 33-residue motifs consisting of two α-helices followed by a β– hairpin loop. These repeats stack on top of each other with an overall helical twist (**Figure 1.3**) (35). Conserved cysteines in the C-terminal ankyrin repeat and the linker preceding S1 are important for activation by membrane-permeable electrophiles (36, 37). These cysteines are solvent-accessible and proximal to the TRP box helix, suggesting a link between covalent modification of cysteines and channel gating (38). Due to similar transmembrane topology, parallels may be drawn between TRPV1 and TRPA1. Resiniferatoxin (RTX), a potent TRPV1 vanilloid agonist, binds in a pocket deep in the transmembrane domain, consisting of the S4-S5 linker helix, the S1-S4 bundle, and the pore (33). Although an electron density much smaller than the chemical structure of capsaicin was observed, capsaicin is likely in a similar orientation as RTX (39). The analogous pocket in TRPA1 may serve as a binding site for nonelectrophilic compounds with modulatory activity, which likely bind in the transmembrane core due to their lipophilic nature. For example, terpenes, the largest class of natural products, contribute to human life as natural medicines and spices through TRPA1 (40, 41). Mutagenesis and chimeric studies point to S873/T874 in S5 and M912/M953 in pore helix 1 and S6, respectively, as critical for activation by noncovalent TRPA1 modulators, which are less well characterized than the activation mechanisms by electrophiles (**Table 1.1**) (40, 43-46). The TRPA1 cryoEM structure, solved in complex with an antagonist, reveals a binding site between pore helix 1 and S5 for A-967079, one of the most potent mammalian TRPA1 antagonists (32,42). The binding site for
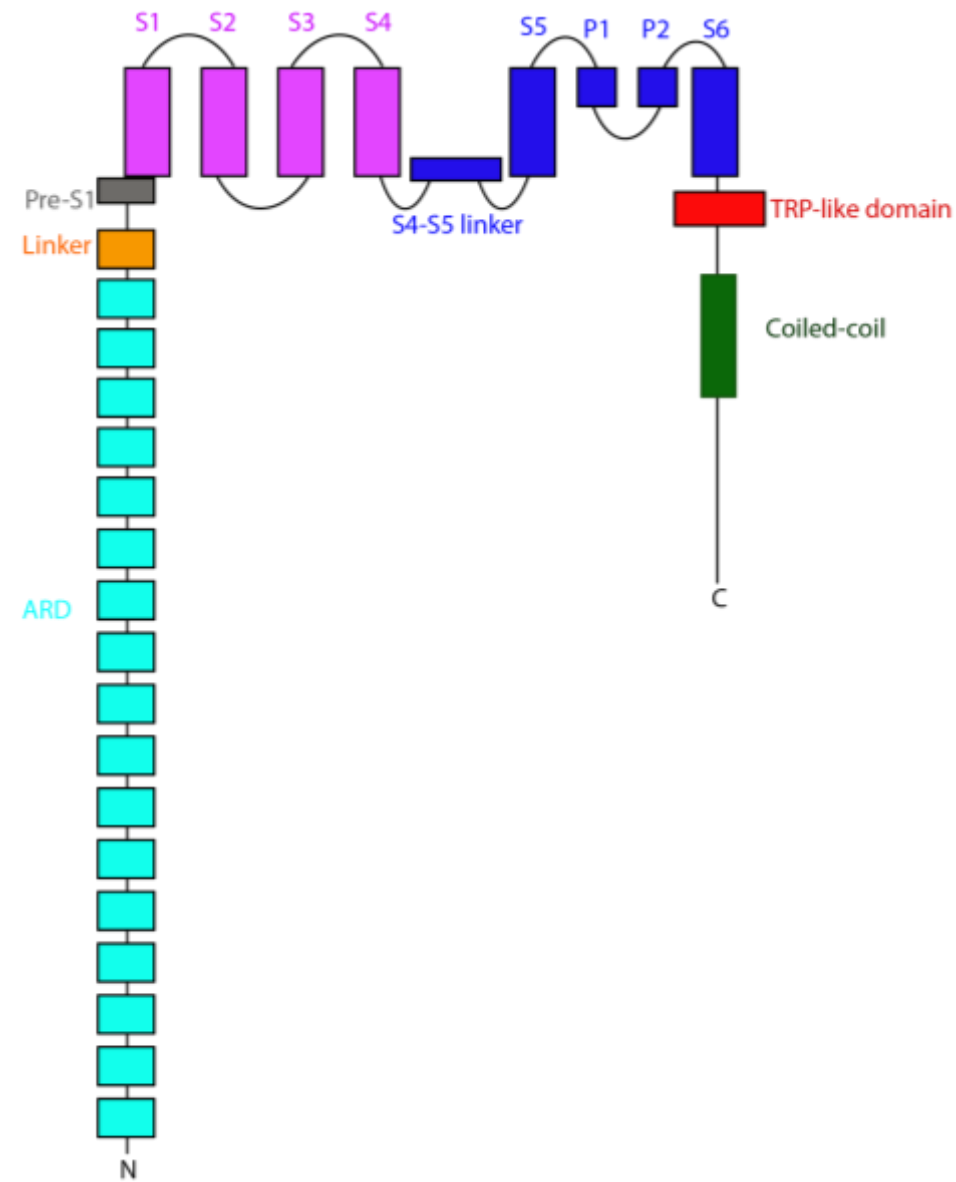
Figure 1.2 Primary structure organization of a TRPA1 subunit with major domains The schematic follows the color scheme from N- to C-terminus: ankyrin repeats, turquoise; linker, orange; pre-S1 (grey); S1-S4 (magenta); S4-S5 linker - S6 (blue); TRP-like domain helix (red); coiled-coil (forest green).
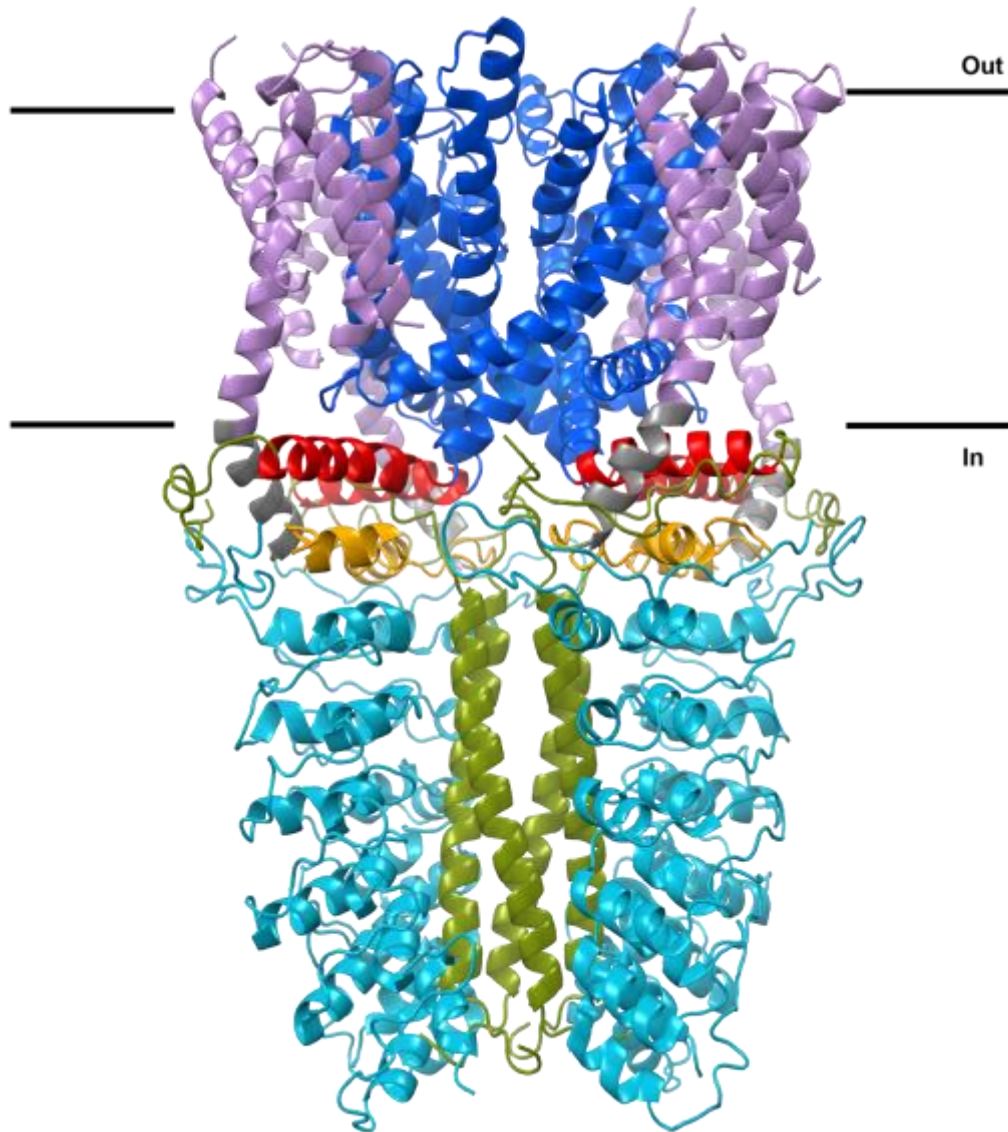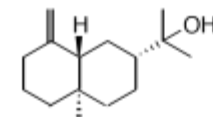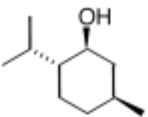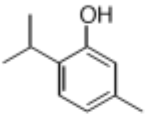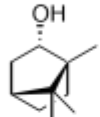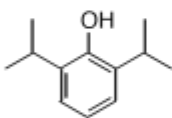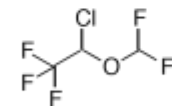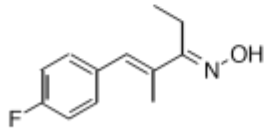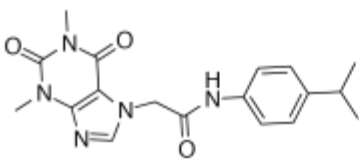
Figure 1.3 CryoEM structure of TRPA1 The cartoon representation follows the color scheme

from N- to C-terminus: ankyrin repeats, turquoise; linker, orange; pre-S1 (grey); S1-S4

(magenta); S4-S5 linker - S6 (blue); TRP-like domain helix (red); coiled-coil (forest green).

Figure adapted from Brewster and Gaudet (38).

Table 1.1 Residues important for TRPA1 sensitivity to noncovalent modulators.

Terpenes		Residues important for TRPA1 activity (location)	References
ß-eudesmol			[40]
Menthol		S873/T874 (S5)	[43]
Thymol			[43]
Borneol			[44]
General anesthetics			
Propofol		M912/M953 (P1/S6)	[45]
Isoflurane			
Selective TRPA1 antagonists			
A-967079		F909 (P1)	[45]
HC-030031		N855 (S4-S5 linker)	[46]

HC-030031, another potent TRPA1 antagonist, was not resolved in the TRPA1 cryoEM structure (32). Mutagenesis and chimeric studies suggest that the binding site for general anesthetics overlaps with that of A-967079 (45).

As the vanilloid binding site in TRPV1 and the A-967079 binding site in TRPA1 are topologically distinct, one hypothesis is that noncovalent TRPA1 agonists influence the channel through one binding site whereas antagonists share a separate binding site in TRPA1. Mutagenesis studies alone cannot distinguish between these two hypotheses due to their caveats: it is unclear whether the observed effects are due to a direct impairment of the ligand interaction or, alternatively, to a steric interference of the ligand access pathway (an allosteric effect) or an indirect effect on channel gating. For example, if a reduced TRPA1 response to a ligand coincides with a small AITC-evoked response, it suggests that multiple gating pathways are affected (a change in gating rather than ligand binding) or that channel expression levels are reduced; it is difficult to rule out these confounding factors. Thus, it remains unclear which residues directly contribute to a binding pocket for noncovalent TRPA1 agonists. What other structural and chemical biology techniques would lead to a direct identification of how nonelectrophilic agonists and antagonists interact with TRPA1? Solving a structure of TRPA1 in complex with a noncovalent agonist would lead to a direct answer but many of these structurally simple modulators undergo transient, low-affinity interactions with TRPA1, complicating the use of structural techniques. An alternative and direct method of identifying a ligand binding site is to use an analogue bearing a photoaffinity group whose activation by light results in irreversible covalent binding. Indeed, photocrosslinking has been used to identify propofol binding sites in several channels, including the GABA$_A$ receptor, which is responsible for propofol's anesthetic effect (47, 48).

Propofol as a chemical tool to identify druggable pockets in TRPA1

General anesthetics, employed in millions of surgeries worldwide, exert both beneficial and undesirable effects. Some general anesthetics stimulate peripheral nociceptors, eliciting a noxious pain upon injection (49, 50). Recently, TRPA1 has been found to be the major nociceptive channel in the anesthetic-induced pain pathway. Propofol, the most widely used intravenous anesthetic, activates TRPA1; the incidence of pain upon injection has been reported to be in 28-90% of patients (51). Understanding how propofol causes pain through TRPA1 requires identification of its binding site(s) in TRPA1. Such site(s) could overlap with the binding pocket(s) for other noxious noncovalent TRP channel agonists or antagonists, facilitating the detection of druggable pockets to rationally design novel TRPA1-targeting analgesic and anti-inflammatory drugs.

Propofol is an intriguing chemical tool to understand how nonelectrophilic modulators interact with TRPA1. For one, propofol shares a similar pharmacophore with other TRPA1 agonists, such as menthol and thymol (Table 1.1). Also, propofol, with its simple chemical structure and strongly activating hydroxyl group, is amenable to chemical manipulation to introduce functional groups, such as photoreactive moieties for photoaffinity labeling. In addition, a bimodal action on mouse TRPA1 (mTRPA1), consisting of activation at lower concentrations and inhibition at high concentrations, has been observed for both propofol and menthol (49, 50, 52). It is unclear whether this induced block at high concentrations is due to an agonist-dependent desensitization or direct inhibition of the channel through a second, lower affinity site, possibly through a direct block of the TRPA1 pore. TRPA1 inhibition and desensitization are attractive therapies for pain relief as mice with a genetic deletion of TRPA1 display significantly reduced nociceptive behaviors in preclinical pain models (17, 18).

It is imperative to develop more patient-friendly anesthetics, especially as no novel class

of anesthetics has been developed for almost half a century and many anesthetics still suffer from

patient drawbacks (53, 54). Thus, understanding where propofol binds in TRPA1 has profound

implications in both basic and translational research. This thesis focuses on the utility of

crosslinkable analogues, combined with small molecule structure-function studies, to directly

identify the binding-site residues of propofol in TRPA1. Although there are no crosslinking

studies to date to probe a TRP channel, several photoreactive analogs of propofol have been

applied to photolabel pentameric ligand-gated ion channels and other biological targets (**Figure
1.4**) (47, 55-57).

Design of photoaffinity probes to label propofol binding-site residues in TRPA1

Generally, proteins realize their biological functions through direct interactions with

other molecules such as ligands. There are many methods to investigate protein-ligand

interactions, each replete with their own pros and cons. For example, the structure of protein-

ligand complexes at atomic resolution provides global data on the protein and the ligand-binding

site, but this technique is particularly difficult for large membrane proteins and ligands with low

affinity for their targets. Currently, propofol-binding sites have only been directly identified,

through X-ray crystallography, in three proteins: the *Gloeobacter* Ligand-gated Ion Channel

(GLIC), a bacterial homolog of vertebrate Cys-loop ligand-gated ion channels, apoferritin and

human serum albumin (HSA) (58-60). But these proteins are an exception and not the norm in

terms of ease of handling. For one, apoferritin and HSA are commercially available. Second,

prokaryotic pentameric ligand-gated ion channels (pLGICs), such as GLIC, provide an

opportunity for probing ligand interactions due to their relative ease of expression in bacterial
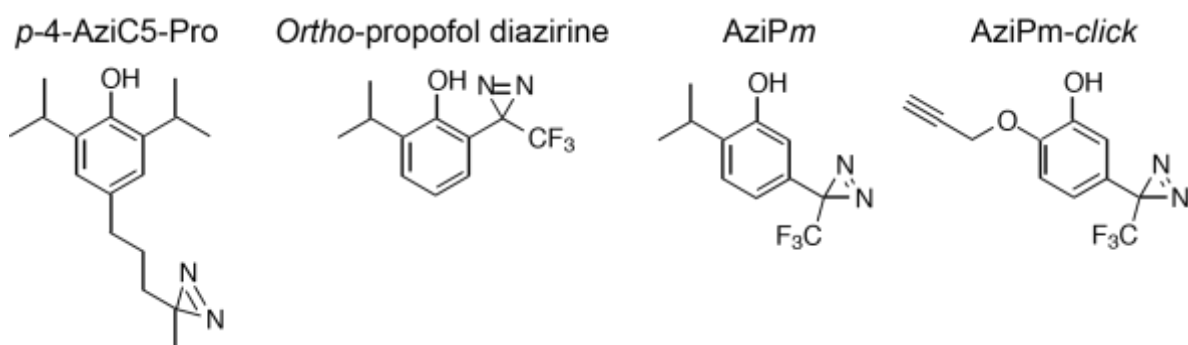
Figure 1.4 Chemical structures of photoreactive analogues of propofol (47, 55-57).

systems and their propensity to yield X-ray diffraction data (61). Also, GLIC, a homolog of nicotinic acetylcholine receptors, is inhibited by propofol, thus the relationship between the binding site and the potentiating site in mammalian channels is still a mystery (47). Propofol binds many large membrane proteins, such as $GABA_A$ and TRPA1, whose structures have only been recently solved (32,62). Thus, it is imperative to explore additional methods to identify ligand-binding sites to gain a complete picture of propofol activation in its targets.

Cysteine accessibility is another commonly used technique to not only define the topology of transmembrane proteins but also assess protein conformational change mechanisms and probe ligand-binding sites (63). This method was used to define a propofol-binding site in $GABA_A$ (64). In this experiment, researchers investigated if propofol protects cysteine residues, which have been substituted for the potential propofol-binding residues, from covalent modification by sulfhydryl-reactive reagents. However, propofol binding induces a conformational change in the $GABA_A$ receptor that affects reaction rates with the engineered cysteine (65). Thus, defining a reference state of the receptor that allows comparison of sulfhydryl reaction rates in the absence and presence of propofol is an issue. In addition, it is difficult to uncouple direct propofol interaction with the residue from allosteric conformational changes. For example, the protection could be due to an allosteric effect, as propofol-induced conformational changes may reduce the accessibility at the engineered positon. Thus, alternative methods that directly identify a drug's binding site would be beneficial.

Photoaffinity labeling is a complementary technique to directly probe the location of drug binding sites (66). Frank Westheimer and colleagues first introduced the concept of photoaffinity labeling over 50 years ago and it is now becoming an in important method in medicinal chemistry and drug discovery (67,68). In this technique, a photoreactive moiety is introduced

into an otherwise reversibly binding chemical probe (69,70). Upon light activation, the photoreactive group forms a reactive intermediate that rapidly reacts with and binds to nearby molecules. Thus, photoaffinity labeling is a direct method that results in irreversible covalent binding between a ligand and protein. The ideal traits of a photoaffinity probe include similarity to parent compound with comparable activity, little steric interference with binding, propensity to undergo intermolecular crosslinking over intramolecular crosslinking, and stability in the dark across a wide pH range (71). The probe should also be activated at a wavelength that limits damage to the protein of interest but still generates highly reactive intermediates capable of forming covalent adducts. In many cases, photoaffinity probes do not simultaneously exhibit each of these characteristics. The effort required in optimizing the probe may be comparable to that in optimizing an early drug lead (70-72). Thus, synthesizing a library of photoaffinity probes increases the probability of generating probes that retain many of these features. In Chapter 2, I will describe the synthesis of three compounds that are photoreactive derivatives of propofol.

A small library of crosslinkable analogues of propofol exists (**Table 1.2**). However, one metric to improve on is the number of synthetic steps to generate the crosslinkable analogue. Using a minimal number of synthetic steps is efficient, in terms of process chemistry, and generally cuts costs and waste. In addition, Figure 1.4 illustrates that few photoreactive propofol analogues contain its parent structure with two isopropyl ortho substituents, which are important for propofol activation as slight modifications to the core of alkyl phenols reduce TRPA1 activation (73). Thus, improving this attribute not only increases the likelihood of retaining channel activation but also downstream detection of crosslinked peptides that are spatially proximal to the native binding site. Furthermore, it is advantageous to expand the probe library

Table 1.2 Predicted physicochemical properties and synthesis comparison of crosslinkable probes. Calculated using Advanced Chemistry Development (ACD/Labs) Software V11.02.

Chemical	Mass (Da)	Density (g/mL)	cLogP	# of synthetic steps
Propofol	178	0.95	3.6	-
p-4-AziC5-Pro	274	1.10	4.9	8
Ortho-propofol diazirine	244	1.38	2.9	7
AziP*m*	244	1.38	3.8	12
AziP*m*-click	270	1.35	1.6	7

because photolabeling moieties may abrogate the ability of the compounds to modulate channel function, and none of the existing photoreactive propofol analogs have yet been tested to determine whether they activate TRPA1.

This thesis highlights a goal of chemical biology: using small molecules to answer biological questions by directly probing living systems. In Chapter 2, I demonstrate relatively simple synthetic strategies towards three photoreactive propofol analogues, two of which are also functionalized with alkyne handles for biorthogonal reactions (*i.e.* click chemistry). In Chapter 3, I use a fluorescence-based assay to determine which probes retain activation of TRPA1. In addition, a minimal structure-activity relationship (SAR) demonstrates the effects of modifying the propofol pharmacophore on TRPA1 activation. In Chapter 4, in collaboration with Kellie Woll from Roderic Eckenhoff's laboratory, I used a photoreactive analogue of propofol to photolabel TRPA1-expressing membranes. Upon pulldown of crosslinked complex, digestion of photolabeled TRPA1 peptides and mass spectrometry, two crosslinked residues were directly identified in TRPA1, the first ligand photocrosslinking study applied to a TRP channel.

References

1. **Martina, M.,** 2012. Ion channel screening: advances in technologies and analysis. *Ion channel screening: advances in technologies and analysis*, p.4.

2. **Clare, J.J.,** 2010. Targeting ion channels for drug discovery. *Discovery medicine*, *9*(46), pp.253-260.

3. **Rask-Andersen, M., Almén, M.S. and Schiöth, H.B.,** 2011. Trends in the exploitation of novel drug targets. *Nature reviews Drug discovery*, *10*(8), pp.579-590.

4. **Clapham, D.E.,** 2003. TRP channels as cellular sensors. *Nature*, *426*(6966), pp.517-524.

5. **Kuang, Q., Purhonen, P. and Hebert, H.,** 2015. Structure of potassium channels. *Cellular and Molecular Life Sciences*, *72*(19), pp.3677-3693.

6. **Catterall, W.A. and Swanson, T.M.,** 2015. Structural basis for pharmacology of voltage-gated sodium and calcium channels. *Molecular pharmacology*, *88*(1), pp.141-150.

7. **James, Z.M., Borst, A.J., Haitin, Y., Frenz, B., DiMaio, F., Zagotta, W.N. and Veesler, D.,** 2017. CryoEM structure of a prokaryotic cyclic nucleotide-gated ion channel. *Proceedings of the National Academy of Sciences*, p.201700248.

8. **Whicher, J.R. and MacKinnon, R.,** 2016. Structure of the voltage-gated K+ channel Eag1 reveals an alternative voltage sensing mechanism. *Science*, *353*(6300), pp.664-669.

9. **Voets, T., Talavera, K., Owsianik, G. and Nilius, B.,** 2005. Sensing with TRP channels. *Nature chemical biology*, *1*(2), pp.85-92.

10. **Macpherson, L.J., Dubin, A.E., Evans, M.J., Marr, F., Schultz, P.G., Cravatt, B.F. and Patapoutian, A.,** 2007. Noxious compounds activate TRPA1 ion channels through covalent modification of cysteines. *Nature*, *445*(7127), pp.541-545.

11. **Story, G.M., Peier, A.M., Reeve, A.J., Eid, S.R., Mosbacher, J., Hricik, T.R., Earley, T.J., Hergarden, A.C., Andersson, D.A., Hwang, S.W. and McIntyre, P.,** 2003.

ANKTM1, a TRP-like channel expressed in nociceptive neurons, is activated by cold temperatures. *Cell*, *112*(6), pp.819-829.

12. **Del Camino, D., Murphy, S., Heiry, M., Barrett, L.B., Earley, T.J., Cook, C.A., Petrus, M.J., Zhao, M., D'Amours, M., Deering, N. and Brenner, G.J.,** 2010. TRPA1 contributes to cold hypersensitivity. *Journal of Neuroscience*, *30*(45), pp.15165-15174.

13. **Petrus, M., Peier, A.M., Bandell, M., Hwang, S.W., Huynh, T., Olney, N., Jegla, T. and Patapoutian, A.,** 2007. A role of TRPA1 in mechanical hyperalgesia is revealed by pharmacological inhibition. *Molecular pain*, *3*(1), p.40.

14. **Trevisani, Marcello, Jan Siemens, Serena Materazzi, Diana M. Bautista, Romina Nassini, Barbara Campi, Noritaka Imamachi** *et al.* "4-Hydroxynonenal, an endogenous aldehyde, causes pain and neurogenic inflammation through activation of the irritant receptor TRPA1." *Proceedings of the National Academy of Sciences* 104, no. 33 (2007): 13519-13524.

15. **Meseguer, V., Alpizar, Y.A., Luis, E., Tajada, S., Denlinger, B., Fajardo, O., Manenschijn, J.A., Fernández-Peña, C., Talavera, A., Kichko, T. and Navia, B.,** 2014. TRPA1 channels mediate acute neurogenic inflammation and pain produced by bacterial endotoxins. *Nature communications*, *5*.

16. **Bautista, D.M., Jordt, S.E., Nikai, T., Tsuruda, P.R., Read, A.J., Poblete, J., Yamoah, E.N., Basbaum, A.I. and Julius, D.,** 2006. TRPA1 mediates the inflammatory actions of environmental irritants and proalgesic agents. *Cell*, *124*(6), pp.1269-1282.

17. **Kwan, K.Y., Allchorne, A.J., Vollrath, M.A., Christensen, A.P., Zhang, D.S., Woolf, C.J. and Corey, D.P.,** 2006. TRPA1 contributes to cold, mechanical, and chemical nociception but is not essential for hair-cell transduction. *Neuron*, *50*(2), pp.277-289.

18. **Horváth, Á., Tékus, V., Boros, M., Pozsgai, G., Botz, B., Borbély, É., Szolcsányi, J., Pintér, E. and Helyes, Z.,** 2016. Transient receptor potential ankyrin 1 (TRPA1) receptor is involved in chronic arthritis: in vivo study using TRPA1-deficient mice. *Arthritis research & therapy*, *18*(1), p.6.

19. **Trevisan, G., Benemei, S., Materazzi, S., De Logu, F., De Siena, G., Fusi, C., Rossato, M.F., Coppi, E., Marone, I.M., Ferreira, J. and Geppetti, P.,** 2016. TRPA1

mediates trigeminal neuropathic pain in mice downstream of monocytes/macrophages and oxidative stress. *Brain*, p.aww038.

20. **Riera, C.E., Huising, M.O., Follett, P., Leblanc, M., Halloran, J., Van Andel, R., de Magalhaes Filho, C.D., Merkwirth, C. and Dillin, A.,** 2014. TRPV1 pain receptors regulate longevity and metabolism by neuropeptide signaling. *Cell*, *157*(5), pp.1023-1036.

21. **Nilius, B. and Appendino, G.,** 2013. Spices: the savory and beneficial science of pungency. In *Reviews of Physiology, Biochemistry and Pharmacology, Vol. 164* (pp. 1-76). Springer International Publishing.

22. **Ahn, S.J., Badenes-Pérez, F.R. and Heckel, D.G.,** 2011. A host-plant specialist, Helicoverpa assulta, is more tolerant to capsaicin from Capsicum annuum than other noctuid species. *Journal of insect physiology*, *57*(9), pp.1212-1219.

23. **Jordt, S.E. and Julius, D.,** 2002. Molecular basis for species-specific sensitivity to "hot" chili peppers. *Cell*, *108*(3), pp.421-430.

24. **Gavva, N.R., Klionsky, L., Qu, Y., Shi, L., Tamir, R., Edenson, S., Zhang, T.J., Viswanadhan, V.N., Toth, A., Pearce, L.V. and Vanderah, T.W.,** 2004. Molecular determinants of vanilloid sensitivity in TRPV1. *Journal of Biological Chemistry*, *279*(19), pp.20283-20295.

25. **Ohkita, Masashi,** *et al.* "Molecular cloning and functional characterization of Xenopus tropicalis frog transient receptor potential vanilloid 1 reveal its functional evolution for heat, acid, and capsaicin sensitivities in terrestrial vertebrates." *Journal of Biological Chemistry* 287.4 (2012): 2388-2397.

26. **Bautista, D.M., Movahed, P., Hinman, A., Axelsson, H.E., Sterner, O., Högestätt, E.D., Julius, D., Jordt, S.E. and Zygmunt, P.M.,** 2005. Pungent products from garlic activate the sensory ion channel TRPA1. *Proceedings of the National Academy of Sciences of the United States of America*, *102*(34), pp.12248-12252.

27. **Escalera, J., von Hehn, C.A., Bessac, B.F., Sivula, M. and Jordt, S.E.,** 2008. TRPA1 mediates the noxious effects of natural sesquiterpene deterrents. *Journal of Biological Chemistry*, *283*(35), pp.24136-24144.

28. **Shin, I.S., Masuda, H. and Naohide, K.,** 2004. Bactericidal activity of wasabi (Wasabia japonica) against Helicobacter pylori. *International journal of food microbiology*, *94*(3), pp.255-261.

29. **Bandell, M., Story, G.M., Hwang, S.W., Viswanath, V., Eid, S.R., Petrus, M.J., Earley, T.J. and Patapoutian, A.,** 2004. Noxious cold ion channel TRPA1 is activated by pungent compounds and bradykinin. *Neuron*, *41*(6), pp.849-857.

30. **Kang, K., Pulver, S.R., Panzano, V.C., Chang, E.C., Griffith, L.C., Theobald, D.L. and Garrity, P.A.,** 2010. Analysis of Drosophila TRPA1 reveals an ancient origin for human chemical nociception. *Nature*, *464*(7288), pp.597-600.

31. **Peng, G., Shi, X. and Kadowaki, T.,** 2015. Evolution of TRP channels inferred by their classification in diverse animal species. *Molecular phylogenetics and evolution*, *84*, pp.145-157.

32. **Paulsen, C.E., Armache, J.P., Gao, Y., Cheng, Y. and Julius, D.,** 2015. Structure of the TRPA1 ion channel suggests regulatory mechanisms. *Nature*, *520*(7548), pp.511-517.

33. **Cao, E., Liao, M., Cheng, Y. and Julius, D.,** 2013. TRPV1 structures in distinct conformations reveal activation mechanisms. *Nature*, *504*(7478), pp.113-118.

34. **Gao, Y., Cao, E., Julius, D. and Cheng, Y.,** 2016. TRPV1 structures in nanodiscs reveal mechanisms of ligand and lipid action. *Nature*.

35. **Gaudet, R.,** 2008. A primer on ankyrin repeat function in TRP channels and beyond. *Molecular BioSystems*, *4*(5), pp.372-379.

36. **Hinman, A., Chuang, H.H., Bautista, D.M. and Julius, D.,** 2006. TRP channel activation by reversible covalent modification. *Proceedings of the National Academy of Sciences*, *103*(51), pp.19564-19568.

37. **Kim, S.H., Lee, Y., Akitake, B., Woodward, O.M., Guggino, W.B. and Montell, C.,** 2010. Drosophila TRPA1 channel mediates chemical avoidance in gustatory receptor neurons. *Proceedings of the National Academy of Sciences*, *107*(18), pp.8440-8445.

38. **Brewster, M.S. and Gaudet, R.,** 2015. How the TRPA1 receptor transmits painful stimuli: Inner workings revealed by electron cryomicroscopy. *BioEssays*, *37*(11), pp.1184-1192.

39. **Yang, F., Xiao, X., Cheng, W., Yang, W., Yu, P., Song, Z., Yarov-Yarovoy, V. and Zheng, J.,** 2015. Structural mechanism underlying capsaicin binding and activation of the TRPV1 ion channel. *Nature chemical biology*, *11*(7), pp.518-524.

40. **Ohara, K., Fukuda, T., Okada, H., Kitao, S., Ishida, Y., Kato, K., Takahashi, C., Katayama, M., Uchida, K. and Tominaga, M.,** 2015. Identification of significant amino acids in multiple transmembrane domains of human transient receptor potential ankyrin 1 (TRPA1) for activation by eudesmol, an oxygenized sesquiterpene in hop essential oil. *Journal of Biological Chemistry*, *290*(5), pp.3161-3171.

41. **Vennekens, R., Vriens, J. and Nilius, B.,** 2008. Herbal compounds and toxins modulating TRP channels. *Current neuropharmacology*, *6*(1), pp.79-96.

42. **Chen, J., Joshi, S.K., DiDomenico, S., Perner, R.J., Mikusa, J.P., Gauvin, D.M., Segreti, J.A., Han, P., Zhang, X.F., Niforatos, W. and Bianchi, B.R.,** 2011. Selective blockade of TRPA1 channel attenuates pathological pain without altering noxious cold sensation or body temperature regulation. *Pain*, *152*(5), pp.1165-1172.

43. **Xiao, B., Dubin, A.E., Bursulaya, B., Viswanath, V., Jegla, T.J. and Patapoutian, A.,** 2008. Identification of transmembrane domain 5 as a critical molecular determinant of menthol sensitivity in mammalian TRPA1 channels. *Journal of Neuroscience*, *28*(39), pp.9640-9651.

44. **Takaishi, M., Uchida, K., Fujita, F. and Tominaga, M.,** 2014. Inhibitory effects of monoterpenes on human TRPA1 and the structural basis of their activity. *The Journal of Physiological Sciences*, *64*(1), pp.47-57.

45. **Ton, H.T., Phan, T.X., Abramyan, A.M., Shi, L. and Ahern, G.P.,** 2017. Identification of a putative binding site critical for general anesthetic activation of TRPA1. *Proceedings of the National Academy of Sciences*, p.201618144.

46. **Gupta, R., Saito, S., Mori, Y., Itoh, S.G., Okumura, H. and Tominaga, M.,** 2016. Structural basis of TRPA1 inhibition by HC-030031 utilizing species-specific differences. *Scientific Reports*, *6*.

47. **Yip, G.M., Chen, Z.W., Edge, C.J., Smith, E.H., Dickinson, R., Hohenester, E., Townsend, R.R., Fuchs, K., Sieghart, W., Evers, A.S. and Franks, N.P.,** 2013. A propofol binding site on mammalian GABAA receptors identified by photolabeling. *Nature Chemical Biology*, *9*(11), pp.715-720.

48. **Jurd, R., Arras, M., Lambert, S., Drexler, B., Siegwart, R., Crestani, F., Zaugg, M., Vogt, K.E., Ledermann, B., Antkowiak, B. and Rudolph, U.,** 2003. General anesthetic actions in vivo strongly attenuated by a point mutation in the GABAA receptor β3 subunit. *The FASEB Journal*, *17*(2), pp.250-252.

49. **Matta, J.A., Cornett, P.M., Miyares, R.L., Abe, K., Sahibzada, N. and Ahern, G.P.,** 2008. General anesthetics activate a nociceptive ion channel to enhance pain and inflammation. *Proceedings of the National Academy of Sciences*, *105*(25), pp.8784-8789.

50. **Fischer, M.J., Leffler, A., Niedermirtl, F., Kistner, K., Eberhardt, M., Reeh, P.W. and Nau, C.,** 2010. The general anesthetic propofol excites nociceptors by activating TRPV1 and TRPA1 rather than GABAA receptors. *Journal of Biological Chemistry*, *285*(45), pp.34781-34792.

51. **Picard, P. and Tramèr, M.R.,** 2000. Prevention of pain on injection with propofol: a quantitative systematic review. *Anesthesia & Analgesia*, *90*(4), pp.963-969.

52. **Karashima, Y., Damann, N., Prenen, J., Talavera, K., Segal, A., Voets, T. and Nilius, B.,** 2007. Bimodal action of menthol on the transient receptor potential channel TRPA1. *Journal of Neuroscience*, *27*(37), pp.9874-9884.

53. **Johansson, J.S. and Scharf, D.,** 2001. Towards an understanding of how general anesthetics alter central nervous system protein function. *Regional anesthesia and pain medicine*, *26*(3), pp.267-270.

54. **McKinstry-Wu, A.R., Bu, W., Rai, G., Lea, W.A., Weiser, B.P., Liang, D.F., Simeonov, A., Jadhav, A., Maloney, D.J. and Eckenhoff, R.G.,** 2015. Discovery of a novel general anesthetic chemotype using high-throughput screening. *The Journal of the American Society of Anesthesiologists*, *122*(2), pp.325-333.

55. **Stewart, D.S., Savechenkov, P.Y., Dostalova, Z., Chiara, D.C., Ge, R., Raines, D.E., Cohne, J.B., Forman, S.A., Bruzik, K.S. and Miller, K.W.,** 2011. p-(4-Azipentyl)-propofol: A Potent Photoreactive General Anesthetic Derivative of Propofol. *Journal of medicinal chemistry*, *54*(23), p.8124.

56. **Hall, M.A., Xi, J., Lor, C., Dai, S., Pearce, R., Dailey, W.P. and Eckenhoff, R.G.,** 2010. m-Azipropofol (AziPm) a photoactive analogue of the intravenous general anesthetic propofol. *Journal of medicinal chemistry*, *53*(15), p.5667.

57. **Woll, K.A., Murlidaran, S., Pinch, B.J., Hénin, J., Wang, X., Salari, R., Covarrubias, M., Dailey, W.P., Brannigan, G., Garcia, B.A. and Eckenhoff, R.G.,** 2016. A Novel Bifunctional Alkylphenol Anesthetic Allows Characterization of γ-Aminobutyric Acid, Type A (GABAA), Receptor Subunit Binding Selectivity in Synaptosomes. *Journal of Biological Chemistry*, *291*(39), pp.20473-20486.

58. **Nury, H., Van Renterghem, C., Weng, Y., Tran, A., Baaden, M., Dufresne, V., Changeux, J.P., Sonner, J.M., Delarue, M. and Corringer, P.J.,** 2011. X-ray structures of general anaesthetics bound to a pentameric ligand-gated ion channel. *Nature*, *469*(7330), pp.428-431.

59. **Vedula, L.S., Brannigan, G., Economou, N.J., Xi, J., Hall, M.A., Liu, R., Rossi, M.J., Dailey, W.P., Grasty, K.C., Klein, M.L. and Eckenhoff, R.G.,** 2009. A unitary anesthetic binding site at high resolution. *Journal of Biological Chemistry*, *284*(36), pp.24176-24184.

60. **Bhattacharya, A.A., Curry, S. and Franks, N.P.,** 2000. Binding of the general anesthetics propofol and halothane to human serum albumin high resolution crystal structures. *Journal of Biological Chemistry*, *275*(49), pp.38731-38738.

61. **Labriola, J.M., Pandhare, A., Jansen, M., Blanton, M.P., Corringer, P.J. and Baenziger, J.E.,** 2013. Structural sensitivity of a prokaryotic pentameric ligand-gated ion channel to its membrane environment. *Journal of Biological Chemistry*, *288*(16), pp.11294-11303.6.

62. **Miller, P.S. and Aricescu, A.R.,** 2014. Crystal structure of a human GABAA receptor. *Nature*, *512*(7514), pp.270-275.

63. **Zhu, Q. and Casey, J.R.,** 2007. Topology of transmembrane proteins by scanning cysteine accessibility mutagenesis methodology. *Methods*, *41*(4), pp.439-450.

64. **Bali, M. and Akabas, M.H.,** 2004. Defining the propofol binding site location on the GABAA receptor. *Molecular pharmacology*, *65*(1), pp.68-76.

65. **Williams, D.B. and Akabas, M.H.,** 2002. Structural evidence that propofol stabilizes different GABAA receptor states at potentiating and activating concentrations. *Journal of Neuroscience*, *22*(17), pp.7417-7424.

66. **Dubinsky, L., Krom, B.P. and Meijler, M.M.,** 2012. Diazirine based photoaffinity labeling. *Bioorganic & medicinal chemistry*, *20*(2), pp.554-570.

67. **Singh, A., Thornton, E.R. and Westheimer, F.H.,** 1962. The photolysis of diazoacetylchymotrypsin. *Journal of Biological Chemistry*, *237*(9), pp.PC3006-PC3008.

68. **Lapinsky, D.J.,** 2012. Tandem photoaffinity labeling–bioorthogonal conjugation in medicinal chemistry. *Bioorganic & medicinal chemistry*, *20*(21), pp.6237-6247.

69. **Sadakane, Y. and Hatanaka, Y.,** 2006. Photochemical fishing approaches for identifying target proteins and elucidating the structure of a ligand-binding region using carbene-generating photoreactive probes. *Analytical sciences*, *22*(2), pp.209-218.

70. **Smith, Ewan, and Ian Collins.** "Photoaffinity labeling in target-and binding-site identification." *Future medicinal chemistry* 7.2 (2015): 159-183.

71. **Rappsilber, J.,** 2011. The beginning of a beautiful friendship: cross-linking/mass spectrometry and modelling of proteins and multi-protein complexes. *Journal of structural biology*, *173*(3), pp.530-540.

72. **Hughes, J.P., Rees, S., Kalindjian, S.B. and Philpott, K.L.,** 2011. Principles of early drug discovery. *British journal of pharmacology*, *162*(6), pp.1239-1249.

73. **Lee, S.P., Buber, M.T., Yang, Q., Cerne, R., Cortes, R.Y., Sprous, D.G. and Bryant, R.W.,** 2008. Thymol and related alkyl phenols activate the hTRPA1 channel. *British journal of pharmacology*, *153*(8), pp.1739-1749.

Chapter 2

Design, synthesis, and characterization of propofol photoaffinity probes

Abstract

      Propofol is a widely used general anesthetic that activates the nociceptive TRPA1 ion channel. A complete picture of how propofol acts requires knowledge of where it binds on TRPA1. Photocrosslinking is a strategy to address this outstanding question. Here, I present a strategy for the facile synthesis under mild conditions of three photoreactive probes of propofol. In each analogue, I introduced a photoreactive diazirine group, and two of these analogues bear alkyne groups, enabling bioorthogonal chemistry with azide-containing partners. These synthetic schemes can also be applied to other molecules, including other noncovalent agonists of TRPA1, further broadening the utility of the methods described in this chapter.

Introduction

      TRPA1 has only recently been suggested as the mediator of propofol-induced pain (1,2). Identifying the binding-site location is an important step to design new TRPA1 inhibitors and other modulators that inhibit the channel at the propofol-binding site, reducing pain during propofol administration. This chapter describes the synthesis of photoaffinity probes for this purpose of identifying propofol's binding sites. Although several photoaffinity analogues of propofol have been published (Figure 1.4), expanding the library of crosslinkable analogues provides more tools to understand how propofol interacts with TRPA1 as well as other physiological targets (3-6). In addition, as of this writing, there are no published studies on the functional activity of any photoaffinity analogs of propofol on TRPA1.

      The main photoreactive groups used in photoaffinity labeling are diazirines, azides, and benzophenones. Although azides are frequently used due to ease of synthesis, they require shorter wavelengths for excitation that may damage biological molecules (7). The benzophenone

group is bulky, which can hinder binding to the target protein and increase nonspecific labeling. (8). Aryldiazirines are the most commonly used photoaffinity group due to their chemical stability, longer wavelength activation (~350 nm) and the short half-life of the reactive carbene intermediate (8). However, aryldiazirines often require the incorporation of trifluoromethyldiazirine groups, which typically add more synthetic steps than alkyl diazirines, to stabilize the carbene to favor intermolecular crosslinking. I chose to link the propofol core with a nonpolar spacer to separate the diazirine moiety from the aryl ring. More specifically, the synthetic route I designed first generated alkyl ketones, the synthetically expedient precursors to diazirines (3).

To facilitate the detection and/or isolation of photolabeled protein, radioactive or fluorescent reporter tags are often incorporated into the photoaffinity probe, either during probe synthesis or after photocrosslinking. For example, biotin/epitope tags on the crosslinking molecule can be exploited in affinity purification. On the other hand, alkynes provide even more flexibility: through their click chemistry reactions with azides, alkynes can be used for both detection and isolation of molecule of interest crosslinked to protein (9). That is, the click reaction is a convenient post-crosslinking method to incorporate an azide-containing biotin or fluorescent tag into the photoprobe. This chapter describes the design of two propofol probes with this dual functionality of crosslinking ability and ability to click with azide-containing molecules.

I present the synthesis of a novel set of three photoreactive propofol analogues: XPRO, *o*-XPRO-Click and *p*-XPRO-Click. Each molecule contains a diazirine group separated by a short nonpolar linker in the para position. I separated the alkyl diazirine moiety from the phenyl ring via a short nonpolar linker to facilitate synthetic expediency and to avoid a potential source of

instability. *o*-XPRO-Click and *p*-XPRO-Click also contain alkyne groups in the ortho and para positions (relative to the phenolic hydroxyl group), respectively. Through this derivatization, these molecules have potential utility in not only crosslinking to TRPA1 but also detecting or isolating photolabeled TRPA1 or other propofol targets. The schemes designed in this study are also applicable to the synthesis of photoreactive probes of other noncovalent TRPA1 ligands.

Materials and Methods

General synthetic procedures

Hexamethylenetetramine was purchased from TCI America (Portland, OR). Ruthenium Dichlorobis(μ-methanethioato)bis(pentamethylcyclopentadienyl)diruthenium(III) was purchased from Strem Pharmaceuticals (Newburyport, MA). All other chemicals were purchased from Sigma-Aldrich (St. Louis, MO). Chemicals were used as received from commercial vendors unless otherwise noted. All reactions were run under an atmosphere of dry nitrogen and monitored by thin layer chromatography (TLC) on Merck silica glass plates. Crude products were chromatographed on a Teledyne Isco CombiFlash system (Lincoln, NE). ^{1}H and ^{13}C nuclear magnetic resonance (NMR) spectra were recorded on an Inova 500 MHz nuclear spectrometer in the Harvard Chemistry & Chemical Biology (CCB) facility. Mass spectra of synthesized compounds were acquired on an Agilent 6220 LC-TOF (Santa Clara, CA) in the Harvard Bauer Core.

XPRO absorbance spectrum

UV spectrum data were acquired at a 10-nm wavelength step on a FlexStation 3 Plate Reader (Molecular Devices; Sunny Vale, CA).

Exposure of XPRO in methanol to ultraviolet (UV) light

The photochemical properties of XPRO were examined over time using a FlexStation plate reader. 1.7 µM XPRO was prepared in methanol and absorbance was measured with a cuvette at 348 nm after exposure to 365 nm UV light with a 100W UVP Blak-Ray B100AP (Upland, CA).

Click reaction with o-XPRO-Click and 3-Azido-7-hydroxycoumarin

0.5 mM *o*-XPRO-Click was mixed with 1 mM 3-Azido-7-hydroxycoumarin in 100 mM phosphate buffer, pH 7.5 and 150 mM NaCl. A premixed solution of 0.1 mM $CuSO_4$ and 0.5 TBTA was added, followed by addition of 5 mM sodium ascorbate. The reaction proceeded at 37°C for 1 hour and the sample was excited at 404 nm while emission was measured with the SpectraMax i3 plate reader (Sunnyvale, CA).

Click reaction with p-XPRO-Click and 3-Azido-7-hydroxycoumarin

0.5 mM *p*-XPRO-Click was mixed with 0-3 mM 3-Azido-7-hydroxycoumarin in phosphate-buffered saline. A premixed solution of 0.1 mM $CuSO_4$ and 0.5 mM TBTA was added, followed by addition of 5 mM sodium ascorbate. The reaction proceeded at 37°C for 1 hour and the sample was excited at 404 nm and emission at 480 nm was measured with increasing concentration of 3-Azido-7-hydroxycoumarin using the SpectraMax i3 plate reader.

Preparation of XPRO

4-(4-hydroxy-3,5-diisopropylphenyl)butan-2-one (1)

A similar procedure was adapted with minor modifications from Bunce *et al.* (10) to synthesize **1**. To a 5-mL toluene solution of 2,6-diisopropylphenol (2.83 mL, 15.3 mmol) was added 326 mg of Amberlyst-15. The slurry was stirred at room temperature while a 1-mL toluene solution of methyl vinyl ketone (0.415 mL, 5.1 mmol) was added dropwise. The vessel was heated to 50°C and allowed to proceed for 6 hours, upon which the reaction was partitioned between water and ether. The ether solution was washed with water, brine, and dried over Na_2SO_4 and concentrated *in vacuo*. The residue was purified by column chromatography with increasing concentration of dichloromethane (DCM). The product eluted at 100% DCM/hexanes. The appropriate fractions were combined and concentrated to yield 1 g (80%) of title compound.

^{1}H NMR (500 MHz, $CDCl_3$): δ 6.88 (s, 2H, H_{arom}), 4.69 (s, 1H, ArOH), 3.15 (sept, 2H, *J*=6.9 Hz, CH-i-Pr), 2.88-2.79 (m, 2H, CH_2), 2.79-2.71 (m, 2H, CH_2), 2.16 (s, 3H, H_3C-C=O), 1.27 (d, 12H, *J*=6.9 Hz, H_3C-i-Pr).

^{13}C NMR (125 MHz, $CDCl_3$): δ 208.7 (C=O), 148.3, 133.8, 132.7, 123.2 (CH_{arom}), 45.8, 30.1, 29.7, 27.2, 22.8.

HRMS calc'd for $C_{16}H_{24}O_2$: [M + H] 249.1855. Found: 249.1842.

4-(4-((*tert*-butyldimethylsilyl)oxy)-3,5-diisopropylphenyl)butan-2-one (2)

1.7 mL of dimethylformamide (DMF) was added to **1** (385 mg, 1.55 mmol) with stirring at room temperature, followed by addition of imidazole (369 mg, 5.425 mmol). Once imidazole was in solution, *tert*-butyldimethylsilyl chloride (TBSCl; 701 mg, 4.65 mmol) was added. After proceeding overnight at room temperature, the reaction was partitioned between hexanes and water. The organic layer was washed with water and saturated $NaHCO_3$, dried over Na_2SO_4, and

concentrated *in vacuo*. Following column chromatography on silica (15% ethyl acetate in hexanes as eluent), the appropriate fractions were combined and concentrated to yield 446 mg (79%) of **2** as an orange oil.

^{1}H NMR (500 MHz, CDCl$_3$): δ 6.85 (s, 2H, H$_{arom}$), 3.28 (sept, 2H, *J*=6.8 Hz, CH-i-Pr), 2.87-2.79 (m, 2H, CH$_2$), 2.79-2.71 (m, 2H, CH$_2$), 2.16 (s, 3H, H$_3$C-C=O), 1.16 (d, 12H, *J*=6.8 Hz, H$_3$C-i-Pr), 1.03 (s, 9H, *tert*-butyl), 0.18 (s, 6H, Si-CH$_3$).

^{13}C NMR (125 MHz, CDCl$_3$): δ 208.7 (C=O), 147.4, 139.0, 133.7, 123.1 (CH$_{arom}$), 45.7, 30.1, 29.8, 26.5, 26.1, 23.4, 18.9, -3.3 (H$_3$C-Si).

HRMS calc'd for C$_{22}$H$_{38}$O$_2$Si: [M + H] 363.2719. Found: 363.2719.

4-(4-((*tert*-butyldimethylsilyl)oxy)-3,5-diisopropylphenyl)-3-methyl-3*H*-diazirine (3)

Under an atmosphere of N$_2$, **2** (446 mg, 1.23 mmol) was dissolved in a mixture of methanol (MeOH)-ether (1:1, 4.5 mL) and cooled to -40°C. A solution of 2.0 M NH$_3$ in MeOH (31 mL) was added dropwise with stirring. The reaction was allowed to proceed for 6 hours at -40°C. A solution of hydroxylamine-*O*-sulfonic acid (NH$_2$OSO$_3$H,; 208 mg, 1.845 mmol) in 3.6 mL of methanol was added dropwise. After 1 hour, the flask was kept at -20°C for 3 days with occasional stirring. After completion, the mixture was filtered, dried with Na$_2$SO$_4$, concentrated *in vacuo*, dissolved in a mixture of methanol (18 mL) and triethylamine (TEA; 0.515 mL, 3.69 mmol), and cooled to -10°C. A solution of iodine (I$_2$; 312 mg, 1.23 mmol) in DCM (9 mL) was added dropwise while stirring. Once the solution remained persistently brown in color, the excess iodine was quenched with a 5% solution of Na$_2$S$_2$O$_3$ (4.5 mL), which turned the reaction orange. The mixture was diluted with water and extracted with ether. The combined organic

phases were washed with water and dried over Na_2SO_4. Concentration and column chromatography on silica using 3% ethyl acetate in hexanes yielded 205 mg (45%) of diazirine **3** as an orange oil.

^{1}H NMR (500 MHz, $CDCl_3$): δ 6.83 (s, 2H, H_{arom}), 3.27 (sept, 2H, J=6.9 Hz, HC-i-Pr), 2.43 (m, 2H, CH_2), 1.65 (m, 2H, CH_2), 1.16 (d, 12H, J=6.9 Hz, H_3C-i-Pr), 1.03 (s, 9H, *tert*-butyl), 1.00 (s, 3H, ɑ-*azi*-CH_3) 0.18 (s, 6H, Si-CH_3).

^{13}C NMR (125 MHz, $CDCl_3$): δ 147.3, 139.0, 133.6, 123.1 (CH_{arom}), 36.7, 29.8, 26.5, 26.1, 25.7, 23.4, 19.9, 18.8, -3.3 (H_3C-Si).

HRMS calc'd for $C_{22}H_{39}N_2OSi$: [M + H] 375.2832. Found: 375.2841.

2,6-diisopropyl-4-(2-(3-methyl-3*H*-diazirin-3-yl)ethyl)phenol (4)

Under an atmosphere of N_2, **3** (32 mg, 0.0855 mmol) was deprotected with dropwise addition of tetra-n-butylammonium fluoride (TBAF)-acetic acid (1:2 molar ratio, 1 M TBAF in tetrahydrofuran + neat acetic acid, 0.43 mL) on ice and the reaction was allowed to warm to room temperature overnight to obtain crude product. Column chromatography on silica (5% ethyl acetate in hexanes) yielded 17 mg (76%) of pure **4** as an orange oil after concentration.

^{1}H NMR (500 MHz, $CDCl_3$): δ 6.84 (s, 2H, H_{arom}), 4.66 (s, 1H, ArOH), 3.14 (sept, 2H, J=6.9 Hz, HC-i-Pr), 2.43 (m, 2H, CH_2), 1.65 (m, 2H, CH_2), 1.27 (d, 12H, J=6.9 Hz, H_3C-i-Pr), 1.03 (s, 3H, ɑ-*azi*-CH_3).

^{13}C NMR (125 MHz, $CDCl_3$): δ 148.2, 133.7, 132.6, 123.2 (CH_{arom}), 36.9, 29.9, 27.2, 25.9, 22.8, 20.0.

HRMS calc'd for $C_{16}H_{24}N_2O$: [M + H] 261.1967. Found: 261.1964.

Preparation of o-XPRO-Click

4-(4-hydroxy-3-isopropylphenyl)butan-2-one (5)

2-isopropylphenol (3 mL, 22.3 mmol, 3.0 eq) and 3 mL of toluene were stirred in an ice-cold flask under an atmosphere of N_2. Then, Amberlyst-15 (475 mg) was added. Methyl vinyl ketone (0.45 mL, 7.43 mmol, 1.0 eq) in 2 mL of toluene was added dropwise. The reaction was warmed to 40°C for 8 hours, then partitioned between ether and water. The ether solution as washed with water, brine, dried over Na_2SO_4 and concentrated under vacuum. Column chromatography on silica (30% ethyl acetate in hexanes as eluent) yielded 2 g (44%) of **5** as a pale-yellow oil.

^{1}H NMR (500 MHz, $CDCl_3$): δ 7.01 (s, 1H), 6.88 (dd, J = 8.1, 2.3 Hz, 1H), 6.68 (d, J = 8.0 Hz, 1H), 4.77 (bs, 1H), 3.20 (sept, J = 7.0 Hz, 1H), 2.94- 2.80 (m, 2H), 2.80 − 2.68 (m, 2H), 2.16 (s, 3H), 1.26 (d, J = 6.9 Hz, 6H).

^{13}C NMR: (125 MHz, $CDCl_3$): δ 208.8, 151.2, 134.5, 133.1, 126.3, 126.2, 115.3, 110, 45.7, 30.1, 29.3, 27, 22.6.

HRMS calc'd for $C_{13}H_{18}O_2$: [M + Na] 229.1204. Found: 229.1222.

4-(3-bromo-4-hydroxy-5-isopropylphenyl)butan-2-one (6)

Under an atmosphere of N_2, **5** (393 mg, 1.905 mmol, 1.0 eq) was stirred in DCM (12 mL). N-bromosuccinimide (NBS; 373 mg, 2.1 mmol, 1.1 eq) was dissolved in 1.4 mL of DMF and added dropwise to the mixture. The reaction proceeded overnight at room temperature. The mixture was then diluted with DCM, washed with water, dried over Na_2SO_4, and concentrated *in*

vacuo. Column chromatography on silica (15% ethyl acetate in hexanes as eluent) yielded 300 mg (54%) of a pale-yellow oil.

^{1}H NMR (500 MHz, CDCl$_3$): δ 7.14 (s, 1H), 6.96 (dd, *J* = 8.1, 2.3 Hz, 1H), 6.68 (d, *J* = 8.0 Hz, 1H), 4.77 (bs, 1H), 3.20 (sept, *J* = 7.0 Hz, 1H), 2.94- 2.80 (m, 2H), 2.80 – 2.68 (m, 2H), 2.16 (s, 3H), 1.26 (d, *J* = 6.9 Hz, 6H).

^{13}C NMR: (125 MHz, CDCl$_3$): δ 208.8, 151.2, 134.5, 133.1, 126.3, 126.2, 115.3, 110, 45.7, 30.1, 29.3, 27, 22.6.

HRMS calc'd for C$_{13}$H$_{17}$BrO$_2$: [M + H] 285.0485. Found: 285.0471.

4-(4-hydroxy-3-isopropyl-5-((trimethylsilyl)ethynyl)phenyl)butan-2-one (7)

A dry flask containing **6** (1g, 3.5 mmol, 1.0 eq), triphenylphosphine (PPh$_3$; 92 mg, 0.35 mmol, 0.1 eq), bis(triphenylphosphine)palladium(II)dichloride (PdCl$_2$(PPh$_3$)$_2$; 153 mg, 0.22 mmol, 0.06 eq), copper (I) iodide (CuI; 239 mg, 1.26 mmol, 0.36 eq) and ethynyltrimethylsilane (1 mL, 10.5 mmol, 3.0 eq), and triethylamine (23 mL) was charged with argon. A flow of argon was bubbled through the reaction mixture for 15 minutes. The reaction proceeded overnight at room temperature. The mixture was then diluted with water and DCM. The layers were separated and the aqueous phase was extracted with DCM. The combined organic phases were dried over Na$_2$SO$_4$, and concentrated *in vacuo*. Column chromatography on silica (15% ethyl acetate in hexanes as eluent) yielded 630 mg (59%) of a light brown oil.

^{1}H NMR (500 MHz, CDCl$_3$): δ 7.02 (s, 1H), 6.99 (s, 1H), 5.87 (s, 1H), 3.25 (sept, J = 6.9 Hz, 1H), 2.79 (ddd J = 8.5, 6.8, 1.7 Hz, 2H), 2.72 (ddd, J = 8.5, 7.0, 1.7 Hz, 2H), 2.15 (s, 3H), 1.23 (d, J = 6.8 Hz, 6H).

^{13}C NMR: (125 MHz, CDCl$_3$): δ 208, 152.8, 134.2, 132.4, 127.8, 109, 101.9, 99.6, 45.4, 30.1, 29, 27.5, 22.4, 22.3.

HRMS calc'd for C$_{18}$H$_{26}$O$_2$Si: [M + H] 303.1775. Found: 303.1656.

4-(4-((tert-butyldimethylsilyl)oxy)-3-isopropyl-5-((trimethylsilyl)ethynyl)butan-2-one (8)

Under an atmosphere of N$_2$, 0.75 mL of DMF was added to **7** (100 mg, 0.331 mmol, 1.0 eq) with stirring. Then imidazole (85 mg, 1.34 mmol, 3.75 eq) and *tert*-butyldimethylsilyl chloride (137 mg, 0.91 mmol, 2.75 eq) were added. After proceeding overnight at room temperature, the reaction was partitioned between hexanes and water. The aqueous layer was extracted with hexanes. The combined organic layers were washed with water and saturated NaHCO$_3$, dried over Na$_2$SO$_4$, and concentrated *in vacuo*. Following column chromatography on silica (20% ethyl acetate in hexanes as eluent), the appropriate fractions were combined and concentrated to yield 113 mg (82%) of **4** as a light brown oil.

^{1}H NMR (500 MHz, CDCl$_3$): δ 7.08 (s, 1H), 6.98 (s, 1H), 3.28 (sept, J = 11.4, 8.2, 5.4 Hz, 1H), 2.88 – 2.76 (m, 2H), 2.73 (ddd, J = 9.0, 5.1, 1.9 Hz, 2H), 2.15 (s, 1H), 1.14 (dd, J = 7.1, 2.6 Hz, 6H), 1.05 (s, 9H), 0.24 (d, J = 3.6 Hz, 6H).

^{13}C NMR (125 MHz, CDCl$_3$): δ 208, 151.5, 140, 133.7, 131.5, 127.1, 115.1, 101.1, 97.4, 45.3, 30.1, 29, 26.3, 26.1, 23.1, 18.7, 0, -3.

HRMS calc'd for C$_{24}$H$_{40}$O$_2$Si$_2$: [M + H] 417.2640. Found: 417.2529.

4-(4-((tert-butyldimethylsilyl)oxy)-3-isopropyl-5-((trimethylsilyl)ethynyl)phenethyl)-3-methyl-3*H*-diazirine (9)

Under an atmosphere of N_2, **8** (61 mg, 0.146 mmol, 1.0 eq) was dissolved in a mixture of methanol-ether (1:1, 0.6 mL) and cooled to -40°C. A solution of 2.0 M NH_3 in MeOH (8 mL) was added dropwise with stirring over 6 hours. A solution of hydroxylamine-*O*-sulfonic acid (25 mg, 0.220 mmol, 1.5 eq) in 0.5 mL of methanol was added dropwise with stirring. After 1 hour, the flask was kept at -20°C for 2 days with occasional stirring. The mixture was filtered, dried with Na_2SO_4, concentrated *in vacuo*, dissolved in a mixture of methanol (2.4 mL) and triethylamine (0.062 mL, 0.442 mmol, 3.01 eq.), and cooled to -10°C. The reaction with trimethylamine stirred for 15 minutes at room temperature. A solution of iodine (37 mg, 0.146 mmol, 1.0 eq) in DCM (1.2 mL) was added dropwise while stirring. Once the solution remained persistently brown in color, the excess iodine was quenched with a 5% solution of $Na_2S_2O_3$ (0.7 mL), which turned the reaction yellow. The mixture was diluted with water and the aqueous layer was extracted with ether. The combined organic phases were washed with water and dried over Na_2SO_4. Concentration and column chromatography on silica (20% ethyl acetate in hexanes as eluent) yielded 20 mg (32%) of diazirine **9** as a yellow oil.

^{1}H NMR (500 MHz, $CDCl_3$): δ 7.06 (s, 1H), 6.97 (s, 1H), 3.29 (sept, J = 6.9 Hz, 1H), 2.53 − 2.26 (m, 2H), 1.80 − 1.59 (m, 2H), 1.15 (d, J = 6.9 Hz, 6H), 1.05 (s, 9H), 1.01 (s, 3H), 0.41-0.20 (m, 6H), 0.10 (s, 9H).

^{13}C NMR (125 MHz, $CDCl_3$): δ 151.5, 139.9, 133.5, 131.5, 127.1, 127, 115.1, 104.1, 97.4, 36.5, 29.3, 26.3, 26.1, 25.7, 23.1, 20, 18.7, 0.01, -2.9.

HRMS calc'd for $C_{24}H_{40}N_2OSi_2$: [M + H] 429.2752. Found: 429.2750.

2-ethynyl-6-isopropyl-4-(2-(3-methyl-3H-diazirin-3-yl)ethyl)phenol (10)

Under an atmosphere of N_2, **9** (20 mg, 0.046 mmol, 1.0 eq) from the previous step was deprotected with dropwise addition of TBAF-acetic acid (0.014 mL of 1.0 M in THF + 0.040 mL THF) on ice and the reaction was allowed to warm to room temperature overnight to obtain crude **10**. Column chromatography on silica (10% ethyl acetate in hexanes) yielded 12 mg (53%) of pure **10** as a yellow oil after concentration.

^{1}H NMR (500 MHz, CDCl$_3$): δ 7.03 (s, 1H), 7.00 (s, 1H), 5.79 (s, 1H), 3.46 (s, 1H), 3.28 (sept, J = 6.9 Hz, 1H), 2.39 (m, 2H), 1.63 (m, 2H), 1.24 (d, J = 6.9 Hz, 6H), 1.02 (s, 3H).

^{13}C NMR: (125 MHz, CDCl$_3$): δ 153, 135, 132, 129, 128, 108, 84, 79, 37, 29, 27, 26, 22, 20.

HRMS calc'd for $C_{15}H_{18}N_2O$: [M + H] 243.1497. Found: 243.1502.

Preparation of p-XPRO-Click

4-hydroxy-3,5-diisopropylbenzaldehyde (11)

11 was synthesized as described in López *et al.* (11). A solution of 2,6-diisopropylphenol (2.0 g, 11.2 mmol, 1.0 eq), hexamethylenetetramine (3.15 g, 22.4 mmol, 2.0 eq) and 11 mL of trifluoroacetic acid (F_3CCO_2H) were mixed in a round bottom flask and heated under reflux (90°C) overnight. The reaction mixture was cooled to room temperature and neutralized with NaHCO$_3$. The aqueous layer was extracted with ethyl acetate (EtOAc) and the combined organic layers were concentrated. 3.0 M hydrochloric acid (HCl) was added to the crude product and the mixture was stirred under reflux (80°C) for 3 hours. The precipitate was filtered, washed with water and purified by elution with hexanes/EtOAc (4:1) to yield 2 g of a white solid (90%).

^{1}H NMR (500 MHz, CDCl$_3$): δ 9.88 (s, 1H), 7.64 (s, 2H), 5.41 (s, 1H), 3.19 (sept, J = 6.9 Hz, 2H), 1.33 (d, 12H).

^{13}C NMR: (125 MHz, CDCl$_3$): δ 192.9, 156.9, 134.8, 129.1, 126.7, 27, 22.5.

HRMS calc'd for C$_{13}$H$_{18}$O$_2$: [M + Na] 229.1204. Found: 229.1222.

4-(*tert*-butyldimethylsilyl)oxy)-3,5-diisopropylbenzaldehyde (12)

Under an atmosphere of nitrogen, **11** (204 mg, 0.989 mmol, 1.0 eq) was dissolved in DCM (10 mL) and then triethylamine (0.69 mL, 4.944 mmol, 5.0 eq) and *tert*-butyldimethylsilyl chloride (179 mg, 1.1867 mmol, 1.2 eq) were added. The mixture stirred at room temperature overnight. The mixture was partitioned between hexanes and EtOAc, dried over Na$_2$SO$_4$, and chromatographed on silica (eluted in hexanes) to yield 200 mg of a yellow oil (63%).

^{1}H NMR (500 MHz, CDCl$_3$): δ 9.95 (s, 1H), 7.63 (s, 2H), 3.33 (sept, J = 6.9 Hz, 2H), 1.22 (d, 12H), 1.04 (d, J = 2.4 Hz, 9H), 0.25 (s, 6H).

^{13}C NMR: (125 MHz, CDCl$_3$): δ 191.8, 155.4, 140.2, 130.8, 125.9, 26.8, 26, 23.1, 19, -3.2.

HRMS calc'd for C$_{19}$H$_{32}$O$_2$Si [M + H]: 321.2250. Found: 321.2280.

1-4-((*tert*-butyldimethylsilyl)oxy)-3,5-diisopropylphenyl)prop-2-yn-1-ol (13)

Under an atmosphere of nitrogen, **12** (680 mg, 2.12 mmol, 1.0 eq) was cooled via a dry ice-acetone bath (78°C). To a solution of **12** in 2 mL of anhydrous THF was added dropwise 7 mL of 0.5 M ethynylmagnesium bromide (HCCMgBr) solution in THF. The reaction mixture was allowed to slowly warm to room temperature. After stirring for 3 hours at room temperature, the reaction was quenched with saturated ammonium chloride (NH$_4$Cl), and the mixture was partitioned between DCM and water, and the two layers were separated. The organic layer was

washed with water and dried over Na₂SO₄. Solvent was evaporated off and material was purified with 15% EtOAc/hexanes to give 0.570 g (83 %) as a brownish oil.

^{1}H NMR (500 MHz, CDCl$_3$): δ 7.28 (s, 2H), δ5.58 – 5.33 (m, 1H), 3.32 (sept, J = 6.9 Hz, 2H), 2.76-2.63 (m, 2H), 1.19 (d, 12H), 1.05 (s, 9H), 0.21 (s, 6H).

^{13}C NMR: (125 MHz, CDCl$_3$): δ 149.6, 139.4, 133, 122.1, 83.9, 74.5, 64.8, 26.8, 26.1, 23.3, 18.9, -3.29.

HRMS calc'd for C$_{21}$H$_{34}$O$_2$Si [M + Na]: 369.2226. Found: 369.2229.

4-(4-((*tert*-butyldimethylsilyl)oxy)-3,5-diisopropylphenyl)hex-5-yn-2-one (14)

14 was synthesized according to Nishibayashi *et al*. (12). Under an atmosphere of N$_2$, ammonium tetrafluoroborate (NH$_4$BF$_4$; 7 mg, 0.066 mmol, 0.1 eq) and [Cp*RuCl(μ$_2$-SMe)$_2$RuCp*Cl] (21 mg, 0.033 mmol, 0.05 eq) were placed in a round-bottomed flask. Anhydrous acetone (40 mL) was added, and then the mixture was stirred at room temperature. After addition of **13** (230 mg, 0.66 mmol, 1.0 eq), the reaction flask was kept at reflux temperature for 5 hours. The reaction mixture was treated with brine (20 mL) and extracted with diethyl ether (20 ml x 3). The ether layer was dried over anhydrous Na$_2$SO$_4$. The extract was concentrated under reduced pressure and purified over SiO$_2$ with EtOAc-*n*-hexane (1/9) to give **14** as a light brown oil (83% yield).

^{1}H NMR (500 MHz, CDCl$_3$): δ 7.04 (s, 2H), δ 4.13 (ddd, J =9.2, 5.5, 2.4 Hz, 1H), 3.29 (hept, J = 6.9 Hz, 2H), 2.98 (dd, J = 16.1, 9.1 Hz, 1H) 2.78 (dd, J = 16.2, 5.5 Hz, 1H), 2.28 (s, 1H), 2.16 (s, 3H), 1.17 (d, 12H), 1.03 (s, 9H), 0.19 (s, 6H).

^{13}C NMR: (125 MHz, CDCl$_3$): δ 206.2 148.2, 139.3, 132.9, 130.9, 128.8, 122.2, 85.5, 70.9, 52.1, 38.7, 32.7, 30.7, 29, 26.7, 26.1, 23.4, 23, 18.9, -3.3.

HRMS calc'd for C$_{24}$H$_{38}$O$_2$Si [M + H]: 387.2719. Found: 387.2787.

3-(2-(4-((*tert*-butyldimethylsilyl)oxy)-3,5-diisopropylphenyl)but-3-yn-1-yl)-3-methyl-3*H*-diazirine (15)

The ketone **14** (160 mg, 0.425 mmol) was dissolved in methanol (1.5 mL) and cooled to -40°C with dry ice/acetonitrile bath. A solution of 2.0 M ammonia in methanol (11 mL) was added dropwise with stirring. The reaction mixture was warmed up to -30°C and stirred at this temperature for 6 hours. A solution of hydroxylamine-*O*-sulfonic acid (74 mg, 0.64 mmol) in 1.2 mL of methanol was added dropwise and the solution was stirred at -20°C for 2 days. After completion, the reaction mixture was evaporated under reduced pressure and dissolved in a mixture of methanol (6.4 mL) and trimethylamine (0.192 mL, 1.28 mmol) and cooled to -10°C. A saturated solution of iodine (109 mg, 0.425 mmol) in dichloromethane (3.2 mL) was added dropwise until the mixture remained light-brown in color. The excess iodine was quenched with 5% solution of Na$_2$S$_2$O$_3$ (1.5 mL). The mixture was partitioned between water and ether. The organic phase was collected and washed with water and brine (20 mL each) and dried over Na$_2$SO$_4$. Rotary evaporation and chromatography using 1% ethyl acetate afforded **15** as a light brown oil (80 mg, 52 %).

^{1}H NMR (500 MHz, CDCl$_3$): δ 7.05 (s, 2H), δ 3.50 (ddd, *J* =8.9, 6.5, 2.5 Hz, 1H), 3.29 (hept, *J* = 13.8, 6.9 Hz, 2H), 1.17 (d, 12H), 1.04 (s, 9H), 0.97 (s, 3H), 0.19 (s, 6H).

^{13}C NMR: (125 MHz, CDCl$_3$): δ 148.2, 139.3, 132.9, 130.9, 122.3, 71.3.5, 44.3, 32.5, 26.7, 26.1, 23.4, 20.3, 18.9, -3.3.

HRMS calc'd for $C_{24}H_{38}N_2OSi$ [M + H]: 399.2832. Found: 399.2830.

2,6-diisopropyl-4-(1-(3-methyl-3H-diazirin-3-yl)but-3-yn-2-yl)phenol (16)

Under an atmosphere of N_2, **15** (30 mg, 0.075 mmol, 1.0 eq) was placed in a flask and then 0.113 mL of TBAF (1.0 M in THF) and 0.013 mL of acetic acid were added while stirring. The reaction proceeded overnight and was purified via SiO_2 with EtOAc/hexanes) to yield **16** in 55% yield.

^{1}H NMR (500 MHz, CDCl$_3$): δ 7.04 (s, 2H), δ 4.73 (s, 1H), 3.50 (ddd, J = 9.0, 6.5, 2.5 Hz, 1H), 3.15 (hept, J = 6.9 Hz, 2H), 1.89-1.68 (m, 2H), 1.28 (d, J = 6.8 Hz, 12H), 1.03 (s, 3H).

^{13}C NMR: (125 MHz, CDCl$_3$): δ 149.0, 133.9, 132.0, 122.4, 85.5, 71.4, 44.2, 32.5, 27.3, 24.8, 22.7, 20.4.

HRMS calc'd for $C_{18}H_{24}N_2O$ [M + H]: 285.1967. Found: 285.1981.

Results

Below, I describe the synthetic schemes for XPRO, *o*-XPRO-Click, and *p*-XPRO-Click with corresponding ^{1}H spectra. ^{1}H and ^{13}C NMR spectra for XPRO, *o*-XPRO-Click, and *p*-XPRO-Click intermediates are listed in the appendix.

Propofol is a synthetic precursor to XPRO

One of the ideal traits of a photoaffinity label is chemical similarity to the parent probe. Studies have shown that Amberlyst-15, a heterogeneous acid catalyst, promotes reactions between alkyl phenols and α-β-unsaturated ketones (10). Since alkyl ketones serve as

synthetically expedient precursors to alkyl diazirines, I chose to incorporate them into the parent propofol molecule using this mild method. Thus, I adapted this strategy to generate a photoreactive derivative of propofol (XPRO) that retains the propofol core structure.

Heterogeneous acid catalysis is very important in many areas of chemical and energy industries. Amberlyst-15 ion exchange resin, a source of sulfonic acid, catalyzes the addition of phenols to α,ß-unsaturated ketones under mild conditions (**i, Figure 2.1A**). I initially used concentrated sulfuric acid as a reagent for the addition, but Amberlyst-15 is easy to measure, safe to use, and easily removed after reaction completion, upon which it can be regenerated. The remaining steps for the synthesis of XPRO include standard protection of the phenolic hydroxyl group (**ii, Figure 2.1A**), diazirination (**iii, Figure 2.1A**), and deprotection of the silyl ether (**iv, Figure 2.1A**), yielding XPRO, a photoreactive derivative that retains the propofol core (**Figure 2.1**). ^{1}H NMR corresponds to the chemical structure of XPRO (**Figure 2.2**). Taken together, the results demonstrate that Amberlyst-15 is an effective catalyst for promoting the addition of propofol to α,ß-unsaturated ketones under mild conditions, with high yield and minimal laboratory operations. Armed with this useful reagent, I applied Amberlyst-15 to the synthesis of another propofol photolabel with added functionality.

o-XPRO-Click is functionalized with a diazirine moiety and an ortho-alkyne group in 6 steps

Alkynes are useful affinity handles for biorthogonal chemistry, thus I designed synthetic schemes to further functionalize diazirine-bearing probes of propofol (**Figures 2.1 B and C**). I exploited a useful property of Amberlyst-15: it catalyzes the regioselective addition of alkyl phenols, with addition occurring preferentially at the para position (10). Starting from 2-
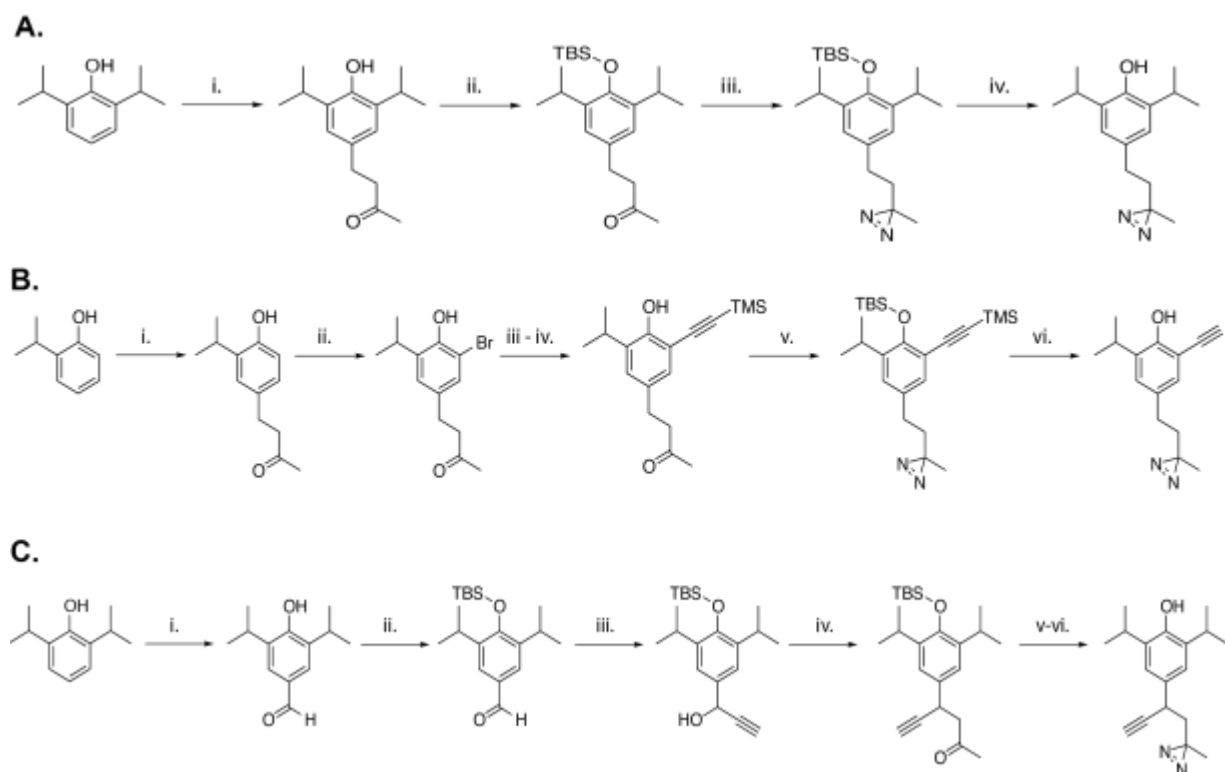
Figure 2.1 Synthetic scheme of XPRO, *o* and *p*-XPRO-Click (A) XPRO synthetic scheme. **i:** Methyl vinyl ketone, Amberlyst-15, **ii:** TBSCl, imidazole **iii:** (a) NH₃, MeOH, NH₂OSO₃H, (b) I₂, TEA **iv:** TBAF-acetic acid. **(B)** *o*-XPRO-Click synthetic scheme. **i:** Methyl vinyl ketone, Amberlyst-15 **ii:** NBS, **iii:** TBSCl, imidazole **iv:** PdCl₂(PPh₃)₂, PPh₃, TEA, CuI, Trimethylsilylacetylene **v:** (a) NH₃, MeOH, NH₂OSO₃H (b) I₂, TEA **vi:** TBAF-acetic acid. **(C)** *p*-XPRO-Click synthetic scheme. **i:** F₃CCO₂H, hexamethylenetetramine, HCl **ii:** TEA, TBSCl, imidazole **iii:** HCCMgBr, THF, NH₄Cl **iv:** cat. Cp*RuCl(μ₂-SMe)₂RuCp*Cl, NH₄BF₄, acetone **v:** (a) NH₃, MeOH, NH₂OSO₃H, (b) I₂, TEA **vi:** TBAF-acetic acid.
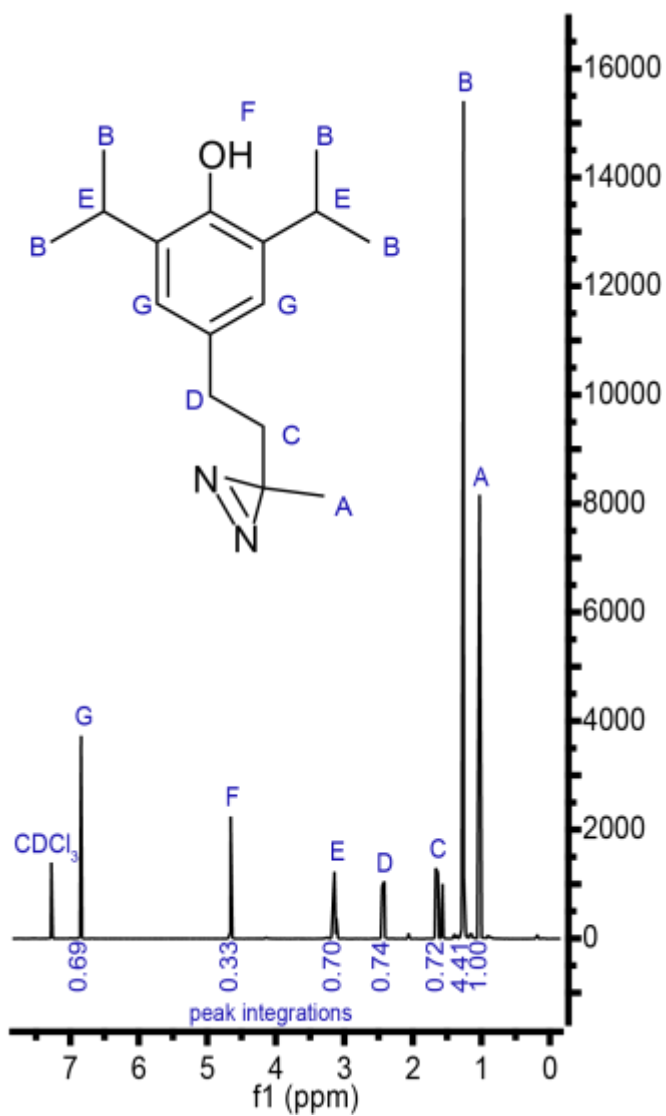
Figure 2.2 ¹H NMR of XPRO.

as 2-isopropylphenol, the reagent in isopropylphenol, I employed Amberlyst-15 to facilitate addition of the phenol to methyl vinyl ketone, generating the alkyl ketone (**i, Figure 2.1B**), the synthetically expedient precursor to the alkyl diazirine group. Amberlyst-15 was particularly useful in the synthesis of *o*-XPRO-Click, as 2-isopropylphenol is amenable to undesirable polysubstitution reactions, due to the absence of an alkyl group in the ortho position.

After installation of the alkyl ketone, I incorporated a bromine at the ortho position (**ii, Figure 2.1B**), relative to the phenolic hydroxyl group; aryl halides are widely used as substrates in coupling with terminal alkynes to form aryl alkynes (13,14). I employed Sonogashira coupling to provide the alkyne moiety using a palladium catalyst, a copper catalyst, and a base (**iii, Figure 2.1B**). Standard diazirine synthesis conditions consisting of phenol protection (**iv, Figure 2.1B**), diazirination (**v, Figure 2.1B**) and deprotection (**vi, Figure 2.1B**) result in *o*-XPRO-Click; ^{1}H NMR conforms to the structure of *o*-XPRO-Click (**Figure 2.3**).

p-XPRO-Click is functionalized with a diazirine moiety and a para-alkyne group in six steps

I reasoned that the propofol core may be important for propofol activation of TRPA1. Thus, to retain the propofol core in a clickable photoreactive analogue, I also synthesized *p*-XPRO-Click as an alternative to *o*-XPRO-Click. However, they were synthesized by different means. In the case of *p*-XPRO-Click, Duff formylation generated the aldehyde (**i, Figure 2.1C**), which, after phenol protection (**ii, Figure 2.1C**), engaged in a Grignard reaction with ethynyl magnesium bromide (**iii, Figure 2.1C**), producing a secondary alcohol bearing an alkyne group. Propargylic alkylation proceeded under very mild and neutral reaction conditions (**iv, Figure 2.1C**). Diazirination (**v, Figure 2.1C**) and deprotection (**vi, Figure 2.1C**) resulted in *p*-XPRO-Click. ^{1}H NMR conforms to the structure of *p*-XPRO-Click (**Figure 2.4**).
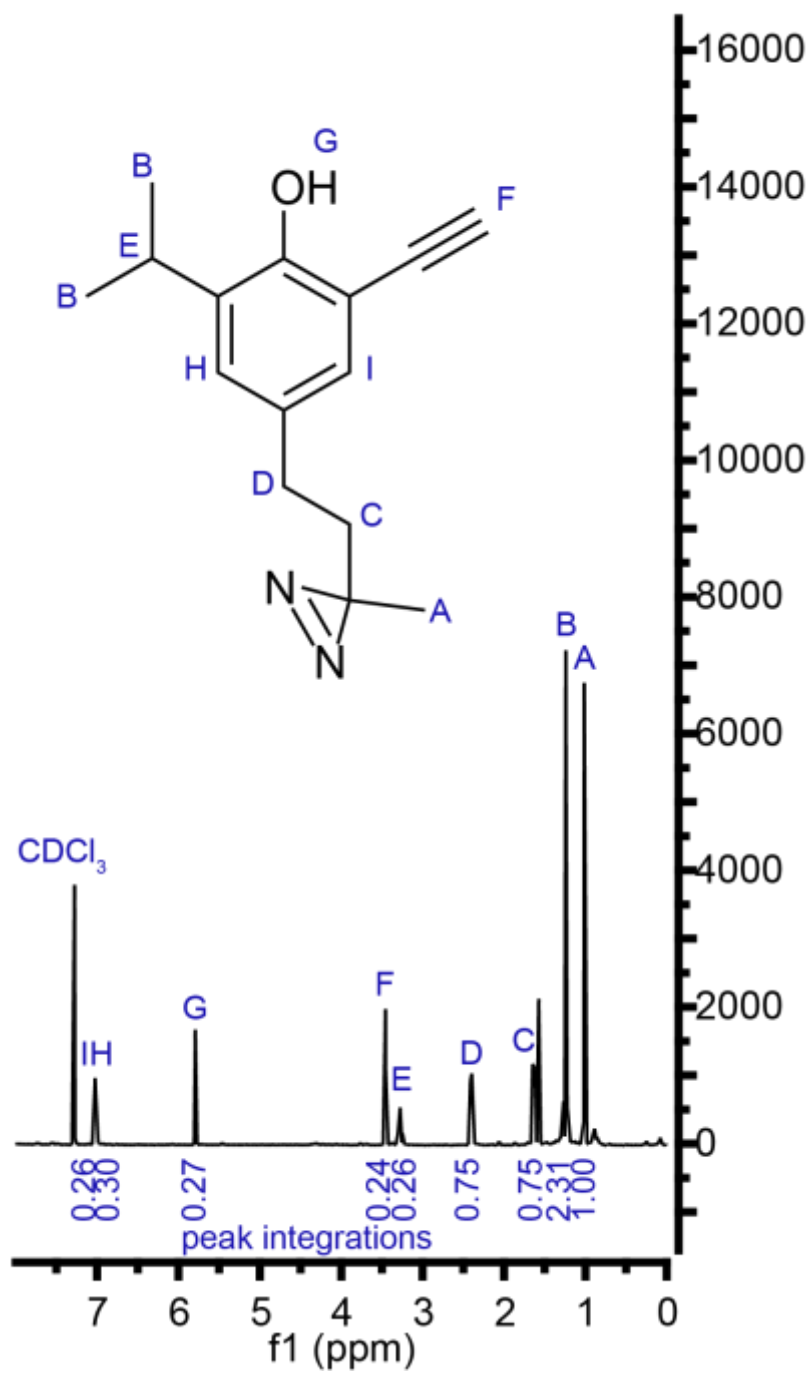
Figure 2.3 ^{1}H NMR of *o*-XPRO-Click.
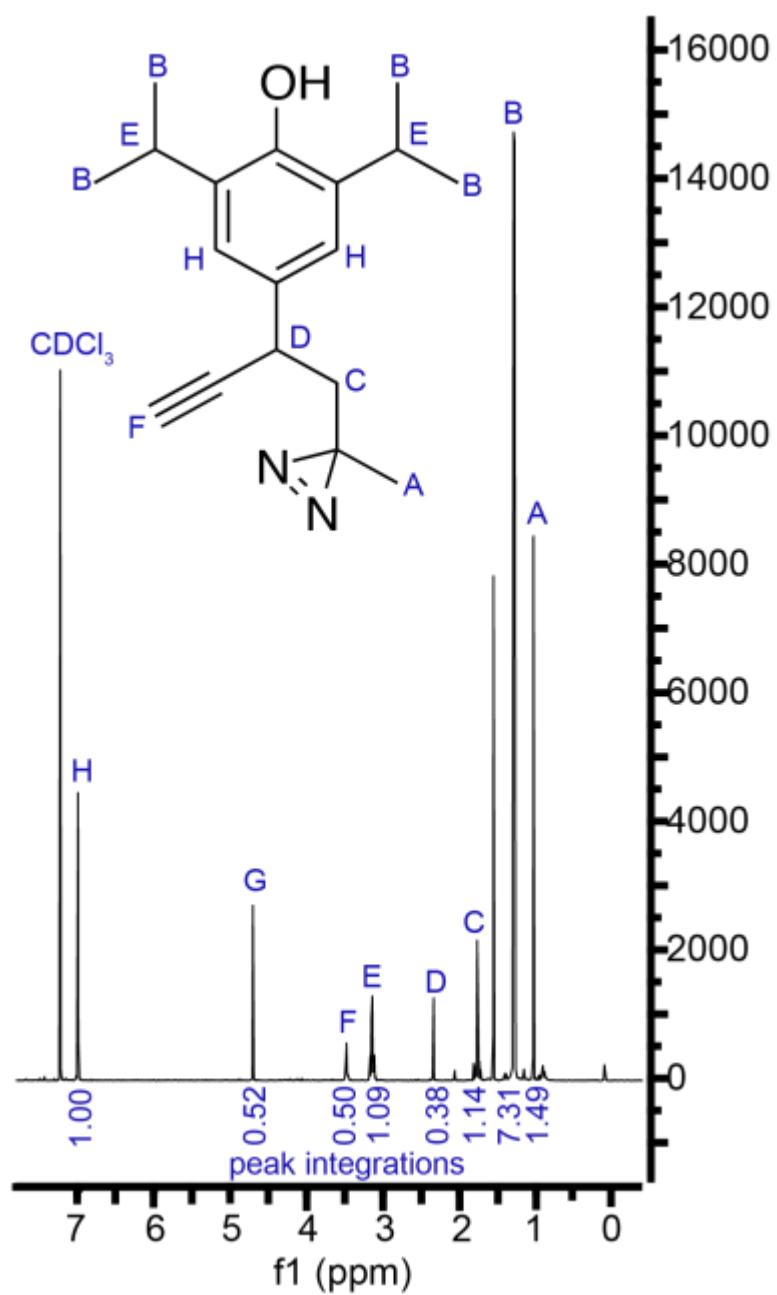
Figure 2.4 ¹H NMR of *p*-XPRO-Click.

Characterization of functional properties of XPRO, o-XPRO-Click, and p-XPRO-Click

I first tested the ability of the diazirine moiety to undergo crosslinking in solution. XPRO contains a diazirine moiety that absorbs UV light at ~ 350 nm (**Figure 2.5A**), consistent with prior studies of diazirine-containing compounds (15). Upon UV exposure, the absorbance of the solution containing XPRO decreases approximately exponentially. I interpret this result as the diazirine moiety reacting with neighboring molecules of methanol. Mass spectrometry of the solution at the final time point corresponds to the molecular weight of XPRO-methanol adduct, which is consistent with my proposed mechanism (**Figure 2.5B**).

I then tested whether *o*-and *p*-XPRO-Click conjugate with azide-bearing moieties such as 3-azido-7-hydroxycoumarin (coumarin azide), whose fluorescence increases upon a successful click reaction with an alkyne partner (16). In this way, coumarin azide is used as a model to assay click chemistry conditions with alkyne-containing chemicals and biomolecules. Thus, I used coumarin azide as a model for the "clickability" of *o*-and *p*-XPRO-Click. Although some background fluorescence is observed for coumarin azide (dotted line), little background fluorescence at the excitation wavelength of coumarin azide is observed for *o*-XPRO-Click (dashed line). The click-reaction with o-XPRO-Click and coumarin azide results in the highest increase in fluorescence after 1 hour of copper-catalyzed click chemistry (**Figure 2.6A**). Similarly, *p*-XPRO-Click reacts with coumarin azide over a range of concentrations, resulting in an increase in fluorescence due to formation of azide-alkyne product **(Figure 2.6B)**. The ratio of the concentration of *p*-XPRO-Click: coumarin azide to elicit a successful click reaction, 1:2, is consistent with previous studies (16).
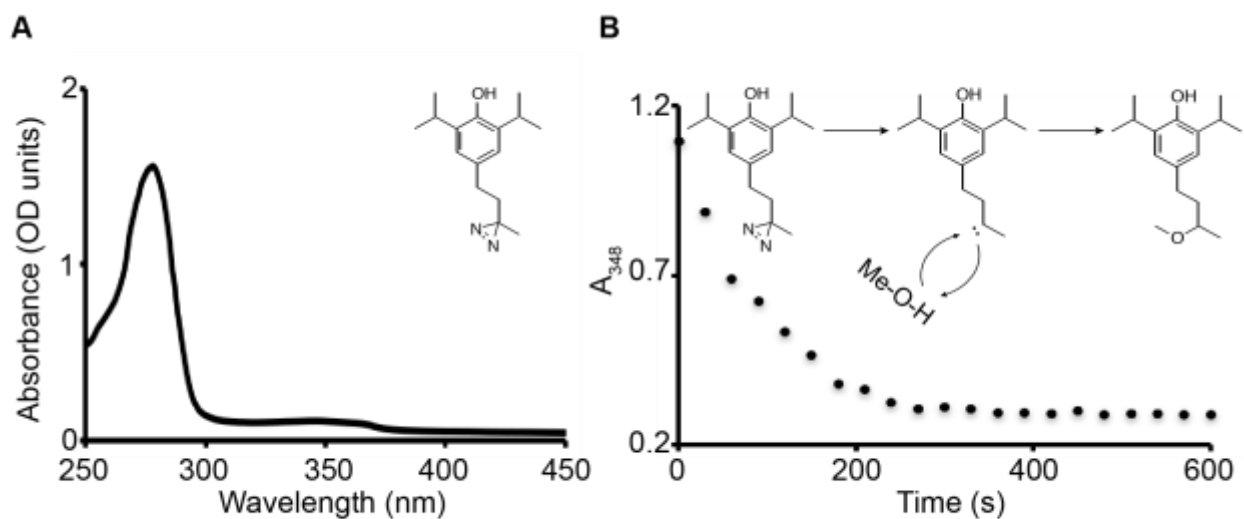
Figure 2.5 Characterization of XPRO crosslinking (**A**) XPRO UV spectrum plotting

absorbance as a function of wavelength. The absorption in the 300-350 nm region is due to the

diazirine moiety. (**B**) Proposed XPRO crosslinking reaction in a methanolic solution. Upon UV

exposure, the absorbance of the diazirine moiety at 348 nm (A_{348}) decreases in a methanolic

solution of XPRO. Mass spectrometry identified a peak that corresponds to a XPRO-methanol

adduct, suggesting diazirine insertion into methanol solvent.
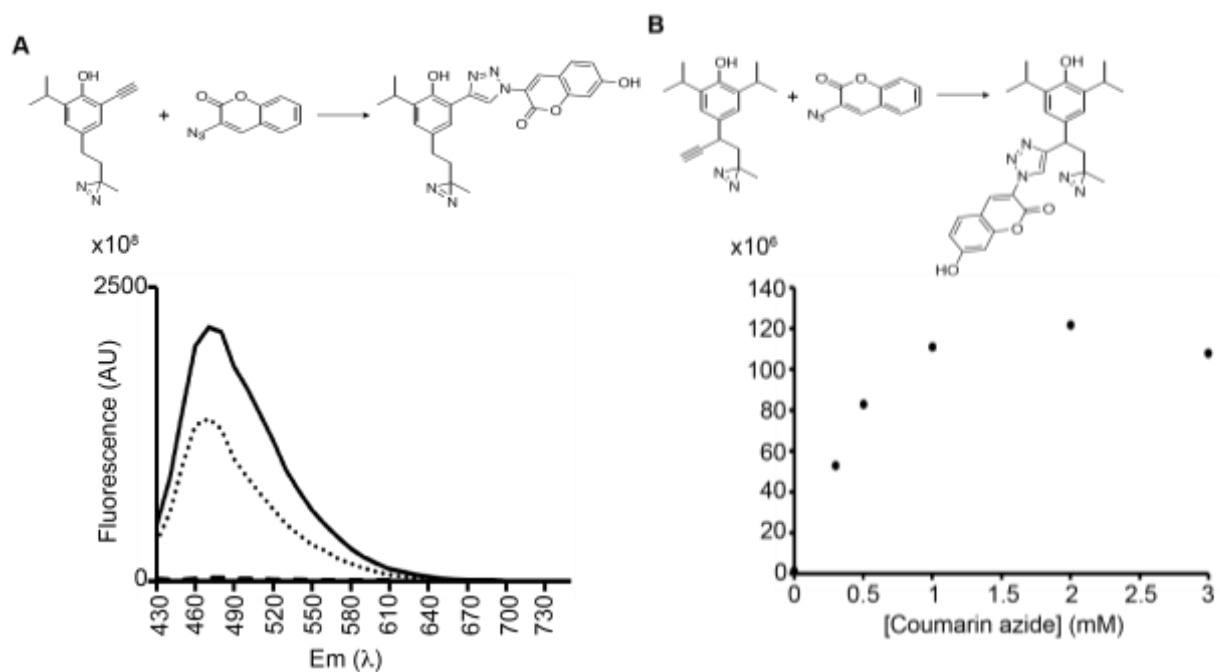
Figure 2.6 Characterization of *o* and *p*-XPRO-Click clickability (**A**) *o*-XPRO-Click

conjugates with coumarin azide, a chromophore whose fluorescence increases upon successful

click reaction. Upon excitation at 404 nm, clicked coumarin azide exhibits a fluorescence

increase. Dashed lines: *o*-XPRO-Click; dotted line: coumarin azide; solid line: *p*-XPRO-Click

incubated with coumarin azide under copper-catalyzed conditions. (**B**) *p*-XPRO-Click (0.5 mM)

reacts with coumarin azide, resulting in an increase in fluorescence upon click reaction.

Discussion

Designing direct and practical chemical syntheses that are cost-effective and is a major challenge in research and development (17). In the synthetic strategies I developed for XPRO, *o*-XPRO-Click, and *p*-XPRO-Click, I strived to adhere to these principles.

One of the principles of green chemistry is the use of selective catalytic reagents (18-20). In the synthesis of XPRO, I adapted a procedure that uses Amberlyst-15 to promote addition at the para position of alkyl phenols to α-β-unsaturated ketones as precursors to chemicals used in the flavoring and fragrance industry (10). Amberlyst-15 is a useful heterogeneous acid catalyst because it is safe to use and easy to handle, facilitating recovery and separation after reaction completion. The ability to catalyze regioselective additions to phenols will also be useful in synthesizing crosslinkable analogues of propofol and other alkyl phenols that do not have both ortho positions blocked off. This is the case for several nonelectrophilic TRPA1 agonists, such as thymol, menthol, and other terpenes (Table 1.1).

In addition to functionalizing the molecules with diazirines, I installed alkyne groups in two of the three compounds, for click chemistry reactions with azide-containing partners. Analogues containing an alkyne group can be used to identify new biological targets or in detection/isolation of photolabeled protein of interest, using azide-containing reporters. In step iv of *p*-XPRO-Click synthesis (Figure 2.1C), I used a regioselective, ruthenium-catalyzed C-C bond formation that occurs under very mild conditions to provide the *p*-XPRO-Click precursor. Although diazirines and alkynes present diverse applications with the propofol core, it is imperative to test activation of TRPA1 by these photoreactive derivatives. For example, the switching an isopropyl group for an alkyne in the ortho position may result in reduced activation

of TRPA1. Thus, in the next chapter I present my work to test this hypothesis and whether the

molecules I synthesized retain TRPA1 activation. In addition, I conducted a structure-activity

analysis with propofol analogues that have modified chemical groups substituted for the propofol

head group and the ortho and para positions. These results provide insight into the structural

determinant for activation of TRPA1 by propofol and its analogues, and into the advantages and

disadvantages, in terms of TRPA1 structure-function studies, of the three photoreactive propofol

compounds I described in the chapter 2.

References

1. **Matta, J.A., Cornett, P.M., Miyares, R.L., Abe, K., Sahibzada, N. and Ahern, G.P.,** 2008. General anesthetics activate a nociceptive ion channel to enhance pain and inflammation. *Proceedings of the National Academy of Sciences*, *105*(25), pp.8784-8789.

2. **Fischer, M.J., Leffler, A., Niedermirtl, F., Kistner, K., Eberhardt, M., Reeh, P.W. and Nau, C.,** 2010. The general anesthetic propofol excites nociceptors by activating TRPV1 and TRPA1 rather than GABAA receptors. *Journal of Biological Chemistry*, *285*(45), pp.34781-34792.

3. **Stewart, D.S., Savechenkov, P.Y., Dostalova, Z., Chiara, D.C., Ge, R., Raines, D.E., Cohne, J.B., Forman, S.A., Bruzik, K.S. and Miller, K.W.,** 2011. p-(4-Azipentyl)-propofol: A Potent Photoreactive General Anesthetic Derivative of Propofol. *Journal of medicinal chemistry*, *54*(23), p.8124.

4. **Yip, G.M., Chen, Z.W., Edge, C.J., Smith, E.H., Dickinson, R., Hohenester, E., Townsend, R.R., Fuchs, K., Sieghart, W., Evers, A.S. and Franks, N.P.,** 2013. A propofol binding site on mammalian GABAA receptors identified by photolabeling. *Nature Chemical Biology*, *9*(11), pp.715-720.

5. **Hall, M.A., Xi, J., Lor, C., Dai, S., Pearce, R., Dailey, W.P. and Eckenhoff, R.G.,** 2010. m-Azipropofol (AziPm) a photoactive analogue of the intravenous general anesthetic propofol. *Journal of medicinal chemistry*, *53*(15), p.5667.

6. **Woll, K.A., Murlidaran, S., Pinch, B.J., Hénin, J., Wang, X., Salari, R., Covarrubias, M., Dailey, W.P., Brannigan, G., Garcia, B.A. and Eckenhoff, R.G.,** 2016. A Novel Bifunctional Alkylphenol Anesthetic Allows Characterization of γ-Aminobutyric Acid, Type A (GABAA), Receptor Subunit Binding Selectivity in Synaptosomes. *Journal of Biological Chemistry*, *291*(39), pp.20473-20486.

7. **Sadakane, Y. and Hatanaka, Y.,** 2006. Photochemical fishing approaches for identifying target proteins and elucidating the structure of a ligand-binding region using carbene-generating photoreactive probes. *Analytical sciences*, *22*(2), pp.209-218.

8. **Terstappen, G.C., Schlüpen, C., Raggiaschi, R. and Gaviraghi, G.,** 2007. Target deconvolution strategies in drug discovery. *Nature Reviews Drug Discovery*, *6*(11), pp.891-903.

9. **Totobenazara, Jane, and Anthony J. Burke.** "New click-chemistry methods for 1, 2, 3-triazoles synthesis: recent advances and applications." *Tetrahedron Letters* 56.22 (2015): 2853-2859.

10. **Bunce, R.A. and Reeves, H.D.,** 1989. Amberlyst-15 catalyzed addition of phenols to α, β-unsaturated ketones. *Synthetic Communications*, *19*(5-6), pp.1109-1117.

11. **López, A., Parra, A., Jarava-Barrera, C. and Tortosa, M.,** 2015. Copper-catalyzed silylation of p-quinone methides: new entry to dibenzylic silanes. *Chemical Communications*, *51*(100), pp.17684-17687.

12. **Nishibayashi, Y., Wakiji, I., Ishii, Y., Uemura, S. and Hidai, M.,** 2001. Ruthenium-Catalyzed Propargylic Alkylation of Propargylic Alcohols with Ketones: Straightforward Synthesis of γ-Keto Acetylenes. *Journal of the American Chemical Society*, *123*(14), pp.3393-3394.

13. **Schilz, M. and Plenio, H.,** 2012. A guide to Sonogashira cross-coupling reactions: the influence of substituents in aryl bromides, acetylenes, and phosphines. *The Journal of organic chemistry*, *77*(6), pp.2798-2807.

14. **Chinchilla, R. and Nájera, C.,** 2011. Recent advances in Sonogashira reactions. *Chemical Society Reviews*, *40*(10), pp.5084-5121.

15. **MacKinnon, A.L. and Taunton, J.,** 2009. Target Identification by Diazirine Photo-Cross-Linking and Click Chemistry. *Current protocols in chemical biology*, pp.55-73.

16. **Hong, V., Presolski, S.I., Ma, C. and Finn, M.G.,** 2009. Analysis and Optimization of Copper-Catalyzed Azide–Alkyne Cycloaddition for Bioconjugation. *Angewandte Chemie International Edition*, *48*(52), pp.9879-9883.

17. **Lombardo, M. and Trombini, C.,** 2009. Catalysis in aqueous media for the synthesis of drug-like molecules. *Current opinion in drug discovery & development*, *13*(6), pp.717-732.

18. **Anastas, P.T. and Warner, J.C.,** 1998. Principles of green chemistry. *Green chemistry: Theory and practice*, pp.29-56.

19. **Tucker, J.L. and Faul, M.M.,** 2016. Industrial research: Drug companies must adopt green chemistry. *Nature*, *534*(7605), pp.27-29.

20. **Zhang, W. and Cue, B.,** 2012. *Green techniques for organic synthesis and medicinal chemistry*. John Wiley & Sons.

Chapter 3

Biological evaluation of propofol analogues as TRPA1 modulators

Abstract

It is difficult to predict *a priori* whether photo-affinity probes retain biological activity that is similar to that of the parent compound. Thus, it is important to validate the biological activity of the photo-affinity compounds synthesized in this study. I used a calcium flux assay, which is widely applied in functional assays of ion channels. I conducted small molecule structure-function studies by varying the propofol head group and the ortho and para positions on the ring. I demonstrate that polar substituents in the position ortho to the phenolic hydroxyl group and halogenated propofol analogues can affect TRPA1 activation. I also demonstrate that AziP*m*, a published crosslinkable analogue, activates TRPA1 in a bimodal fashion, inhibiting the channel at higher concentrations. These data identify structural and chemical features important for propofol activation of TRPA1, and provide the first evidence of TRPA1 activation by crosslinkable propofol analogues.

Introduction

Photoaffinity analogues of propofol have been used to probe its protein targets (1-4). However, no crosslinking studies have been applied to TRPA1. Thus, it remains unclear whether these molecules activate TRPA1. In the best-case scenario, the analogue contains the parent molecule core backbone to mimic physiological interactions and retains a potency similar to that of the parent molecule at the target receptor. These considerations are rarely achieved in practice as synthetic drugs, generally, can tolerate few structural modifications without affecting channel activity (4,5). Thus, it is advantageous to expand the limited library of crosslinkable analogues of propofol and test multiple molecules in functional assays to determine the most promising candidates for crosslinking to TRPA1.

TRPA1 activation is measured in several ways. TRPA1, which is part of the same channel superfamily as the voltage and ligand-gated potassium channels, exhibits voltage-dependent properties (6-8). Thus, voltage clamp electrophysiological methods, in which the voltage across the membrane is maintained at a desired value to permit the measurement of ionic current across the cell membrane at a given voltage, are ways to measure TRPA1 activation (9,10). Although patch-clamp electrophysiology is considered the gold standard to directly record ion channel activity at the single cell or single channel level, it is usually a low-throughput, labor-intensive technique (11). Although fluorescence-based assays do not directly measure ionic current, they can be used to measure intracellular ionic concentrations. Since TRPA1 is a calcium-permeable channel, calcium-binding dyes are widely used to measure the increase in intracellular calcium resulting from TRPA1 activation (12-14). In addition, these dyes are often used with fluorescence plate readers, facilitating high-throughput screening.

TRPA1 is activated by a diverse range of noncovalent agonists that are structurally similar such as propofol, menthol, thymol and other alkyl phenols (15-17). A bimodal sensitivity of mouse and rat TRPA1, with activation at lower concentrations (low micromolar range) and channel block at higher concentrations, has been reported for menthol, propofol, and thymol (15-18). It has been suggested that menthol-induced block of TRPA1 is related to menthol's analgesic property (19,20). Species-specific differences exist for menthol and propofol-induced activation of TRPA1. Studies show that menthol activates, but does not inhibit, human TRPA1 (15,16). In addition, resurging currents were observed for rat TRPA1 after termination of propofol in concentrations above 10 μM but not for human TRPA1, even with 300 μM propofol (17). Mouse-human chimeras and chimeras between menthol/propofol-insensitive species and mammalian TRPA1 point to residues in the fifth transmembrane segment that are important for

TRPA1 activation (16,21). Structure-activity relationship studies of alkyl phenols have also revealed the effect of bulkiness and hydrophobicity in the ortho position, adjacent to the phenolic hydroxyl group of propofol and thymol, on TRPA1 activation (22). Using commercially available alkyl phenols, researchers found a positive correlation between calculated LogP (cLogP) value and TRPA1 activation (22). However, few studies have demonstrated the effect of substituting the propofol head group and the adjacent ortho position with polar chemical groups.

I performed functional assays, using calcium influx and binding to a fluorescent indicator as a measure of TRPA1 activation, with XPRO, *o*-XPRO-Click, and *p*-XPRO-Click to determine their promise in future crosslinking experiments. The results, described below, enable me to prioritize probes that mimic the potency of TRPA1 activation by propofol. In addition, I conducted small molecule structure-function studies to provide insights into the structural determinants for propofol activation. I modified the propofol head group or the ortho and para positions to assay their effect on TRPA1 activation. These results provide the first evidence of TRPA1 activation by crosslinkable propofol analogues, reveal that the polar head group is critical for propofol activation of TRPA1, that substitution of an isopropyl group for an alkyne reduces TRPA1 activation, and that derivatization of propofol with bromine in the para position reduces its activation of TRPA1.

Materials and Methods

Cloning and Expression

Silent mutations a660c and t2163c were introduced into the mouse TRPM8 cDNA (provided by Ardem Patapoutian) to remove two NdeI sites. Full-length TRPA1 was amplified by PCR and ligated between the NdeI and NotI sites of a modified pFastBac1 vector encoding a

C-terminal FLAG-tag, pFastBac-CFlag. Rat TRPV1 baculovirus (23) stock was obtained from Sze-Yi Lau. Cloning and generation of the Bacmid DNA were performed by David Sola Del Valle and Christopher Phelps. Mutants were generated by Quikchange mutagenesis protocol (Stratagene) and all clones were verified by DNA sequencing.

Human TRPA1 (hTRPA1) in pcDNA3-cFLAG (provided by Monique Brewster) was cloned into pFastBac1-CFLAG vector. The vector was digested with NdeI and NotI and treated with calf intestinal alkaline phosphatase. PCR of hTRPA1-FLAG consisted of the annealing region of the forward primer binding to the NdeI restriction site flanking hTRPA1-cFLAG open reading frame (ORF) as well as the 21 base pairs 3' of this site. The overhang includes 24 base pairs that are homologous to the sequence 5' of the NdeI site in pFB-CFLAG. The reverse primer binds to the last 29 base pairs of the hTRPA1-cFLAG ORF. This includes all of the FLAG tag and 4 base pairs of the NotI restriction site found immediately 5' of the FLAG tag. This sequence is homologous to pFB-CFLAG immediately 3' of the NotI site.

Forward primer (sequence format is overhang in **bold** and annealing in unbolded text): **CGTCCCACCATCGGGCGCGGATCT**CATATGAAGCGCAGCCTGAGGAAGATG (annealing temperature: 74°C). Reverse primer: CTTATCGTCGTCATCCTTGTAATCAGCGG (annealing temperature: 73°C). Agarose gel electrophoresis of restriction digests and PCR reactions were then followed by gel extraction of bands of the expected sizes. Gibson assembly (24) was used to ligate DNA fragments. Plasmid was transformed into *E. coli* DH5α and correct clones were identified by sequencing of isolated plasmid.

Bacmid DNA was produced by transformation of the resulting vector into DH10Bac cells and then transfected into Sf21 cells using standard protocols to produce baculovirus. Sf21 cells

were grown and maintained at 27°C in Hink's TNM-FH medium (Mediatech, Manassas, VA) supplemented with 10% fetal bovine serum and 10 µg/mL gentamicin.

HEK293 cell culture

HEK293 cells were cultured in Dulbecco's modified Eagle's medium (DMEM) supplemented with 10% fetal bovine serum, 100 units/mL penicillin, 100 µg/mL streptomycin and 10 µg/mL gentamicin. Cells were grown in an incubator at 37°C with humidified 5% CO_2 and 95% air.

HEK293 cell transfection

4.5 µg of hTRPA1-cFLAG pcDNA was added to a 1.5 mL Eppendorf tube and 0.67 mL of 250 mM calcium chloride ($CaCl_2$) was added dropwise. The media was aspirated and cells were washed with 2 mL of phosphate-buffered saline. 1 mL of trypsin was added and cells were resuspended in 9 mL of DMEM. Cells were spun down for 2 minutes at 700 RPM. Media was aspirated and cells were resuspended in 10 mL of fresh DMEM media. $CaCl_2$/DNA was added dropwise to HEPES-buffered sodium phosphate and this mixture was added to cells (1.1×10^6 cells/mL). Cells were seeded in poly-lysine coated plates and placed in a 37°C incubator. The media was gently aspirated and replaced with 0.2 mL/well on the following day. Cells were then moved to a 30°C incubator prior to calcium influx assays.

Sf21 cell calcium-influx assay

Sf21 cells (0.4×10^5 cells in 100 µL) were seeded into each well of a 96-well plate, infected with baculovirus and incubated 44-48 h at 27°C. I replaced the medium with 50 µL bath

solution containing (in mM): 150 sodium gluconate, 10 HEPES, 2 CaCl$_2$, 10 NaCl, and 10 D-glucose, 0.02% Pluronic F-127, pH 7.2) containing 5 µM Fura-2-AM. After 45 min, unabsorbed dye was washed away with 180 µL bath solution, replacing with 50 µL of fresh bath solution after 1 h. Experiments were conducted on a Flexstation III (Molecular Devices, Sunnyvale, CA) with excitation at 340/380 nm and emission measured at 510 nm. Test agonists were added at 60 s and 1 mM AITC was added at 180 s as a positive control for TRPA1 expression. 75 nM capsaicin or 1% Triton X-100 was used as a positive control for TRPV1 or Fura-2 loaded cells. Expression while Compound stocks of tested agonists were made in DMSO and diluted 1:1000 in bath solution immediately before assay measurement. The net change in Fura-2 340/380 fluorescence ratio (ΔRatio) was calculated as the Fura-2 340/380 fluorescence ratio minus the 340/380 ratio of the baseline prior to ligand addition (0-60 s). Data were then averaged after baseline subtraction was performed for each individual trace.

Results

Functional assay setup and validation

As a first step in obtaining functional data, I explored different TRPA1 homologs and different expression systems. I transfected insect cells with either human or mouse TRPA1, however, only mouse TRPA1 was functional in my hands. Thus, I expressed mouse TRPA1 in all subsequent functional assays. In addition, I expressed functional human TRPA1 by transient transfection in human embryonic kidney cells (HEK) 293 cells. However, I settled on the baculovirus expression system in insect cells for several reasons, described below.

Our lab has previously shown that insect cells are suitable for functional TRP channel expression (25, 26). Insect cells offer abundant protein expression with posttranslational

modifications analogous to those of mammalian cells and they are amenable to both adherent and suspension cultures (27,28). Also, insect cells are easier and cheaper to handle than adherent cells such as HEK 293 cells, which is important for scale-up (29). Thus, baculovirus expression systems are powerful systems to yield high protein levels in insect cells. The benefits of this system include ease of baculovirus infection and high rates of infectivity, which allows for more consistent and robust protein expression across experiments. In addition, baculoviruses are not pathogenic to humans (30). This expression system is also easily adaptable to 96-well plates, facilitating high-throughput screening. The baculovirus expression system in insect cells is the principal heterologous expression system for eukaryotic integral membrane production and has so far yielded the largest number of eukaryotic integral membrane proteins, which are notoriously difficult to express in large quantities (31,32). In addition, TRPV1 in Sf21 insect cells was validated previously in the Gaudet lab (23). I also show that TRPA1 expression for both the human and mouse homologs is robust in baculovirus-infected insect cells (**Figure 3.1**).

To enable high-throughput measurements of TRPA1 activation, I adapted a well-known fluorescence-based calcium assay. I chose to use Fura-2AM, a ratiometric fluorescent Ca^{2+}-binding indicator (33). After Fura-2AM is applied to cells, it readily crosses the plasma membrane. Endogenous intracellular esterases remove the acetoxymethyl (AM) groups, generating the negatively-charged Fura-2 indicator that is now trapped inside the cell. Upon ligand binding and activation, TRPA1 allows calcium to flow down its concentration gradient into the cell, binding Fura-2 and resulting in an absorption shift: the Ca^{2+}-bound and unbound forms of Fura-2 are excited at 340 nm and 380 nm, respectively. The emitted light is measured at 510 nm. The Fura-2 340/380 nm excitation ratio permits measurement of the intracellular Ca^{2+}
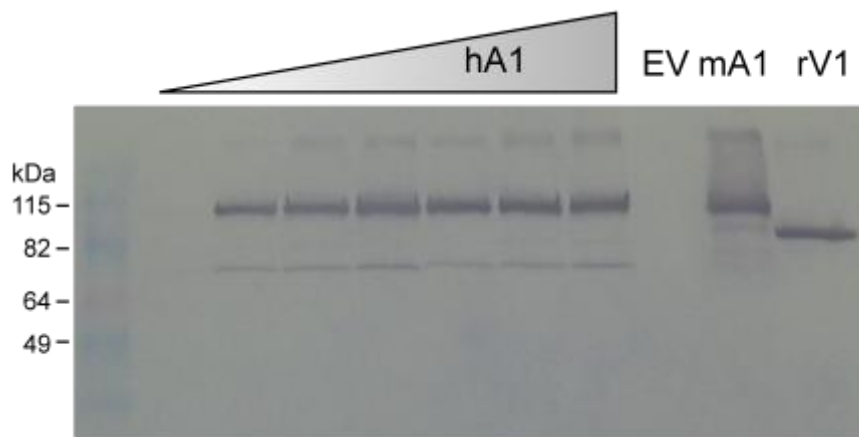
Figure 3.1 Robust TRPA1 expression in baculovirus-infected insect cells α–FLAG western blot of baculovirus-infected insect cells expressing human TRPA1 (hTRPA1), mouse TRPA1 (mTRPA1), and rat TRPV1 (rTRPV1). 0.6×10^6 insect cells (0.5 mL) were infected in a 24 well plate with 1,5, 10, 20, 50, and 100 µL of hTRPA1-encoding baculovirus or 15 µL of mock baculovirus, mTRPA1-encoding baculovirus or rat TRPV1-encoding baculovirus. The molecular weights of TRPA1 and TRPV1 are ~ 120 kDa and ~95 kDa, respectively. TRPA1 and TRPV1 bands were not observed in empty vector-infected insect cells.

concentration, it increases with increasing intracellular Ca^{2+}. Thus, Fura-2 is a ratiometric dye, minimizing confounding variables across samples such as differences in cell thickness or uneven dye loading, as both parts of the ratio would be affected. In this assay, I use activation as a proxy for ligand binding; that is, if a compound specifically activates TRPA1, I infer that it binds the channels. The caveat is that binding of compounds that do not activate TRPA1 will go undetected.

To validate that the assay is working, I conduct a time course of the 340/380 fluorescence ratio. In the assay, there are three distinct stages: 0-60 s, 60 s, and 180 s correspond to basal conditions, addition of test agonist, and addition of TRPA1/TRPV1 agonist as a positive control for protein expression, respectively. For example, addition of 40 μM propofol at 60 s elicits a greater rise in $[Ca^{2+}]_i$ than o-XPRO-Click in mouse TRPA1-expressing insect cells, resulting in an increase in the 340/380 ratio of the Fura-2 dye. Expression of TRPA1 in all samples was confirmed by activation with 1 mM AITC, an electrophilic TRPA1 agonist, added at 180 s (**Figure 3.2A**). However, neither propofol nor XPRO-Click activates rat TRPV1, as addition of propofol or XPRO-Click at 60 s did not elicit a rise in $[Ca^{2+}]_i$ in rTRPV1-expressing insect cells. Capsaicin, a TRPV1-specific agonist added at 180 s, did elicit a rise in $[Ca^{2+}]_i$, thus confirming TRPV1 expression in all samples. (**Figure 3.2B**). Propofol activates TRPA1 to a greater degree than XPRO-Click across all tested concentrations; the overall dose-response behavior of propofol is consistent with published data (**Figure 3.2C**) (17,18).

Propofol, XPRO, and p-XPRO-Click elicit higher TRPA1 activation than o-XPRO-Click

I next tested the ability of the two other crosslinkable molecules that I synthesized, XPRO and p-XPRO-Click, to activate TRPA1. These molecules have similar chemical
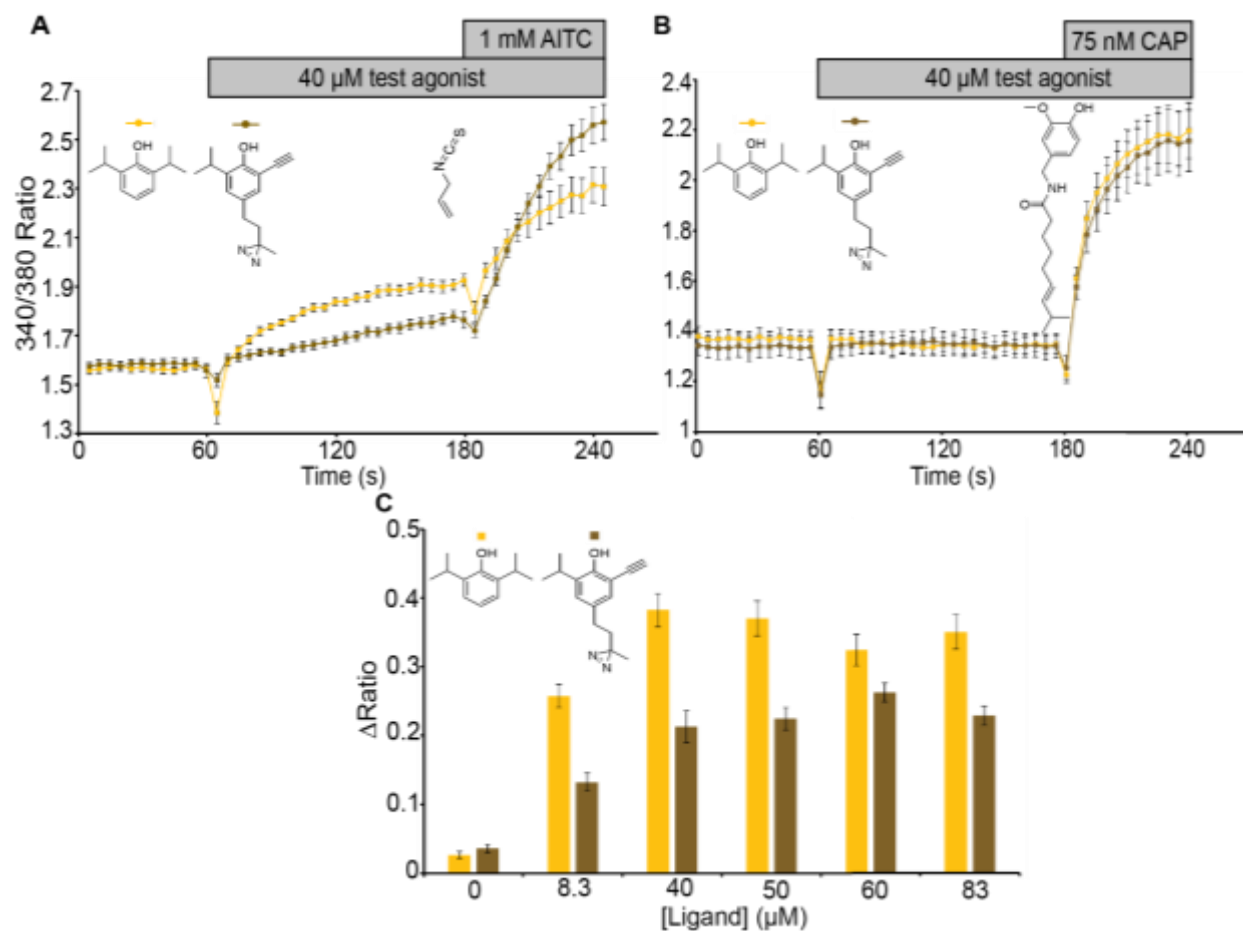
Figure 3.2 Propofol is a stronger TRPA1 agonist than *o*-XPRO-Click Propofol corresponds to the yellow traces and *o*-XPRO-Click corresponds to brown traces. (**A**) Time course of the 340/380 fluorescence ratio. Fluorescence levels increase upon addition of propofol and *o*-XPRO-Click. AITC is added at 180 s to confirm mouse TRPA1 (mTRPA1) expression. Data represent mean +/- SEM for n=11-14. (**B**) Propofol or *o*-XPRO-Click did not activate rat TRPV1 (rTRPV1) while capsaicin, a TRPV1-selective agonist activates TRPV1. Data represent mean +/- SEM for n=6-7. (**C**) Histogram depicts the maximal response to tested ligand concentrations. Data represent mean +/- SEM for n=10-14. The net change in Fura-2 340/380 fluorescence ratio (ΔRatio) was calculated as the Fura-2 340/380 fluorescence ratio minus the 340/380 ratio of the baseline prior to ligand addition (0-60 s).

structures and physicochemical properties; both molecules contain the parent propofol core.

Addition of 60 μM XPRO at 60 s elicited a greater rise in $[Ca^{2+}]_i$ than propofol in TRPA1-expressing insect cells. Expression of TRPA1 in all samples was confirmed by activation with AITC added at 180 s. (**Figure 3.3A**). Neither propofol nor XPRO activated TRPV1 while capsaicin, which serves as s positive control for TRPV1 expression, was a potent TRPV1 agonist (**Figure 3.3B**). XPRO activated TRPA1 at least as well as propofol across all tested concentrations, with 100 μM XPRO eliciting the highest 340/380 response (**Figure 3.3C**).

p-XPRO-Click also activated TRPA1 at least as well as propofol (**Figure 3.4**). Addition of 60 μM *p*-XPRO-Click at 60 s elicited a greater rise in $[Ca^{2+}]_i$ than propofol in TRPA1-expressing insect cells. Expression of TRPA1 in all samples was confirmed by activation with AITC added at 180 s (**Figure 3.4A**). *p*-XPRO-Click did not activate TRPV1 while capsaicin did activate TRPV1 (**Figure 3.4B**). *p*-XPRO-Click activated TRPA1 at least as well as propofol across most of the tested concentrations (**Figure 3.4C**).

Taken together, Ca^{2+}-influx assays demonstrate that XPRO and *p*-XPRO-Click retain TRPA1 activation that is similar to that of propofol while *o*-XPRO-Click is less effective than propofol in activating TRPA1.

AziPm and propofol produce similar calcium-influx responses in TRPA1

I next tested the ability of a published crosslinkable analogue of propofol to activate TRPA1. AziP*m* (gift from Roderic Eckenhoff at the University of Pennsylvania) has been used to photolabel ion channels such as GABA_A (34,35). I tested whether AziP*m* activates TRPA1 with the goal of expanding the library of crosslinkable propofol analogues that activate TRPA1. Upon addition at 60 s, AziP*m* and propofol produced similar response profiles in TRPA1
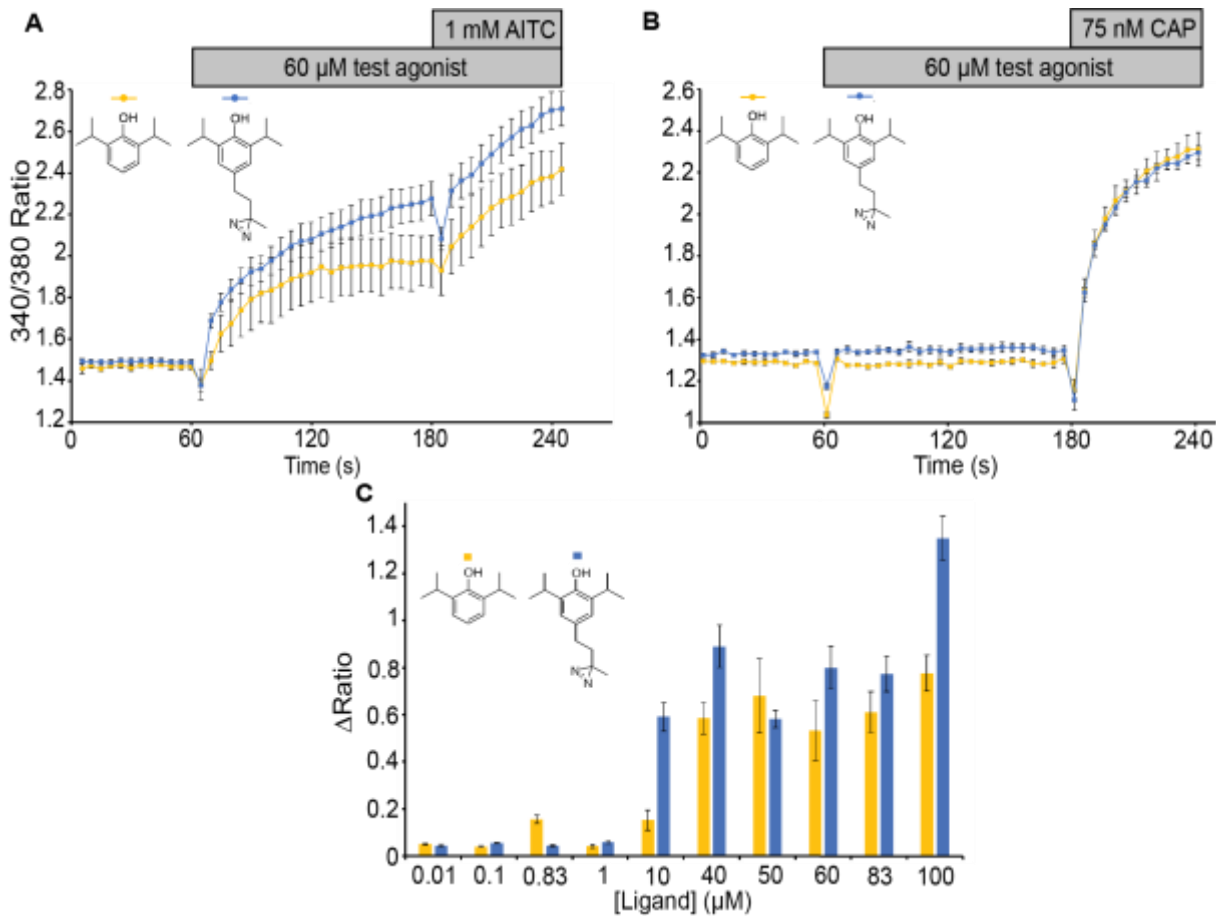
Figure 3.3 XPRO and propofol share similar TRPA1 potency Propofol corresponds to the yellow traces and XPRO corresponds to the blue traces. **(A)** Time course of the 340/380 fluorescence ratio. Fluorescence levels increase upon addition of propofol and XPRO-Click. AITC is added at 180s to confirm TRPA1 expression. Data represent mean +/- SEM for n=4-12. **(B)** Neither XPRO nor propofol activates rat TRPV1. Addition of propofol and XPRO at 60 s did not elicit a rise in $[Ca^{2+}]_i$ in rTRPV1-expressing insect cells. Capsaicin, a TRPV1-specific agonist added at 180 s did not elicit a rise in $[Ca^{2+}]_i$, thus confirming TRPV1 expression in all samples. Data represent mean +/- SEM for n=3-5. **(C)** Histogram depicts the maximal response to tested ligand concretions. XPRO activates TRPA1 to a greater degree than propofol. Data represent mean +/- SEM for n=4-12.
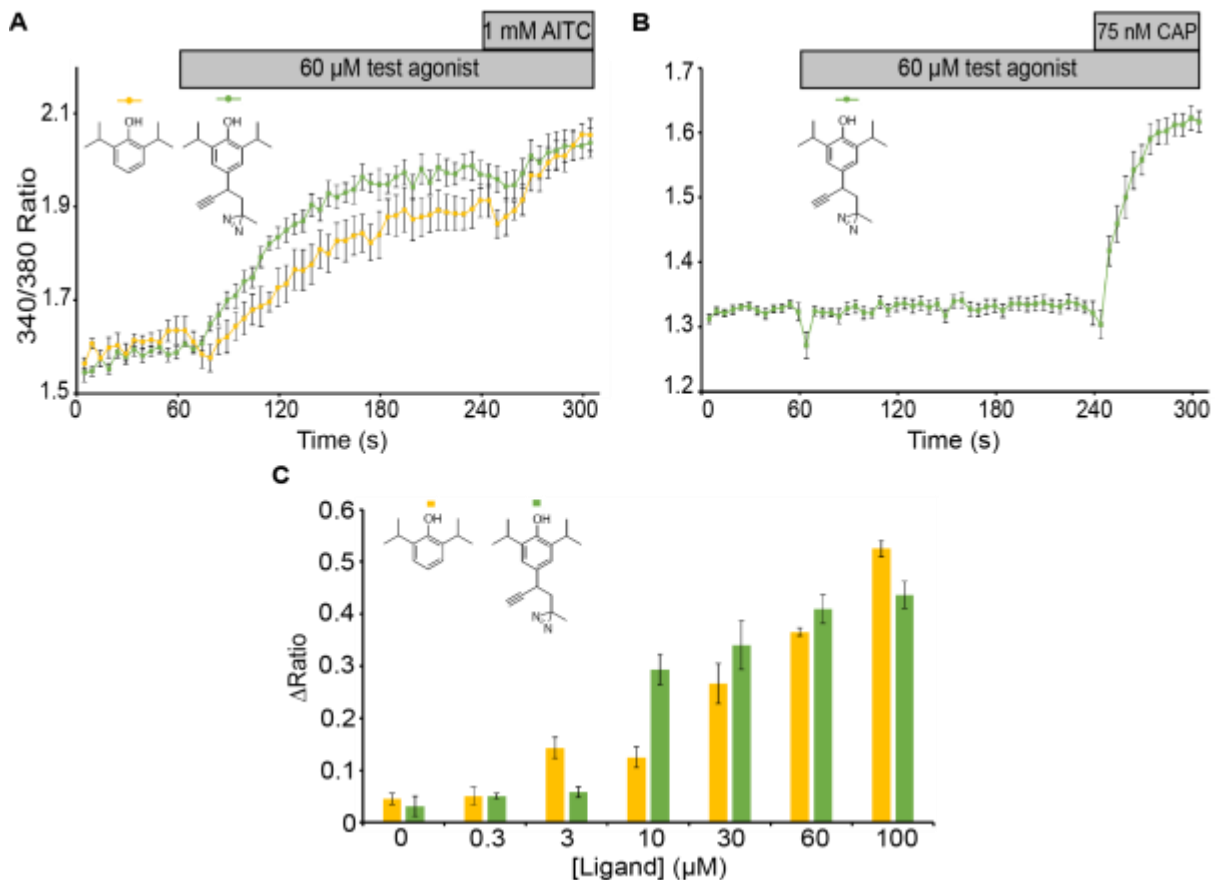
Figure 3.4 *p*-XPRO-Click and propofol share similar TRPA1 potency Propofol corresponds to the yellow traces and *p*-XPRO-Click corresponds to the green traces. **(A)** Addition of 60 μM *p*-XPRO-Click at 60 s elicited a greater rise in $[Ca^{2+}]_i$ than propofol in TRPA1-expressing insect cells. Expression of TRPA1 in all samples was confirmed by activation with AITC added at 180 s. Data represent mean +/- SEM for n=6. **(B)** Neither *p*-XPRO-Click nor propofol activated rat TRPV1. Addition of *p*-XPRO-Click and propofol at 60 s did not elicit a rise in $[Ca^{2+}]_i$ in rTRPV1-expressing insect cells. Capsaicin, added at 180 s, did elicit a rise in $[Ca^{2+}]_i$, thus confirming TRPV1 expression in all samples. Data represent mean +/- SEM for n=12 **(C)** *p*-XPRO-Click activates TRPA1 to a greater degree than propofol. Data represent mean +/- SEM for n=9.

(**Figure 3.5A**). AziP*m* and propofol also exhibited bimodal action on TRPA1 (**Figure 3.5B**).

AziP*m* and propofol-induced calcium flux was specific for TRPA1 as evidenced by the lack of

response observed for empty-vector (**Figure 3.5C**) and TRPV1-infected cells (**Figure 3.5D**).

These data demonstrate the potential of AziP*m* as a probe that mimics propofol activation of

TRPA1.

From the reduced TRPA1 activation observed with *o*-XPRO-Click, I surmised that

modification of the ortho position, adjacent to the phenolic hydroxyl group, influences TRPA1

activation. After obtaining TRPA1 functional data with four photoreactive analogues of

propofol, I then conducted small molecule structure-function studies by varying the chemical

groups on the aromatic ring, including substitutions of the phenolic hydroxyl group and the ortho

and para positions on the propofol core. This minimal structure-activity relationship study is

addressed below.

The phenolic head group is critical for TRPA1 activation

Studies suggest that the propofol hydroxyl group is important for ligand activation, as

fospropofol, a water-soluble analogue that has a charged phosphate group substituted for the

hydroxyl, does not evoke depolarizing currents in TRPA1-positive neurons but retains the ability

to induce anesthesia (36,37). To this end, I tested the ability of 2,6-diisopropyls, in which an

amine or a fluorine replaces the phenolic head group of propofol, to activate TRPA1. 2,6-

diisopropylaniline, which contains an amine in place of the hydroxyl, produced higher calcium

influx in TRPA1-infected cells than propofol (**Figure 3.6A and C**). No activation was observed

with TRPV1-infected cells (**Figure 3.6B**). However, fropofol (a gift from the Eckenhoff lab),

which contains a fluorine in place of the hydroxyl, did not activate TRPA1 (**Figure 3.7A and B**).
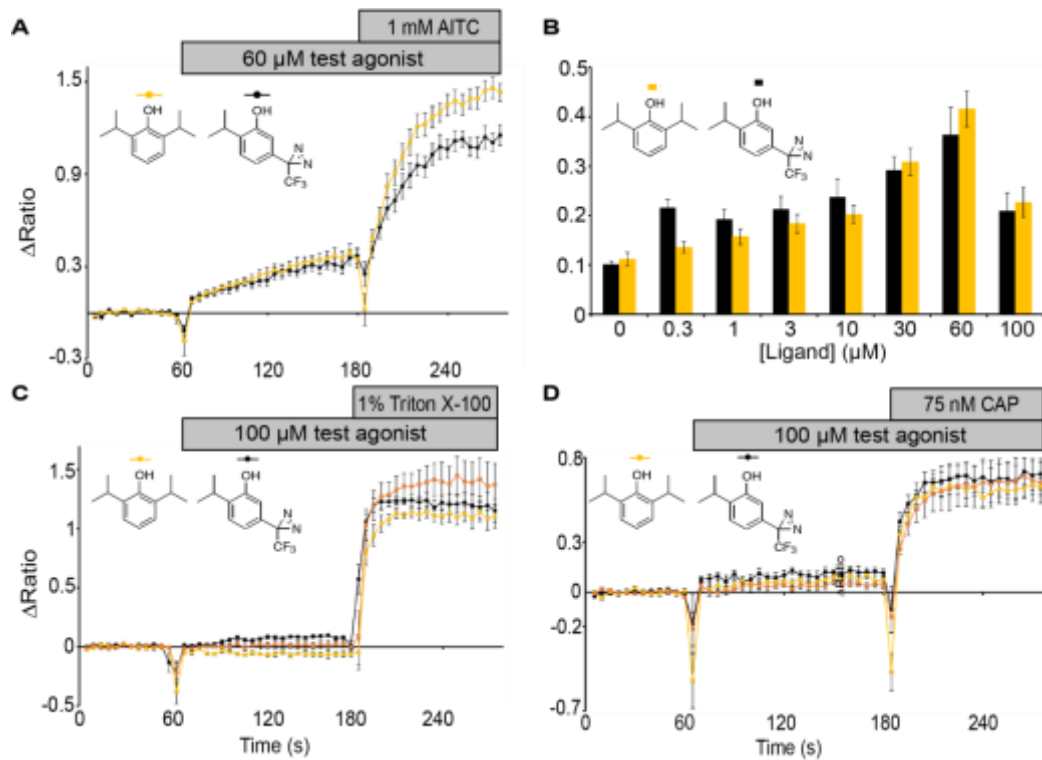
Figure 3.5 AziP*m* activates TRPA1 similarly to propofol AziP*m* corresponds to the black

traces and propofol corresponds to the yellow traces **(A)** Addition of 60 μM AziP*m* and propofol

at 60 s elicited a rise in $[Ca^{2+}]_i$ in TRPA1-expressing insect cells. Expression of TRPA1 in all

samples was confirmed by activation with AITC added at 180 s. Data represent mean +/- SEM

for n=12. **(B)** AziP*m* and propofol exhibit bimodal TRPA1 activity. Data represent mean +/-

SEM for n=12. **(C)** AziPm and propofol do not cause non-specific calcium fluxes. Addition of

AziP*m* and propofol and vehicle (orange) at 60 s did not elicit a rise in $[Ca^{2+}]_i$ in empty vector-

infected insect cells. Additional Triton X-100 detergent at 1% at 180 s did cause large increases

in the 340/380 ratio, confirming cells were effectively loaded with Fura-2. Data represent mean

+/- SEM for n=6. **(D)** Neither AziPm, propofol nor vehicle activate TRPV1. Addition of AziP*m*

and propofol and vehicle (orange) at 60 s did not elicit a rise in $[Ca^{2+}]_i$ in TRPV1-expressing

cells. Capsaicin added at 180 s did elicit a rise in $[Ca^{2+}]_I$ thus confirming TRPV1 expression in

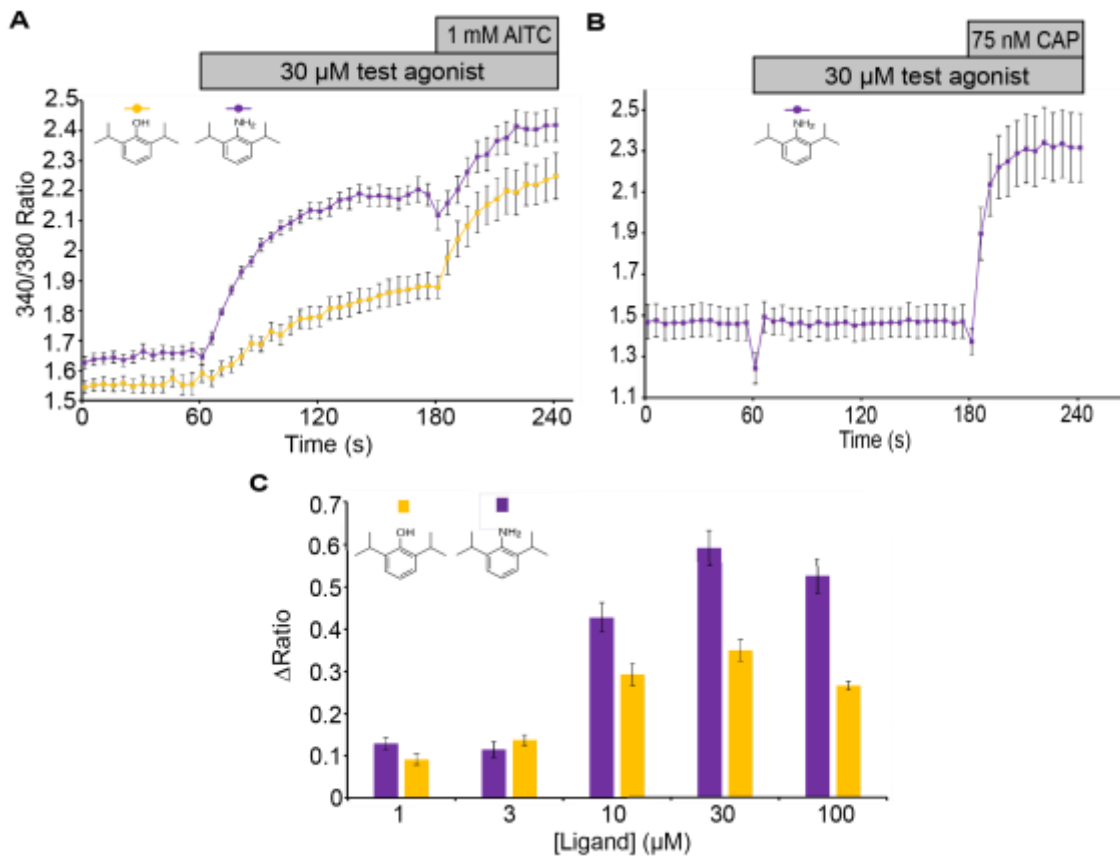all samples. Data represent mean +/- SEM for n=6.

Figure 3.6 2,6-diisopropylaniline is a stronger TRPA1 agonist than propofol 2,6-

diisopropylamine corresponds to purple traces and propofol corresponds to yellow traces. **(A)**

Addition of 30 µM 2,6-Diisopropylaniline at 60 s elicited a greater rise in $[Ca^{2+}]_i$ than propofol

in TRPA1-expressing insect cells. Expression of TRPA1 in all samples was confirmed by

activation with AITC added at 180 s. Data represent mean +/- SEM for n=13. **(B)** Neither 2,6-

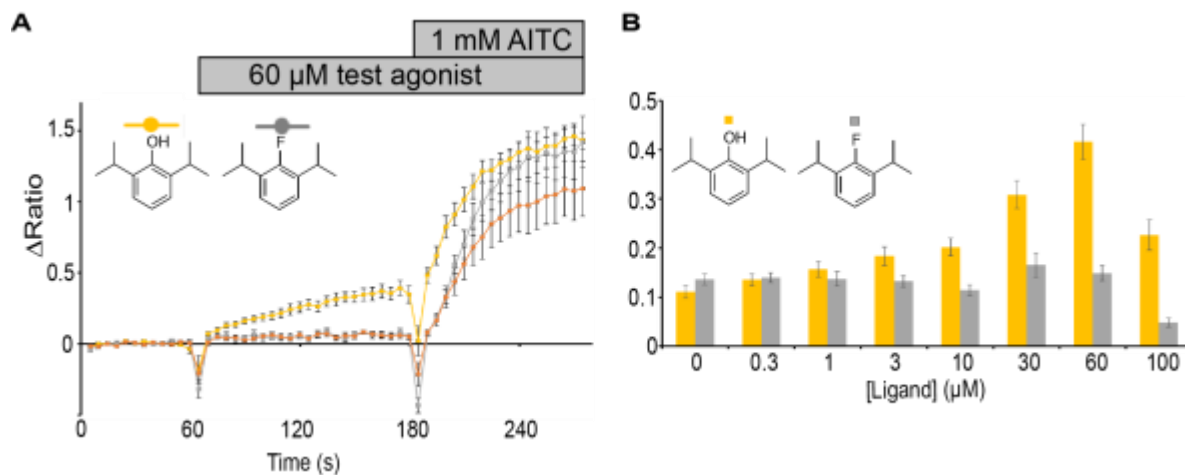Diisopropylaniline nor propofol activates TRPV1.

Figure 3.7 Fropofol does not activate TRPA1 Propofol corresponds to the yellow traces, fropofol corresponds to the grey traces, and vehicle control corresponds to the orange trace. **(A)** Addition of 60 μM fropofol (grey) or vehicle (orange) at 60 s did not elicit a rise in $[Ca^{2+}]_i$ in TRPA1-expressing insect cells. Expression of TRPA1 in all samples was confirmed by activation with AITC added at 180 s. Data represent mean +/- SEM for n=9. **(B)** Fropofol did not elicit a rise in $[Ca^{2+}]_i$ across all tested concentrations. Data represent mean +/- SEM for n=12. The propofol data are reproduced from Figure 3.6 for ease of comparison. The net change in Fura-2 340/380 fluorescence ratio (ΔRatio) was calculated as the Fura-2 340/380 fluorescence ratio minus the 340/380 ratio of the baseline prior to ligand addition (0-60 s). Data were then averaged after baseline subtraction was performed for each individual trace. This was done to permit easier visualization of the difference in response upon ligand addition at 60 s.

Taken together, these results suggest that a polar head group is critical for propofol activation of TRPA1. I next tested activation of TRPA1 by an isomer of propofol, 2,4-diisopropylphenol since it is structurally similar to propofol and other noncovalent TRPA1 agonists such as thymol and menthol.

2,4-diisopropylphenol, an isomer of propofol, exhibits bimodal TRPA1 activation

I tested the effect of varying one of propofol's isopropyl groups. Studies with alkyl phenols such as propofol and thymol have shown that the presence of hydrophobic groups in the ortho and meta positions are important for TRPA1 activation (22). However, this study did not assay TRPA1 activation with compounds that have branched hydrophobic groups in the para position. I first tested 2,4-diisopropylphenol, an isomer of propofol. As discussed previously, several molecules that are structurally similar noncovalent TRPA1 agonists activate mTRPA1 in a bimodal fashion (15-18). Thus, I tested if the bimodal activation could be recapitulated in an isomer of propofol called 2,4-diisopropylphenol. I hypothesized that bimodal activation would occur for this isomer as it does for structurally similar alkyl phenols. Indeed, upon addition at 60 s, 2,4-diisopropylphenol not only activated TRPA1 (**Figure 3.8A**) but also induced lower 340/380 responses at higher concentrations (**Figure 3.8B**). This bimodal activation has been observed for several nonelectrophilic agonists such as propofol and menthol (16-18). These results demonstrate that 2,4-diisopropylphenol activates mouse TRPA1 in a bimodal fashion, which is consistent with activation of mouse TRPA1 by alkyl phenols such as propofol and menthol.

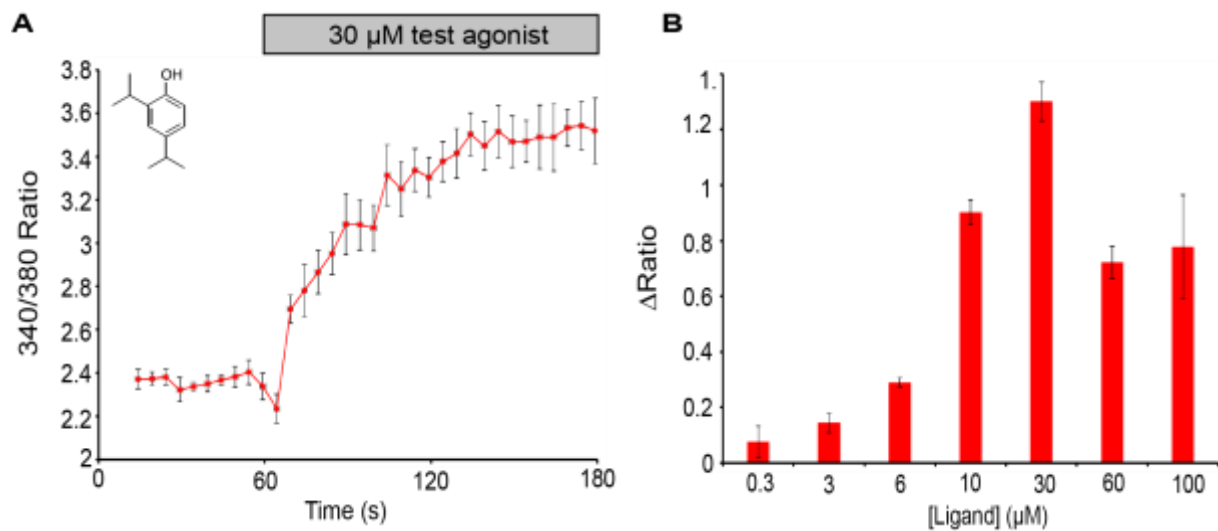*4-bromopropofol does not activate TRPA1*

Figure 3.8 2,4-diisopropylphenol activates TRPA1 in a bimodal fashion (A) Addition of 30

µM 2,4-diisopropylphenol at 60 s elicited a rise in $[Ca^{2+}]_i$ in TRPA1-expressing insect cells Data

represent mean +/- SEM for n=4. **(B)** 2,4-diisopropylphenol exhibited bimodal TRPA1 activation

consisting of activation at lower concentrations and a reduced response at higher concentrations.

Data represent mean +/- SEM for n=4.

I then tested the influence on TRPA1 activation of substituting a halogen into the para position of propofol. Halogenated propofol analogues have recently come to attention as analgesics due to their block of voltage-operated sodium channels (38). A derivative of propofol, 4-bromopropofol, is being pursued for potential treatment of lower back pain (39,40). I synthesized 4-bromopropofol starting from propofol using N-bromosuccinimide. Addition of 10 μM propofol elicited a higher 340/380 response than 4-bromopropofol (**Figure 3.9A**). Up until the predicted aqueous solubility limit of 4-bromopropofol, propofol elicited higher calcium influx than 4-bromopropofol (**Figure 3.9B**). These data suggest that derivatization of propofol with bromine reduces TRPA1 activation.

Discussion

In Chapter 3, the small molecule structure-function study shed light on differences in TRPA1 activation among photoreactive propofol derivatives, thus highlighting promising probes to move forward in crosslinking studies. Through TRPA1 functional assays, I demonstrate that three crosslinkable analogues of propofol effectively activate mouse TRPA1. Second, a bimodal activation profile of TRPA1 by alkyl phenols was observed.

A first observation from my structure-function studies is that XPRO and p-XPRO-Click yield greater TRPA1 activation than propofol. It would be interesting to test TRPA1 activation as a function of chain length. By increasing the length of the *para*-linker, one may gain insight into the nature of the binding pocket, including size and orientation of propofol. The synthetic schemes I developed are amenable to not only increasing the chain length, but also installing alkyl ketones into the chain. A second observation is that XPRO and *p*-XPRO-Click share a different TRPA1 dose-response relationship than propofol, AziP*m* and 2,4-disopropylphenol.
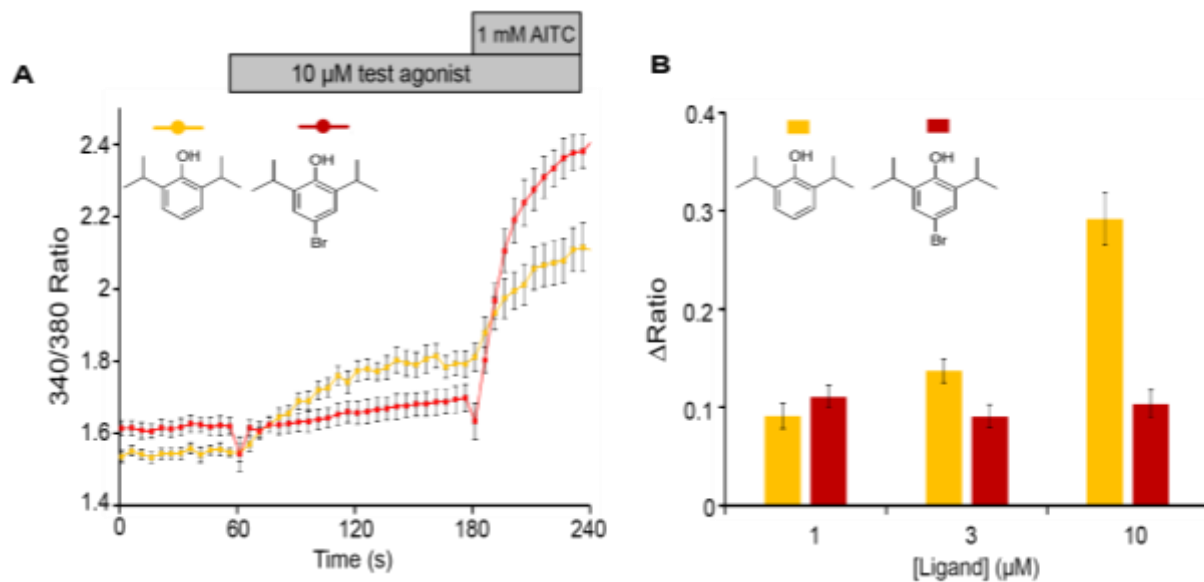
Figure 3.9 4-bromopropofol does not activate TRPA1 4-bromopropofol corresponds to the red

trace while propofol corresponds to the yellow trace. **(A)** Addition of 10 μM propofol (yellow) at

60 s elicited a greater rise in $[Ca^{2+}]_i$ in TRPA1-expressing insect cells than 4-bromopropofol.

Expression of TRPA1 in all samples was confirmed by activation with AITC added at 180 s.

Data represent mean +/- SEM for n=9-12. **(B)** Propofol was a more potent TRPA1 agonist than

4-bromopropofol up until 10 μM. Data represent mean +/- SEM for n=9-12.

While the crosslinkable analogues elicited higher intracellular calcium levels with increasing concentration of probe, propofol and its analogues, which are devoid of a nonpolar spacer, exhibited bimodal activation of mouse TRPA1. A similar bimodal activation profile has been reported for other nonelectrophilic agonists such as menthol and thymol (15-17).

The functional assays presented in Chapter 3 present the first TRPA1 evaluation of crosslinkable propofol analogues. These results highlight the promise of these probes in labeling propofol-binding sites in TRPA1. With a small library of photoactive probes that retain TRPA1 activation, I am now positioned for crosslinking studies. In Chapter 4 I discuss the use of a photoreactive derivative of propofol that modified residues in TRPA1.

References

1. **Stewart, D.S., Savechenkov, P.Y., Dostalova, Z., Chiara, D.C., Ge, R., Raines, D.E., Cohne, J.B., Forman, S.A., Bruzik, K.S. and Miller, K.W.,** 2011. p-(4-Azipentyl)-propofol: A Potent Photoreactive General Anesthetic Derivative of Propofol. *Journal of medicinal chemistry*, *54*(23), p.8124.

2. **Hall, M.A., Xi, J., Lor, C., Dai, S., Pearce, R., Dailey, W.P. and Eckenhoff, R.G.,** 2010. m-Azipropofol (AziPm) a photoactive analogue of the intravenous general anesthetic propofol. *Journal of medicinal chemistry*, *53*(15), p.5667.

3. **Woll, K.A., Murlidaran, S., Pinch, B.J., Hénin, J., Wang, X., Salari, R., Covarrubias, M., Dailey, W.P., Brannigan, G., Garcia, B.A. and Eckenhoff, R.G.,** 2016. A Novel Bifunctional Alkylphenol Anesthetic Allows Characterization of γ-Aminobutyric Acid, Type A (GABAA), Receptor Subunit Binding Selectivity in Synaptosomes. *Journal of Biological Chemistry*, *291*(39), pp.20473-20486.

4. **Yip, G.M., Chen, Z.W., Edge, C.J., Smith, E.H., Dickinson, R., Hohenester, E., Townsend, R.R., Fuchs, K., Sieghart, W., Evers, A.S. and Franks, N.P.,** 2013. A propofol binding site on mammalian GABAA receptors identified by photolabeling. *Nature Chemical Biology*, *9*(11), pp.715-720.

5. **Nassar, A.E.F., Kamel, A.M. and Clarimont, C.,** 2004. Improving the decision-making process in the structural modification of drug candidates: enhancing metabolic stability. *Drug discovery today*, *9*(23), pp.1020-1028.

6. **Caterina, M.J.,** 2013. Boosting that tan with a bit of voltage. *Channels*, *7*(6), pp.417-417.

7. **Harteneck, C., Plant, T.D. and Schultz, G.,** 2000. From worm to man: three subfamilies of TRP channels. *Trends in neurosciences*, *23*(4), pp.159-166.

8. **Gaudet, R.,** 2007. Structural insights into the function of TRP channels.

9. **Motter, A.L. and Ahern, G.P.,** 2012. TRPA1 is a polyunsaturated fatty acid sensor in mammals. *PLoS One*, *7*(6), p.e38439.

10. **Kistner, K., Siklosi, N., Babes, A., Khalil, M., Selescu, T., Zimmermann, K., Wirtz, S., Becker, C., Neurath, M.F., Reeh, P.W. and Engel, M.A.,** 2016. Systemic desensitization through TRPA1 channels by capsazepine and mustard oil-a novel strategy against inflammation and pain. *Scientific Reports*, *6*.

11. **Yu, H.B., Li, M., Wang, W.P. and Wang, X.L.,** 2016. High throughput screening technologies for ion channels. *Acta Pharmacologica Sinica*, *37*(1), pp.34-43.

12**. Karashima, Y., Prenen, J., Talavera, K., Janssens, A., Voets, T. and Nilius, B.,** 2010. Agonist-induced changes in Ca^{2+} permeation through the nociceptor cation channel TRPA1. *Biophysical journal*, *98*(5), pp.773-783.

13. **Son, H.J., Kim, Y., Misaka, T., Noh, B.S. and Rhyu, M.R.,** 2012. Activation of the chemosensory ion channels TRPA1 and TRPV1 by hydroalcohol extract of Kalopanax pictus leaves. *Biomol. Ther*, *20*, pp.550-555.

14. **Gupta, R., Saito, S., Mori, Y., Itoh, S.G., Okumura, H. and Tominaga, M.,** 2016. Structural basis of TRPA1 inhibition by HC-030031 utilizing species-specific differences. *Scientific Reports*, *6*.

15. **Karashima, Y., Damann, N., Prenen, J., Talavera, K., Segal, A., Voets, T. and Nilius, B.,** 2007. Bimodal action of menthol on the transient receptor potential channel TRPA1. *Journal of Neuroscience*, *27*(37), pp.9874-9884.

16. **Xiao, B., Dubin, A.E., Bursulaya, B., Viswanath, V., Jegla, T.J. and Patapoutian, A.,** 2008. Identification of transmembrane domain 5 as a critical molecular determinant of menthol sensitivity in mammalian TRPA1 channels. *Journal of Neuroscience*, *28*(39), pp.9640-9651.

17. **Fischer, M.J., Leffler, A., Niedermirtl, F., Kistner, K., Eberhardt, M., Reeh, P.W. and Nau, C.,** 2010. The general anesthetic propofol excites nociceptors by activating TRPV1 and TRPA1 rather than GABAA receptors. *Journal of Biological Chemistry*, *285*(45), pp.34781-34792.

18. **Matta, J.A., Cornett, P.M., Miyares, R.L., Abe, K., Sahibzada, N. and Ahern, G.P.,** 2008. General anesthetics activate a nociceptive ion channel to enhance pain and inflammation. *Proceedings of the National Academy of Sciences*, *105*(25), pp.8784-8789.

19. **Galeotti, N., Mannelli, L.D.C., Mazzanti, G., Bartolini, A. and Ghelardini, C.,** 2002. Menthol: a natural analgesic compound. *Neuroscience letters*, *322*(3), pp.145-148.

20. **Macpherson, L.J., Hwang, S.W., Miyamoto, T., Dubin, A.E., Patapoutian, A. and Story, G.M.,** 2006. More than cool: promiscuous relationships of menthol and other sensory compounds. *Molecular and Cellular Neuroscience*, *32*(4), pp.335-343.

21. **Ton, H.T., Phan, T.X., Abramyan, A.M., Shi, L. and Ahern, G.P.,** 2017. Identification of a putative binding site critical for general anesthetic activation of TRPA1. *Proceedings of the National Academy of Sciences*, p.201618144.

22. **Lee, S.P., Buber, M.T., Yang, Q., Cerne, R., Cortes, R.Y., Sprous, D.G. and Bryant, R.W.,** 2008. Thymol and related alkyl phenols activate the hTRPA1 channel. *British journal of pharmacology*, *153*(8), pp.1739-1749.

23. **Lishko, P.V., Procko, E., Jin, X., Phelps, C.B. and Gaudet, R.,** 2007. The ankyrin repeats of TRPV1 bind multiple ligands and modulate channel sensitivity. *Neuron*, *54*(6), pp.905-918.

24. **Gibson, D.G., Young, L., Chuang, R.Y., Venter, J.C., Hutchison, C.A. and Smith, H.O.,** 2009. Enzymatic assembly of DNA molecules up to several hundred kilobases. *Nature methods*, *6*(5), pp.343-345.

25. **Phelps, C.B. and Gaudet, R.,** 2007. The role of the N terminus and transmembrane domain of TRPM8 in channel localization and tetramerization. *Journal of Biological Chemistry*, *282*(50), pp.36474-36480.

26. **Phelps, C.B., Wang, R.R., Choo, S.S. and Gaudet, R.,** 2010. Differential regulation of TRPV1, TRPV3, and TRPV4 sensitivity through a conserved binding site on the ankyrin repeat domain. *Journal of Biological Chemistry*, *285*(1), pp.731-740.

27. **Khan, K.H.,** 2013. Gene expression in mammalian cells and its applications. *Adv Pharm Bull*, *3*(2), pp.257-63.

28. **Altmann, F., Staudacher, E., Wilson, I.B. and März, L.,** 1999. Insect cells as hosts for the expression of recombinant glycoproteins. *Glycoconjugate journal*, *16*(2), pp.109-123.

29**. Bernaudat, F., Frelet-Barrand, A., Pochon, N., Dementin, S., Hivin, P., Boutigny, S., Rioux, J.B., Salvi, D., Seigneurin-Berny, D., Richaud, P. and Joyard, J.,** 2011. Heterologous expression of membrane proteins: choosing the appropriate host. *PloS one*, *6*(12), p.e29191.

30. **van Loo, N.D., Fortunati, E., Ehlert, E., Rabelink, M., Grosveld, F. and Scholte, B.J.,** 2001. Baculovirus infection of nondividing mammalian cells: mechanisms of entry and nuclear transport of capsids. *Journal of virology*, *75*(2), pp.961-970.

31. **He, Y., Wang, K. and Yan, N.,** 2014. The recombinant expression systems for structure determination of eukaryotic membrane proteins. *Protein & cell*, *5*(9), pp.658-672.

32. **Contreras-Gómez, A., Sánchez-Mirón, A., García-Camacho, F., Molina-Grima, E. and Chisti, Y.,** 2014. Protein production using the baculovirus-insect cell expression system. *Biotechnology progress*, *30*(1), pp.1-18.

33. **Grynkiewicz, G., Poenie, M. and Tsien, R.Y.,** 1985. A new generation of Ca2+ indicators with greatly improved fluorescence properties. *Journal of Biological Chemistry*, *260*(6), pp.3440-3450.

34. **Hall, M.A., Xi, J., Lor, C., Dai, S., Pearce, R., Dailey, W.P. and Eckenhoff, R.G.,** 2010. m-Azipropofol (AziPm) a photoactive analogue of the intravenous general anesthetic propofol. *Journal of medicinal chemistry*, *53*(15), p.5667.

35. **Jayakar, S.S., Zhou, X., Chiara, D.C., Dostalova, Z., Savechenkov, P.Y., Bruzik, K.S., Dailey, W.P., Miller, K.W., Eckenhoff, R.G. and Cohen, J.B.,** 2014. Multiple propofol-binding sites in a γ-aminobutyric acid type A receptor (GABAAR) identified using a photoreactive propofol analog. *Journal of Biological Chemistry*, *289*(40), pp.27456-27468.

36. **Patwardhan, A., Edelmayer, R., Annabi, E., Price, T., Malan, P. and Dussor, G.,** 2012. Receptor specificity defines algogenic properties of propofol and fospropofol. *Anesthesia and analgesia*, *115*(4), p.837.

37. **Welliver, M. and Rugari, S.M.,** 2009. New drug, fospropofol disodium: a propofol prodrug. *AANA journal*, *77*(4).

38. **Haeseler, G., Karst, M., Foadi, N., Gudehus, S., Roeder, A., Hecker, H., Dengler, R. and Leuwer, M.,** 2008. High-affinity blockade of voltage-operated skeletal muscle and neuronal

sodium channels by halogenated propofol analogues. *British journal of pharmacology*, *155*(2), pp.265-275.

39. **Leuwer, M., O'neill, P., Berry, N. and Haeseler, G.,** The University Of Dundee, 2013. *Compounds for use in the treatment of pain*. U.S. Patent 8,507,724.

40. **Eckle, V.S., Grasshoff, C., Mirakaj, V., O'neill, P.M., Berry, N.G., Leuwer, M. and Antkowiak, B.,** 2014. 4-bromopropofol decreases action potential generation in spinal neurons by inducing a glycine receptor-mediated tonic conductance. *British journal of pharmacology*, *171*(24), pp.5790-5801.

Chapter 4

Towards a model of propofol-induced activation of TRPA1

Most of the work presented in this chapter represents a collaboration with Kellie Woll, a postdoctoral fellow in Roderic Eckenhoff's lab at the University of Pennsylvania. I conducted initial mass spectrometry trials testing mouse TRPA1-FLAG coverage of peptides generated by protease digestion. Ertugrul Cansizoglu, a postdoctoral fellow in Judith Steen's lab (Harvard Medical School), performed mass spectrometry analysis to detect TRPA1 digested peptides. For photolabeling studies with AziP*m*, I expressed mouse TRPA-FLAG in insect cells and isolated insect cell membranes. Kellie Woll performed photoaffinity labeling studies with AziP*m* and TRPA1-rich membranes and conducted mass spectrometry analysis of photolabeled TRPA1 peptides.

Abstract

A complete picture of how the general anesthetic propofol induces a painful sensation requires identification of where it binds in TRPA1. Mutagenesis studies suggest a role for the pocket that is shared by the antagonist A-967079, comprising residues in the S5, S6, and first pore helix in TRPA1. However, the inherent caveats associated with mutagenesis experiments necessitate complementary studies to further elucidate physiological binding sites and mechanisms. In addition, if anesthetics and antagonists share an overlapping binding site, it becomes important to investigate how these molecules produce opposite functional effects on TRPA1 gating. Thus, the aim of this chapter is to explore the location of photolabeled residues in the structure of the TRPA1 channel. Photoaffinity labeling TRPA1-containing membranes with AziP*m*, a photoactive derivative of propofol, directly identified two modified residues on the S6 helix of TRPA1, likely corresponding to two different binding sites. V954 overlaps with the A-967079 antagonist binding site while E969 lies at the nexus of the end of S6 and the TRP box helix in TRPA1. The identification of propofol binding sites will not only drive drug design efforts to hinder anesthetic-induced activation of TRPA1 but also help elucidate the molecular mechanisms of noncovalent TRPA1 agonists and highlight conserved structural gating elements in TRP channels.

Introduction

Although TRPA1 is a major contributor to propofol-induced pain, where propofol binds to TRPA1 and how this binding translates to channel opening and Ca^{2+} influx is not clear (1,2). A complete picture of propofol's mechanism of action requires identification of where it binds to

TRPA1. By using an analogue of the test drug that forms an irreversible covalent bond upon light exposure, photocrosslinking is a direct method of identifying a drug's binding site(s) (3,4).

We chose AziP*m* for initial crosslinking studies because it has been studied and validated with other propofol protein targets and it resembles the propofol in chemical structure and TRPA1 activation, suggesting AziP*m* will bind in the same location as the parent compound (5,6). AziP*m* contains a trifluoromethyl diazirine group, which promotes formation of the carbene over the long-lived diazo intermediate, which can dissociate from the binding pocket and react non-specifically with the protein target (7). Also, photoinsertion of the carbene into proteins can proceed in high yield (8). Finally, the structure-activity studies in Chapter 3 demonstrated that compounds with just one isopropyl group that is ortho to the phenolic hydroxyl group, AziP*m* and 2,4-diisopropylphenol, activate TRPA1 similarly to propofol. AziP*m* is thus a promising tool for at least the initial characterization of propofol binding sites in TRPA1.

Previous studies identified two distinct domains in TRPA1 that are important for activation by reactive electrophiles and nonelectrophilic agonists. Electrophilic TRPA1 activators, such as allyl isothiocyante (AITC) from wasabi, covalently modify N-terminal cysteines located intracellularly in TRPA1 (9,10). However, nonelectrophilic agonists such as propofol, menthol, thymol, and β-eudesmol, and cannabinoids are hydrophobic and likely bind within the TRPA1 transmembrane domain (11-14). Mutational and chimeric studies suggest that the S5 and S6 segments, which surround the ion-conducting pore, are important for activation by nonreactive chemicals, such as menthol and propofol (11,15). To circumvent the known limitations in mutagenesis, complementary studies are necessary for a more complete understanding of how noncovalent TRPA1 agonists bind and gate TRPA1.

Photoaffinity labeling is a useful strategy to generate reactive chemical species that covalently crosslink nonelectrophilic agonists to TRPA1. Through photolabeling, this study directly identified two modified residues on the S6 helix of TRPA1, likely corresponding to two distinct binding sites. One residue overlaps with the site identified in the cryoEM structure of antagonist-bound TRPA1 while the other lies at the nexus of the end of the S6 helix and the beginning of the TRP box helix, a region important for TRP channel gating (16-19). As general anesthetic-induced activation of TRPA1 elicits a pain response in many patients, identifying propofol-binding sites will facilitate the development of drugs that block this deleterious effect, shed light on the molecular mechanisms of noncovalent TRPA1 agonists, and underscore conserved gating elements in TRP channels.

Materials and Methods

General immunoprecipitation of mouse TRPA1 (mTRPA1) from whole cell lysates of baculovirus-infected insect cells

A 13-mL culture of Sf21 insect cells (at a density of $1-1.5 \times 10^6$ cells/mL) was infected with 130 µL of mTRPA1-FLAG baculovirus (or appropriate FLAG-tagged construct) and harvested 48 h post-infection via centrifugation at 3000 rpm, frozen in liquid nitrogen and stored at -80°C. Cell pellets were resuspended in 0.75 mL of lysis buffer (50 mM Tris-HCl, pH 7.5, 150 mM NaCl, 1mM EDTA, pH 8.0, 1 mM PMSF, 1X Complete protease inhibitor tablets and 1% n-Dodecyl-β-D-Maltoside (DDM) and incubated for 2 hours with rocking at 4°C. While samples were incubating, M2 Anti-FLAG agarose beads (Sigma; 50 µL of a 50% slurry per pull down sample) were resuspended by gentle inversion and washed 2X with 1 mL stock buffer (50 mM Tris-HCl, pH 7.5, 150 mM NaCl, and 1 mM EDTA, pH 8.0). The cell lysate was centrifuged for

20 minutes at 4°C and the supernatant was transferred to a tube containing beads, rocked for 1 hour at 4°C, then centrifuged for 2 minutes at 1000 rpm. The supernatant was saved as "flow-through". The beads were washed 3-5X with wash buffer (stock buffer + 1 mM phenylmethylsulfonyl fluoride (PMSF), 1X Complete protease inhibitor tablet, and 0.03% DDM). The wash buffer was discarded and the protein was eluted by adding 80 µL of 2X SDS sample buffer (200 mM Tris-HCl, pH 6.8, 8% sodium dodecyl sulfate (SDS), 0.04% Bromophenol blue, 40% glycerol). Samples were then spun down before loading onto sodium dodecyl sulfate polyacrylamide gel electrophoresis (SDS-PAGE) gel.

Preparation of mTRPA1-containing membranes

Sf21 cells (66 mL at 1.25 x 10^6 cells/mL) were infected with mTRPA1-FLAG baculovirus and harvested 48 h post-infection, frozen in liquid nitrogen and stored at -80°C. Membranes were prepared at 4°C. Cells were resuspended and homogenized in 3.5 mL lysis buffer (20 mM HEPES, pH 7.2, protease inhibitor cocktail containing 1 mM 4-(2-aminoethyl)benzenesulfonyl fluoride hydrochloride (AEBSF), 800 nM Aprotinin, 50 µM Bestatin, 15 µM E64, 20 µM Leupeptin, 10 µM Pepstatin A, 5 mM ethylenediaminetetraacetic acid (EDTA), and 1 mM PMSF). This was a commercial Halt Protease Inhibitor Cocktail-100X (Thermo Scientific, Waltham, MA). Successful lysis was confirmed by visualizing cells under light microscope using Trypan Blue. The homogenate was centrifuged 15 min at 1000 *g*. The cleared supernatant was centrifuged at 55,000 rpm in a Ti90 rotor (Beckman-Coulter, Brea, CA) for 45 min at 4°C, and the resulting membrane pellets resuspended at 1 mg/mL total protein in lysis buffer and stored in 50 µL aliquots at -80°C.

SDS-PAGE and western blot of mTRPA1-FLAG

15 µL of sample was loaded per lane of a 12% SDS-PAGE gel. Samples were separated at 200 volts over 1 hour. While samples were electrophoresed, the polyvinylidene fluoride (PVDF) membrane was washed with methanol and submerged in 1X transfer buffer with six filter papers. Three filter papers were placed on the electroblotting apparatus, followed by the gel, membrane, and three filter papers. The proteins were transferred to the PVDF membrane at a current of 200 mA for 1 hour. The membrane was rinsed with TBS-T (TBS + 0.1% Tween-20). The membrane was blocked with 3% bovine serum albumin (BSA)/tris-buffered saline-tween 20 (TBS-T) for 1 hour and then incubated with M2 Anti-FLAG antibody conjugated with alkaline phosphatase diluted 1:1000 with TBS-T for 1 hour. The membrane was rinsed with TBS-T and washed 3X with TBS-T. Two mL of 1-Step nitro-blue tetrazolium chloride (NBT)/5-bromo-4-chloro-3-indolylphosphate toluidine salt (BCIP) (Thermos Scientific, Waltham, MA) was placed on the membrane to initiate the staining. After ~ 10 minutes of gentle swirling, the membrane was rinsed with water.

In-gel digestion of mTRPA1-containing bands

The SDS-polyacrylamide gel was stained with Coomassie Blue to visualize the protein bands and washed with water to remove excess background stain. The TRPA1-containing bands were excised from the gel and cut into cubes and destained with 50 mM ammonium bicarbonate (NH_4CO_3) and 50% acetonitrile. Acetonitrile (0.5 mL) was added until the gel pieces shrunk. Acetonitrile and 100 mM NH_4HCO_3 were used 3X alternatively to dehydrate and rehydrate the gel pieces. 10 mM dithiothreitol (DTT) was added to reduce disulfide bonds and 55 mM iodoacetamide (IAA) was used to alkylate free cysteine residues. Gel slices were spun down and dried in a Speedvac and then proteins were digested with 50 µL of freshly prepared 20 ng/µL

chymotrypsin (Roche applied science sequencing grade) and/or trypsin (Promega sequencing grade modified). In the case of the combination of trypsin and chymotrypsin in 25 mM NH_4HCO_3 for 24-48 hours at 37ºC. Digested peptides were extracted with 50 µL of 60% acetonitrile and 30 mM $NH_4HCO_3$and samples were resuspended in mass spectrometry (MS) loading buffer (5% acetonitrile and 0.1% formic acid). Mass spectrometry analysis, using a Q Exactive mass spectrometer (Thermo Fisher Scientific) coupled with Eksigent LC system (AB Sciex, Framingham, MA) over a 120-minute gradient to obtain protease-digested TRPA1 peptides, was conducted in Judith Steen's lab (Harvard Medical School).

Results

In-gel protease digestion of TRPA1-FLAG yields peptides that are detected by mass spectrometry

I expressed mouse TRPA1, carrying a C-terminal FLAG tag, in Sf21 insect cells and lysed whole cells, releasing membranes containing TRPA1-FLAG. I performed immunoprecipitation of TRPA1-FLAG, performed SDS-PAGE, excised the TRPA1-containing band and tested three protease digestion conditions (trypsin, chymotrypsin, and a double digest with both proteases) to determine which conditions provide not only the highest protein coverage but particularly provide high coverage of the hydrophobic peptides that are in the transmembrane domain, which is likely where the lipophilic propofol binds.

In my hands, 100% sequence coverage of TRPA1 was obtained with the sequential digestion of chymotrypsin and trypsin while single digestion with chymotrypsin or trypsin yielded 98% and 88% sequence coverage, respectively (**Figure 4.1**). In the trypsin digestion, most of the residues in the cytoplasmic domains were detected, however, there was a paucity of

Figure 4.1 TRPA1 peptides detected via MS projected onto mTRPA1 topology. Dark blue, sky blue, and teal correspond to detected peptides with relative high, medium, and low abundance, respectively. White circles correspond to undetected peptides and bolded circles correspond to predicted protease cleavage sites. Two-dimensional projections of TRPA1 were generated using the web-accessible Protter software. **(Top)** Mass spectrometry of TRPA1 subjected to trypsin digestion yields 88% sequence coverage of TRPA1 (**Middle**) Mass spectrometry of TRPA1 subjected to chymotrypsin digestion yields 98% sequence coverage of TRPA1 (**Bottom**) Mass spectrometry of TRPA1 subjected to sequential digestion of trypsin and chymotrypsin yields full sequence coverage of TRPA1.
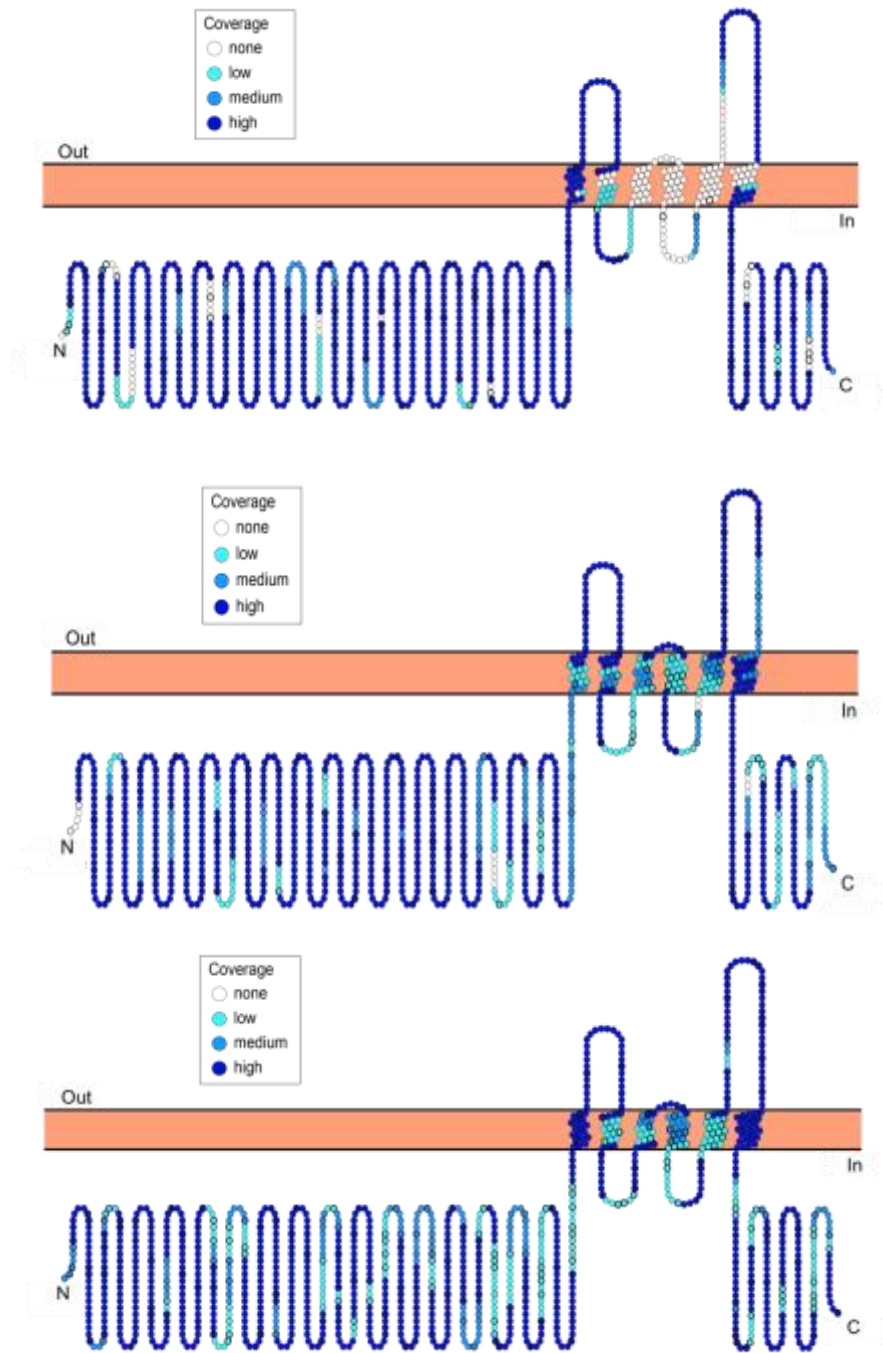
Figure 4.1 TRPA1 peptides detected via MS projected onto TRPA1 topology (continued)

peptides detected in the transmembrane domain (**Figure 4.1**). Chymotrypsin digestion yielded 98% total protein coverage with complete transmembrane domain detection (**Figure 4.1**). Sequential digestion with both chymotrypsin and trypsin not only allowed for detection of all TRPA1 residues but also increased peptide detection in the S1, S4, and S6 transmembrane domains (**Figure 4.1**).

Photolabeled residues projected onto TRPA1 cryoEM structure

With MS conditions facilitating complete detection of TRPA1-digested peptide and a functional assay that revealed three crosslinkable analogues of propofol share similar TRPA1 activation, I initiated a collaboration with a laboratory that uses photoaffinity labeling in proteins and peptide models.

I, along with Kellie Woll, a postdoctoral fellow in the lab of Roderic Eckenhoff (University of Pennsylvania) chose AziP*m*, a photoactive derivative of propofol*)* for initial crosslinking studies because it has been characterized in GABA and ion channels. (5,6). I expressed mouse TRPA1-FLAG in baculovirus-infected insect cells and isolated TRPA1-rich membranes. Kellie performed photoaffinity labeling with AziP*m* and mass spectrometry analyses.

Although one strategy is to photolabel in intact insect cells, TRPA1 may be in a more native confirmation in the membrane than in the artificial detergent environment. Thus, photolabeling was performed in intact insect cell membranes. Photoaffinity labeling with 3 μM AziP*m* identified two residues, V954 and E969 (mouse TRPA1 numbering), located within the S6 helix of TRPA1 (**Figure 4.2**). V954 lies in the middle of S6 within the transmembrane domain while E969 is surface-exposed and closer to the cytoplasmic side (**Figure 4.2**).
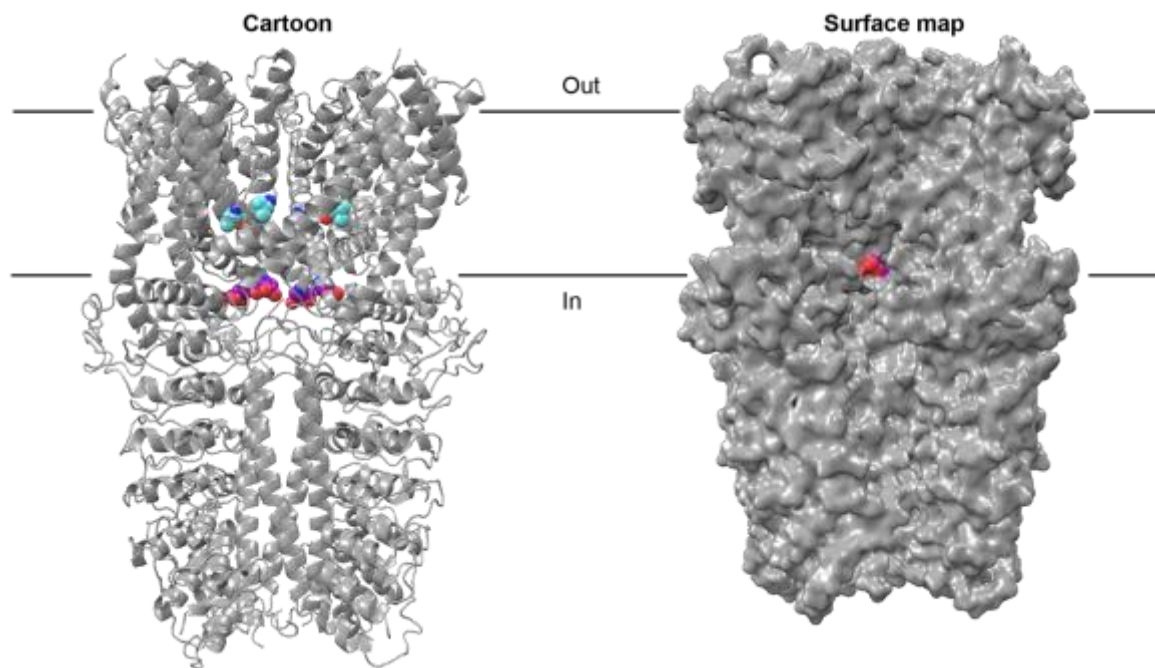
Figure 4.2 CryoEM structure of TRPA1 with residues modified by AziP*m* Residue

numbering refers to human TRPA1; V951 and E966 are colored by element. (**Left**) Membrane

view of human TRPA1 (PDB: 3J9P) with photolabeled residues V951 (sky blue spheres; V954

in mouse) and E966 (magenta spheres; E969 in mouse) shown on each subunit. **(Right)** Surface

view of solvent-exposed E966 (magenta sphere).

V954 forms a pocket with the antagonist binding site in TRPA1

The cryoEM structure of TRPA1 revealed an antagonist binding site with A-967079 (19). AziP*m* photolabeled V954 (V951 in human TRPA1), which overlaps with the A-967079 antagonist-binding site (**Figure 4.3A**). S876 and T877, which lie at the kink connecting the S4-S5 linker and the S5 helix are important for TRPA1 activation by nonelectrophilic agonists such as menthol and eudesmol, are also a part of this pocket (11,13,15).

E969 lies at the bottom of the pore near the TRP-domain helix

In the human TRPA1 structure, E966 (corresponding to E969 in mouse) lies beneath the S4-S5 linker at the junction consisting of the end of the S6 helix and the start of the TRP box helix, which is important for gating in TRP channels (**Figure 4.3B**) (16-19). As the TRP-domain helix makes several important contacts with other intracellular, it may represent an important link between these TRPA1 domains and the channel gate.

Discussion

General anesthetics are widely used drugs that suppress the central nervous system (CNS) and induce a reversible state of unconsciousness. In addition to activating the channels responsible for this immensely useful property, general anesthetics such as propofol also activate TRPA1 in peripheral sensory neurons, eliciting a pain upon injection that many patients experience (1,2). In this chapter, we directly identified two modified residues on the S6 helix of TRPA1 by photoaffinity labeling TRPA1-containing membranes with AziP*m*, a photoactive derivative of propofol. It is important to obtain sufficient coverage of digested peptides to detect
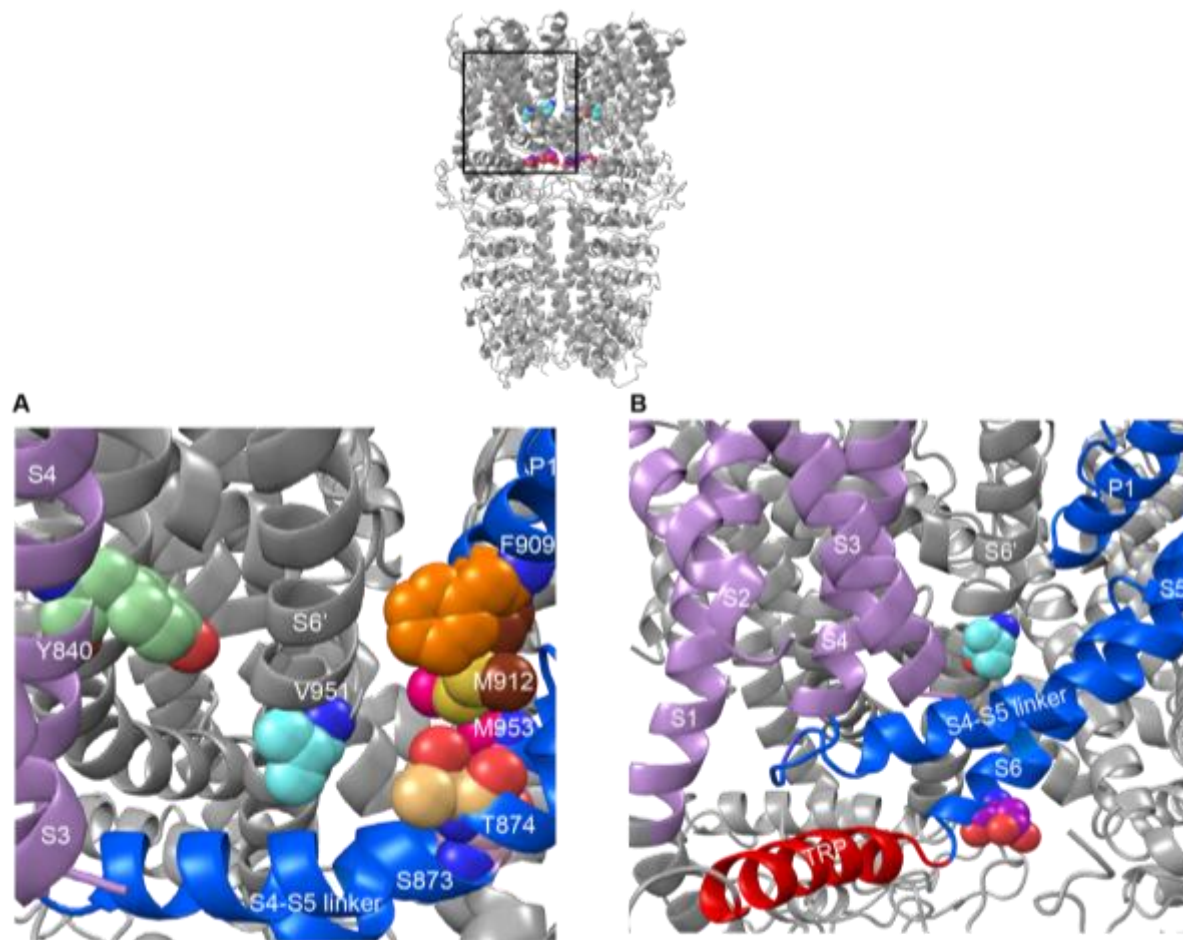
Figure 4.3 Close-up view of V954 and E969 Both panels follow the following color scheme

from N-to C-terminus: S1-S4, lilac; S5-S6, blue; V951, sky blue; E966, magenta; TRP-domain

helix, fire red). Residue numbering refers to human TRPA1. Residues are colored by element.

S6' refers to S6 helix on the adjacent subunit. (**A**) V951 (sky blue spheres) on the S6 helix of one

subunit projects into a pocket formed by S4, the S4-S5 linker and F909 (orange sphere on pore

helix 1) on the adjacent subunit. S873 and T874 are proposed to interact with the hydroxyl group

of the A-967079 antagonists. All other helices have been colored grey for clarification of the

binding pocket. Inset box demarcates close-up view in panel B. (**B**) E966 lies at the nexus of the

end of S6 and the TRP box helix in TRPA1.

as many peptides as possible that may be crosslinked. As predicted, the combination of both chymotrypsin and trypsin provided the most complete TRPA1 coverage. Chymotrypsin, which cleaves peptide amide bonds where the carboxyl side of large hydrophobic amino acid residues, was a protease of choice to get good coverage for the transmembrane regions, due to the abundance of aromatic residues in the TRPA1 transmembrane domain.

We identified two residues through photolabeling TRPA1 with AziP*m*. V954 projects into the S6-pore pocket on the adjacent subunit. The S4-S5 linker transduces activation conformational changes not only in TRP channels but also in voltage-gated channels (20-23). Several residues near the TRPA1 pore pocket, particularly S876 and T877, which are at the kink between the S4-S5 linker and S5 near the lipid-water interface and are conserved in mammals, are important for the response to several molecules that are structurally similar to propofol. S876 is important not only for TRPA1 response to eudesmol but also monoterpenes (13,24). T877, which points toward S6 of the adjacent TRPA1subunit, is also important for activation by monoterpenes such as borneol, 2-methylisoborneol, and fenchyl alcohol (24). The S4-S5 linker is also important for TRPV1 activation. The cryoEM structure of TRPV1 and site-specific mutagenesis combined with functional assays revealed that the capsaicin 'head' binds residues in the S4-S5 linker, which transduces activation conformational changes (25,26). Taken together, the S4-S5 linker, which joins the S1-S4 sensor domain and pore, serves as a signal integrator for TRP channels.

Interestingly, the TRP box helix, which is important for channel gating, is located near the second photolabeled residue. E969, at the bottom of S6, makes contacts with the TRP box helix in TRPA1. The TRP box, a hydrophobic α-helix conserved in various TRP channels, is just C-terminal of the S6 helix. Although TRPA1 lacks a canonical 'TRP box' motif the cryoEM

structure of TRPA1 revealed a TRP box helix structurally analogous to the TRP box helix in

TRPV1 (19), providing further evidence for TRP-domain helices as important sites for TRPA1

regulation. The TRP box helix in TRPA1 makes extensive hydrophobic contacts with the S4-S5

linker as well. In other TRP channels, the TRP box is thought to stabilize the closed state of

TRPV4 (27). The TRP box helix interacts with several intracellular domains, allowing it to serve

as an essential gate for channel function.

A recent study using chimeric channels and mutagenesis identified residues important for

TRPA1 activation by propofol and isoflurane, two general anesthetics (15). In this study,

researchers generated chimeras in which mouse TRPA1 contains the S5 domain of *Drosophila*

TRPA1, which is not activated by propofol or menthol, and tested for activation by propofol and

isoflurane (2,11). Substituting S876 in mouse TRPA1 for V933, the corresponding residue in

Drosophila, hindered activation by isoflurane. This finding is consistent with previous studies

that S876 is critical for activation by nonelectrophilic agonists (11). In addition to testing the

effect of S876 on TRPA1 activation by propofol and isoflurane, they also introduced mutations

at amino acid residues that define the A-967079-binding pocket in the cryoEM structure of

TRPA1. Substituting four amino acid residues onto *Drosophila* TRPA1 conferred some

antagonism, as measured by percent inhibition of AITC-evoked response. Molecular modeling

predicted an important role for two methionines within the A-967079-binding site. The results

presented in this chapter are consistent with their results in pointing to a shared binding site

consisting of S5, S6 and pore helix 1, which form a binding pocket for A-967079. We

photolabeled a second, previously unidentified site in TRPA1 that is on the S6 helix near the

TRP-box helix. However, mutagenesis experiments still need to be performed to determine if

these residues affect channel function. In addition, competition experiments with propofol will help pinpoint which residues comprise the propofol-binding site.

Noncovalent TRPA1 agonists are an important class of molecules with uses in medicine and other industries but their molecular mechanisms remain unclear. The fact that many of these molecules engage in low-affinity interactions with TRPA1 further complicates this pressing issue. As discussed above, photoaffinity labeling is a powerful technique to capture transient ligand interactions with proteins. It also provides a complementary technique to mutagenesis, which has inherent caveats such as the difficulty in ascertaining whether changes in channel function are due to direct binding or are a consequence of an allosteric effect. The results in this chapter highlight the potential "druggability" of the S6-pore pocket in TRPA1, as this site is shared by both TRPA1 agonists and antagonists. In addition, the proximity of E969, identified by photolabeling with a photoreactive analogue of propofol, to the TRP box helix warrants follow-up studies of this result, which may shed light on this important structural element that plays a role in general TRP channel gating.

References

1. **Matta, J.A., Cornett, P.M., Miyares, R.L., Abe, K., Sahibzada, N. and Ahern, G.P.,** 2008. General anesthetics activate a nociceptive ion channel to enhance pain and inflammation. *Proceedings of the National Academy of Sciences*, *105*(25), pp.8784-8789.

2. **Fischer, M.J., Leffler, A., Niedermirtl, F., Kistner, K., Eberhardt, M., Reeh, P.W. and Nau, C.,** 2010. The general anesthetic propofol excites nociceptors by activating TRPV1 and TRPA1 rather than GABAA receptors. *Journal of Biological Chemistry*, *285*(45), pp.34781-34792.

3. **McFedries, A., Schwaid, A. and Saghatelian, A.,** 2013. Methods for the elucidation of protein-small molecule interactions. *Chemistry & biology*, *20*(5), pp.667-673.

4. **MacKinnon, A.L. and Taunton, J.,** 2009. Target Identification by Diazirine Photo-Cross-Linking and Click Chemistry. *Current protocols in chemical biology*, pp.55-73.

5. **Hall, M.A., Xi, J., Lor, C., Dai, S., Pearce, R., Dailey, W.P. and Eckenhoff, R.G.,** 2010. m-Azipropofol (AziPm) a photoactive analogue of the intravenous general anesthetic propofol. *Journal of medicinal chemistry*, *53*(15), p.5667.

6. **Jayakar, S.S., Dailey, W.P., Eckenhoff, R.G. and Cohen, J.B.,** 2013. Identification of propofol binding sites in a nicotinic acetylcholine receptor with a photoreactive propofol analog. *Journal of Biological Chemistry*, *288*(9), pp.6178-6189.

7. **Amy, K.F.,** 2015. Diazo compounds for the bioreversible esterification of proteins. *Chemical science*, *6*(1), pp.752-755.

8. **Brunner, J.,** 1993. New photolabeling and crosslinking methods. *Annual review of biochemistry*, *62*(1), pp.483-514.

9. **Macpherson, L.J., Dubin, A.E., Evans, M.J., Marr, F., Schultz, P.G., Cravatt, B.F. and Patapoutian, A.,** 2007. Noxious compounds activate TRPA1 ion channels through covalent modification of cysteines. *Nature*, *445*(7127), pp.541-545.

10. **Hinman, A., Chuang, H.H., Bautista, D.M. and Julius, D.,** 2006. TRP channel activation by reversible covalent modification. *Proceedings of the National Academy of Sciences*, *103*(51), pp.19564-19568.

11. **Xiao, B., Dubin, A.E., Bursulaya, B., Viswanath, V., Jegla, T.J. and Patapoutian, A.,** 2008. Identification of transmembrane domain 5 as a critical molecular determinant of menthol sensitivity in mammalian TRPA1 channels. *Journal of Neuroscience*, *28*(39), pp.9640-9651.

12. **Lee, S.P., Buber, M.T., Yang, Q., Cerne, R., Cortes, R.Y., Sprous, D.G. and Bryant, R.W.,** 2008. Thymol and related alkyl phenols activate the hTRPA1 channel. *British journal of pharmacology*, *153*(8), pp.1739-1749.

13. **Ohara, K., Fukuda, T., Okada, H., Kitao, S., Ishida, Y., Kato, K., Takahashi, C., Katayama, M., Uchida, K. and Tominaga, M.,** 2015. Identification of significant amino acids in multiple transmembrane domains of human transient receptor potential ankyrin 1 (TRPA1) for activation by eudesmol, an oxygenized sesquiterpene in hop essential oil. *Journal of Biological Chemistry*, *290*(5), pp.3161-3171.

14. **Andersson, D.A., Gentry, C., Alenmyr, L., Killander, D., Lewis, S.E., Andersson, A., Bucher, B., Galzi, J.L., Sterner, O., Bevan, S. and Högestätt, E.D.,** 2011. TRPA1 mediates spinal antinociception induced by acetaminophen and the cannabinoid Δ9-tetrahydrocannabiorcol. *Nature communications*, *2*, p.551.

15. **Ton, H.T., Phan, T.X., Abramyan, A.M., Shi, L. and Ahern, G.P.,** 2017. Identification of a putative binding site critical for general anesthetic activation of TRPA1. *Proceedings of the National Academy of Sciences*, p.201618144.

16. **Liao, M., Cao, E., Julius, D. and Cheng, Y.,** 2013. Structure of the TRPV1 ion channel determined by electron cryo-microscopy. *Nature*, *504*(7478), pp.107-112.

17. **Hellmich, U.A. and Gaudet, R.,** 2014. High-resolution views of TRPV1 and their implications for the TRP channel superfamily. In *Mammalian Transient Receptor Potential (TRP) Cation Channels* (pp. 991-1004). Springer International Publishing.

18. **Venkatachalam, K. and Montell, C.,** 2007. TRP channels. *Annu. Rev. Biochem.*, *76*, pp.387-417.

19. **Paulsen, C.E., Armache, J.P., Gao, Y., Cheng, Y. and Julius, D.,** 2015. Structure of the TRPA1 ion channel suggests regulatory mechanisms. *Nature*, *520*(7548), pp.511-517.

20. **Lu, Z., Klem, A.M. and Ramu, Y.,** 2002. Coupling between voltage sensors and activation gate in voltage-gated K+ channels. *The Journal of general physiology*, *120*(5), pp.663-676.

21. **Yarov-Yarovoy, V., DeCaen, P.G., Westenbroek, R.E., Pan, C.Y., Scheuer, T., Baker, D. and Catterall,** W.A., 2012. Structural basis for gating charge movement in the voltage sensor of a sodium channel. *Proceedings of the National Academy of Sciences*, *109*(2), pp.E93-E102.

22**. Boukalova, S., Marsakova, L., Teisinger, J. and Vlachova, V.,** 2010. Conserved residues within the putative S4–S5 region serve distinct functions among thermosensitive vanilloid transient receptor potential (TRPV) channels. *Journal of Biological Chemistry*, *285*(53), pp.41455-41462.

23. **Voets, T., Owsianik, G., Janssens, A., Talavera, K. and Nilius, B.,** 2007. TRPM8 voltage sensor mutants reveal a mechanism for integrating thermal and chemical stimuli. *Nature chemical biology*, *3*(3), pp.174-182.

24. **Takaishi, M., Uchida, K., Fujita, F. and Tominaga, M.,** 2014. Inhibitory effects of monoterpenes on human TRPA1 and the structural basis of their activity. *The Journal of Physiological Sciences*, *64*(1), pp.47-57.

25. **Cao, E., Liao, M., Cheng, Y. and Julius, D.,** 2013. TRPV1 structures in distinct conformations reveal activation mechanisms. *Nature*, *504*(7478), pp.113-118.

26. **Yang, F., Xiao, X., Cheng, W., Yang, W., Yu, P., Song, Z., Yarov-Yarovoy, V. and Zheng, J.,** 2015. Structural mechanism underlying capsaicin binding and activation of the TRPV1 ion channel. *Nature chemical biology*, *11*(7), pp.518-524.

27. **Teng, J., Loukin, S.H., Anishkin, A. and Kung, C.,** 2015. L596–W733 bond between the start of the S4–S5 linker and the TRP box stabilizes the closed state of TRPV4 channel. *Proceedings of the National Academy of Sciences*, *112*(11), pp.3386-3391.

Chapter 5

Discussion

Despite over 150 years of use, the molecular mechanisms of general anesthetics remain poorly understood. Thus, it is not surprising that TRPA1 has only recently emerged as the major player in the propofol-induced pain pathway (1, 2). In this thesis, I set out to identify the structural determinants for propofol binding in TRPA1. I will discuss the three major themes of this project - design and synthesis of probes, small molecule structure-function studies, and the propofol binding-site residues revealed through crosslinking - in terms of contributions to the TRP channel field and future experiments.

Propofol binds various ligand-gated and voltage-gated ion channels (3). In addition to TRPA1, evidence suggests propofol interacts with voltage-gated Kv1.5 channels, cardiac Nav1.5 sodium channels, and acid-sensing ion channels, further demonstrating the need for a diverse, readily available library of crosslinkable analogues of propofol (4-7). Mutations in the Kv1.5 gene are associated with atrial fibrillation, the most arrhythmia encountered during operating procedures that use anesthesia; adverse cardiovascular effects due to propofol are also related to voltage-gated sodium-channels (8). Thus, XPRO, *o*-XPRO-Click, and *p*-XPRO-Click should be used to identify propofol-binding sites in these ion channels as well. Also, the design of XPRO, *o*-XPRO-Click, and *p*-XPRO-Click is readily adaptable to that of alkyl phenols that are structurally analogous to propofol, such as thymol and carvacrol, which are TRP channel agonists used as flavor enhancers and analgesics (9-11). Moreover, the diazirine synthetic strategies described here could also be applied to other TRPA1/TRPV1 agonists such as zingerone, which contains a 4-carbon linker similar to that of the three XPROs. Zingerone is a vanilloid, like capsaicin and RTX, which are used therapeutically to treat pain (12,13). Thus, the zingerone binding-site location in TRPV1 and TRPA1 could point to shared or disparate binding pockets for the vanillyl moiety.

In addition to the diazirine functionality, the alkynes in *o*-XPRO-Click and *p*-XPRO-Click can serve as handles to generate novel TRPA1 modulators. For example, studies show that replacement of the benzylamide group in capsaicinoids with a tetrazole moiety, the product of the azide-alkyne cycloaddition, creates molecules that activate TRPA1 better than TRPV1 (14,15). This method is analogous to fragment self-assembly, which involves the fusion of two chemical fragments into a larger molecule (16). The copper-catalyzed click reaction can also be exploited for enrichment of photolabeled TRPA1. Immunoprecipitation of photolabeled TRPA1-FLAG, followed by conjugation to a cleavable azide resin utilizing the click chemistry, permits enrichment of photolabeled protein (17). This affinity step may simplify downstream mass spectrometry (MS) analysis by improving the signal-to-noise ratio of crosslinked peptides.

The second theme of this thesis describes the small molecule structure-function studies that reveal that incorporating halogens into propofol analogues can affect activation of TRPA1. Halogens are often incorporated drug discovery endeavors; approximately 40% of drugs currently on the market or in clinical trials are halogenated (18). Halogens form halogen bonds with halogen-bond acceptors such as oxygen, nitrogen, sulfur, and aromatic systems (18). Halogen are analogous to hydrogen bonds and can be used to improve ligand affinity while retaining structurally important interactions (18). One observation upon inspection of published TRPV1 and TRPA1 antagonists is that many of these compounds are aryl halides (19). Capsazepine and A-967079, which contain a chlorine and fluorine atom, respectively, are two examples of TRP channel antagonists that fit this trend.

Like fropofol, the brominated derivatives in this study were weaker than propofol in activation of TRPA1. Interestingly, there are potential applications of brominated propofol analogues to TRPA1; fragment-based drug discovery is one technique where halogenated

compounds are being increasingly used (20,21). This method is based on identifying small chemical fragments that only weakly bind to the protein target, and expanding the ligand library to generate higher affinity leads (22). Fragment screening is often coupled with X-ray crystallography as a powerful tool to probe protein structure and function (23,24). Fragment libraries containing brominated compounds are appealing due to ease of detection of bromine using anomalous scattering (25). In this way, fragments are screened against a protein target to probe ligand surface sites in soaking experiments (26-28). As halogenated propofol analogues are increasingly studied for their potential analgesic effects mediated through glycine receptors and voltage-gated sodium channels, it will be important to understand how these halogenated propofol analogues interact with all their biological targets (29,30).

The final theme of this thesis covers the propofol binding-site residues in TRPA1 identified through photolabeling. V954 (V951 in human TRPA1), one of the two residues identified by photolabeling, lies in the middle of the S6 helix, within range of F909 (human numbering) in pore-helix 1, which is important for antagonism of TRPA1 by A-967079 (31). S6, together with S5, forms the channel gate within 6TM-channels, thus it is conceivable that binding in this region influences channel activity. Mutagenesis experiments substituting V954 for alanine and assaying TRPA1 activation by propofol would provide further evidence for the link between the location of propofol-binding residues and activation at this position. Hannah Zurier, a lab colleague, has generated mutants of the antagonist-binding site and calcium-influx assays with transiently-transfected, mTRPA1-expressing human embryonic kidney (HEK) cells are ongoing to provide an answer.

Compared to V954, which lies within the TMD, E969 is exposed to aqueous solvent and is closer to the protein surface. E969 lies at the junction of the gate-forming S6 helix C-terminus

and the TRP-domain helix, which lies parallel to the membrane underneath the S4-S5 linker. The TRP-domain may be present in more TRP channels and may represent an important, structurally conserved, gating handle (32). Interestingly, a gain-of-function mutation, N855S (human numbering), located at the start of the S4-S5 linker, above the junction of the TRP-domain helix before it radiates outward, causes familial episodic syndrome, characterized by debilitating pain in the upper body (33). Mutations introduced into the TRPV1 S4-S5 linker also lead to increased basal current (34).

At this point, it is difficult to determine which site in TRPA1 corresponds to an agonist or antagonist pocket. To distinguish ligand binding from its consequences on channel function, a combination of mutagenesis and functional assays coupled with crosslinking studies can provide complementary insights. It would be interesting to use AziP*m* at higher concentrations in photolabeling studies with TRPA1. As propofol and AziP*m* exhibit bimodal activation, with inhibition at higher concentrations, higher concentrations of AziP*m* may result in photolabeling of residues involved on channel inhibition. Competition experiments with a crosslinkable analogue and the parent propofol molecule should also be used to distinguish crosslinked peptides due to effects such as ease of ligand accessibility from physiological binding sites.

To sum, the TRP channel field, due to rich pharmacology, is ripe for more chemical biology approaches to understanding where and how small molecules influence protein function. The direct identification of propofol-binding sites in TRPA1 shows how agonist and antagonist sites overlap in a protein. A complete picture of where and how propofol interacts with TRPA1 will be useful for the development of TRPA1 antagonists and novel analgesics that counter the noxious effects of propofol and other general anesthetics that are mediated through TRPA1.

References

1. **Matta, J.A., Cornett, P.M., Miyares, R.L., Abe, K., Sahibzada, N. and Ahern, G.P.,** 2008. General anesthetics activate a nociceptive ion channel to enhance pain and inflammation. *Proceedings of the National Academy of Sciences*, *105*(25), pp.8784-8789.

2. **Fischer, M.J., Leffler, A., Niedermirtl, F., Kistner, K., Eberhardt, M., Reeh, P.W. and Nau, C.,** 2010. The general anesthetic propofol excites nociceptors by activating TRPV1 and TRPA1 rather than GABAA receptors. *Journal of Biological Chemistry*, *285*(45), pp.34781-34792.

3. **Weiser, B.P. and Eckenhoff, R.G.,** 2015. Propofol inhibits SIRT2 deacetylase through a conformation-specific, allosteric site. *Journal of Biological Chemistry*, *290*(13), pp.8559-8568.

4. **Kojima, A., Ito, Y., Ding, W.G., Kitagawa, H. and Matsuura, H.,** 2015. Interaction of propofol with voltage-gated human Kv1. 5 channel through specific amino acids within the pore region. *European journal of pharmacology*, *764*, pp.622-632.

5. **Stoetzer, C., Reuter, S., Doll, T., Foadi, N., Wegner, F. and Leffler, A.,** 2016. Inhibition of the cardiac Na+ channel α-subunit Nav1. 5 by propofol and dexmedetomidine. *Naunyn-Schmiedeberg's archives of pharmacology*, *389*(3), pp.315-325.

6. **Ouyang, W., Wang, G. and Hemmings, H.C.,** 2003. Isoflurane and propofol inhibit voltage-gated sodium channels in isolated rat neurohypophysial nerve terminals. *Molecular pharmacology*, *64*(2), pp.373-381.

7. **Lei, Z., Li, X., Wang, G., Fei, J., Meng, T., Zhang, X., Yu, J., Yu, J. and Li, J.,** 2014. Inhibition of acid-sensing ion channel currents by propofol in rat dorsal root ganglion neurons. *Clinical and Experimental Pharmacology and Physiology*, *41*(4), pp.295-300.

8. **Nielsen, N.H., Winkel, B.G., Kanters, J.K., Schmitt, N., Hofman-Bang, J., Jensen, H.S., Bentzen, B.H., Sigurd, B., Larsen, L.A., Andersen, P.S. and Haunsø, S.,** 2007. Mutations in the Kv1. 5 channel gene KCNA5 in cardiac arrest patients. *Biochemical and biophysical research communications*, *354*(3), pp.776-782.

9. **Mihara, S. and Shibamoto, T.,** 2015. The role of flavor and fragrance chemicals in TRPA1 (transient receptor potential cation channel, member A1) activity associated with allergies. *Allergy, Asthma & Clinical Immunology*, *11*(1), p.11.

10. **de Cássia da Silveira e Sá, R., Andrade, L.N. and de Sousa, D.P.,** 2013. A review on anti-inflammatory activity of monoterpenes. *Molecules*, *18*(1), pp.1227-1254.

11. **Fachini-Queiroz, F.C., Kummer, R., Estevao-Silva, C.F., Carvalho, M.D.D.B., Cunha, J.M., Grespan, R., Bersani-Amado, C.A. and Cuman, R.K.N.,** 2012. Effects of thymol and carvacrol, constituents of Thymus vulgaris L. essential oil, on the inflammatory response. *Evidence-Based Complementary and Alternative Medicine*, *2012*.

12. **Iadarola, M.J. and Gonnella, G.L.,** 2013. Resiniferatoxin for pain treatment: an interventional approach to personalized pain medicine. *The open pain journal*, *6*, p.95.

13. **Fattori, V., Hohmann, M.S., Rossaneis, A.C., Pinho-Ribeiro, F.A. and Verri, W.A.,** 2016. Capsaicin: current understanding of its mechanisms and therapy of pain and other pre-clinical and clinical uses. *Molecules*, *21*(7), p.844.

14. **Appendino, G., Bacchiega, S., Minassi, A., Cascio, M.G., De Petrocellis, L. and Di Marzo, V.,** 2007. The 1, 2, 3-Triazole Ring as a Peptido-and Olefinomimetic Element: Discovery of Click Vanilloids and Cannabinoids. *Angewandte Chemie*, *119*(48), pp.9472-9475.

15. **Del Prete, D., Caprioglio, D., Appendino, G., Minassi, A., Schiano-Moriello, A., Di Marzo, V. and De Petrocellis, L.,** 2015. Discovery of non-electrophilic capsaicinoid-type TRPA1 ligands. *Bioorganic & medicinal chemistry letters*, *25*(5), pp.1009-1011.

16. **Rees, D.C., Congreve, M., Murray, C.W. and Carr, R.,** 2004. Fragment-based lead discovery. *Nature Reviews Drug Discovery*, *3*(8), pp.660-672.

17. **Sibbersen, C., Lykke, L., Gregersen, N., Jørgensen, K.A. and Johannsen, M.,** 2014. A cleavable azide resin for direct click chemistry mediated enrichment of alkyne-labeled proteins. *Chemical Communications*, *50*(81), pp.12098-12100.

18. **Jiang, S., Zhang, L., Cui, D., Yao, Z., Gao, B., Lin, J. and Wei, D.,** 2016. The Important Role of Halogen Bond in Substrate Selectivity of Enzymatic Catalysis. *Scientific Reports*, *6*.

19. **Skerratt, S.** "Chapter Three-Recent Progress in the Discovery and Development of TRPA1 Modulators." *Progress in Medicinal Chemistry* 56 (2017): 81-115.

20. **Jenkins, B.G.,** 1991. Detection of site-specific binding and co-binding of ligands to macromolecules using 19F NMR. *Life sciences*, *48*(13), pp.1227-1240.

21. **Fielding, L.,** 2007. NMR methods for the determination of protein–ligand dissociation constants. *Progress in Nuclear Magnetic Resonance Spectroscopy*, *51*(4), pp.219-242.

22. **Tiefenbrunn, T., Forli, S., Happer, M., Gonzalez, A., Tsai, Y., Soltis, M., Elder, J.H., Olson, A.J. and Stout, C.D.,** 2014. Crystallographic Fragment-Based Drug Discovery: Use of a Brominated Fragment Library Targeting HIV Protease. *Chemical biology & drug design*, *83*(2), pp.141-148.

23. **Bauman, J.D., Patel, D. and Arnold, E.,** 2011. Fragment screening and HIV therapeutics. In *Fragment-Based Drug Discovery and X-Ray Crystallography* (pp. 181-200). Springer Berlin Heidelberg.

24. **Bauman, J.D., Patel, D., Dharia, C., Fromer, M.W., Ahmed, S., Frenkel, Y., Vijayan, R.S.K., Eck, J.T., Ho, W.C., Das, K. and Shatkin, A.J.,** 2013. Detecting allosteric sites of HIV-1 reverse transcriptase by X-ray crystallographic fragment screening. *Journal of medicinal chemistry*, *56*(7), p.2738.

25. **Erlanson, D.A.,** 2011. Introduction to fragment-based drug discovery. In *Fragment-based drug discovery and X-ray crystallography* (pp. 1-32). Springer Berlin Heidelberg.

26. **Davies, T.G. and Tickle, I.J.,** 2011. Fragment screening using X-ray crystallography. In *Fragment-Based Drug Discovery and X-Ray Crystallography* (pp. 33-59). Springer Berlin Heidelberg.

27. **Jeff Blaney, V.N. and Burley, S.K.,** 2006. Fragment-based Lead Discovery and Optimization Using X-Ray Crystallography, Computational Chemistry, and High-through-put Organic Synthesis. *Fragment-based Approaches in Drug Discovery*, *34*.

28. **Patel, D., Bauman, J.D. and Arnold, E.,** 2014. Advantages of crystallographic fragment screening: functional and mechanistic insights from a powerful platform for efficient drug discovery. *Progress in biophysics and molecular biology*, *116*(2), pp.92-100.

29. **Eckle, V.S., Grasshoff, C., Mirakaj, V., O'neill, P.M., Berry, N.G., Leuwer, M. and Antkowiak, B.,** 2014. 4-bromopropofol decreases action potential generation in spinal neurons

by inducing a glycine receptor-mediated tonic conductance. *British journal of pharmacology*, *171*(24), pp.5790-5801.

30. **Haeseler, G., Karst, M., Foadi, N., Gudehus, S., Roeder, A., Hecker, H., Dengler, R. and Leuwer, M.,** 2008. High-affinity blockade of voltage-operated skeletal muscle and neuronal sodium channels by halogenated propofol analogues. *British journal of pharmacology*, *155*(2), pp.265-275.

31**. Paulsen, C.E., Armache, J.P., Gao, Y., Cheng, Y. and Julius, D.,** 2015. Structure of the TRPA1 ion channel suggests regulatory mechanisms. *Nature*, *520*(7548), pp.511-517.

32. **Brewster, M.S. and Gaudet, R.,** 2015. How the TRPA1 receptor transmits painful stimuli: Inner workings revealed by electron cryomicroscopy. *BioEssays*, *37*(11), pp.1184-1192.

33. **Kremeyer, B., Lopera, F., Cox, J.J., Momin, A., Rugiero, F., Marsh, S., Woods, C.G., Jones, N.G., Paterson, K.J., Fricker, F.R. and Villegas, A.,** 2010. A gain-of-function mutation in TRPA1 causes familial episodic pain syndrome. *Neuron*, *66*(5), pp.671-680.

34. **Boukalova, S., Touska, F., Marsakova, L., Hynkova, A., Sura, L., Chvojka, S., Dittert, I. and Vlachova, V.,** 2014. Gain-of-function mutations in the transient receptor potential channels TRPV1 and TRPA1: how painful?. *Physiological Research*, *63*, p.S205.

Appendix

Supplementary ^{1}H and ^{13}C NMR spectra
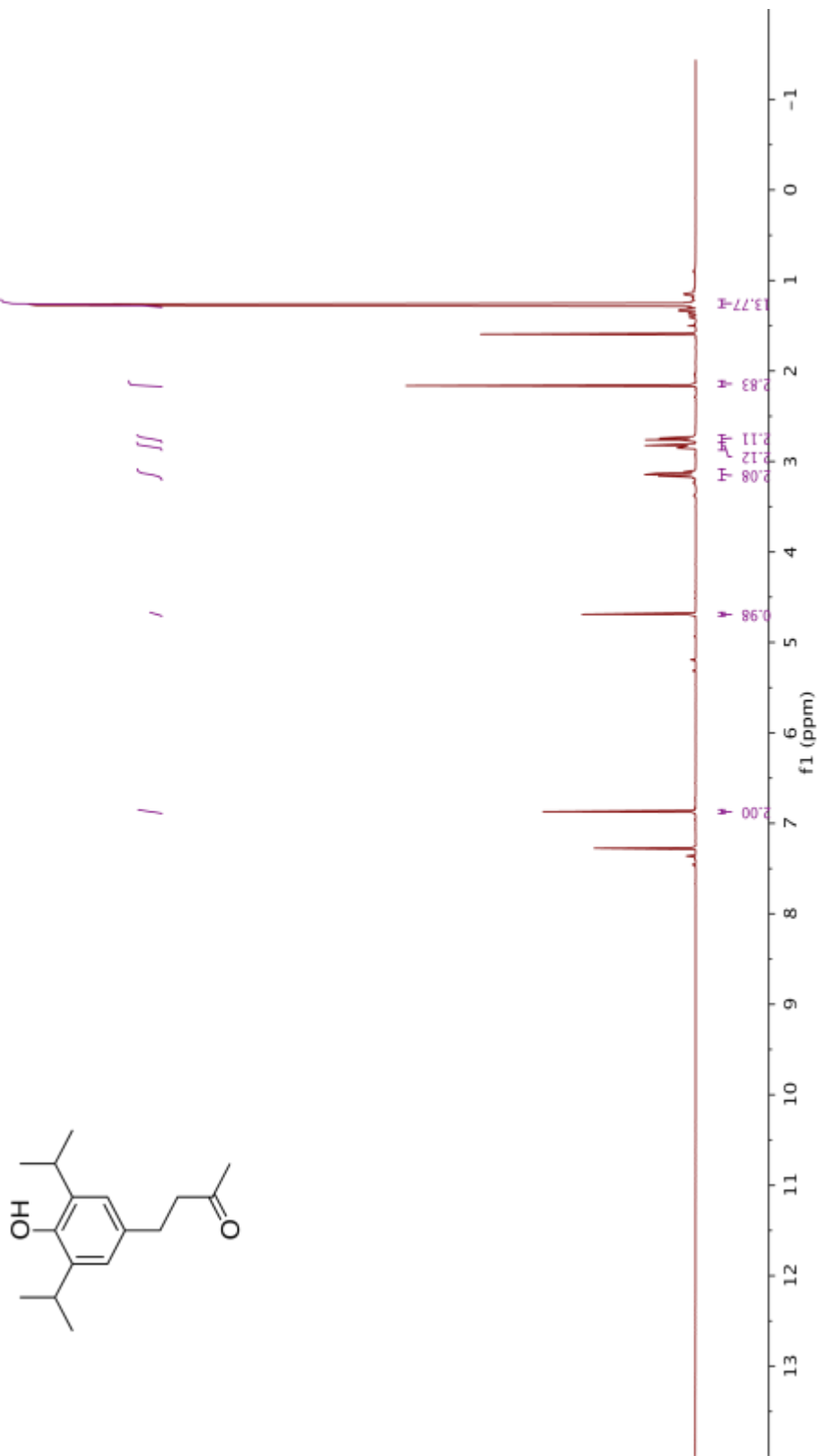
Figure A.1 ^{1}H NMR of 4-(4-Hydroxy-3,5-diisopropylphenyl)butan-2-one

113
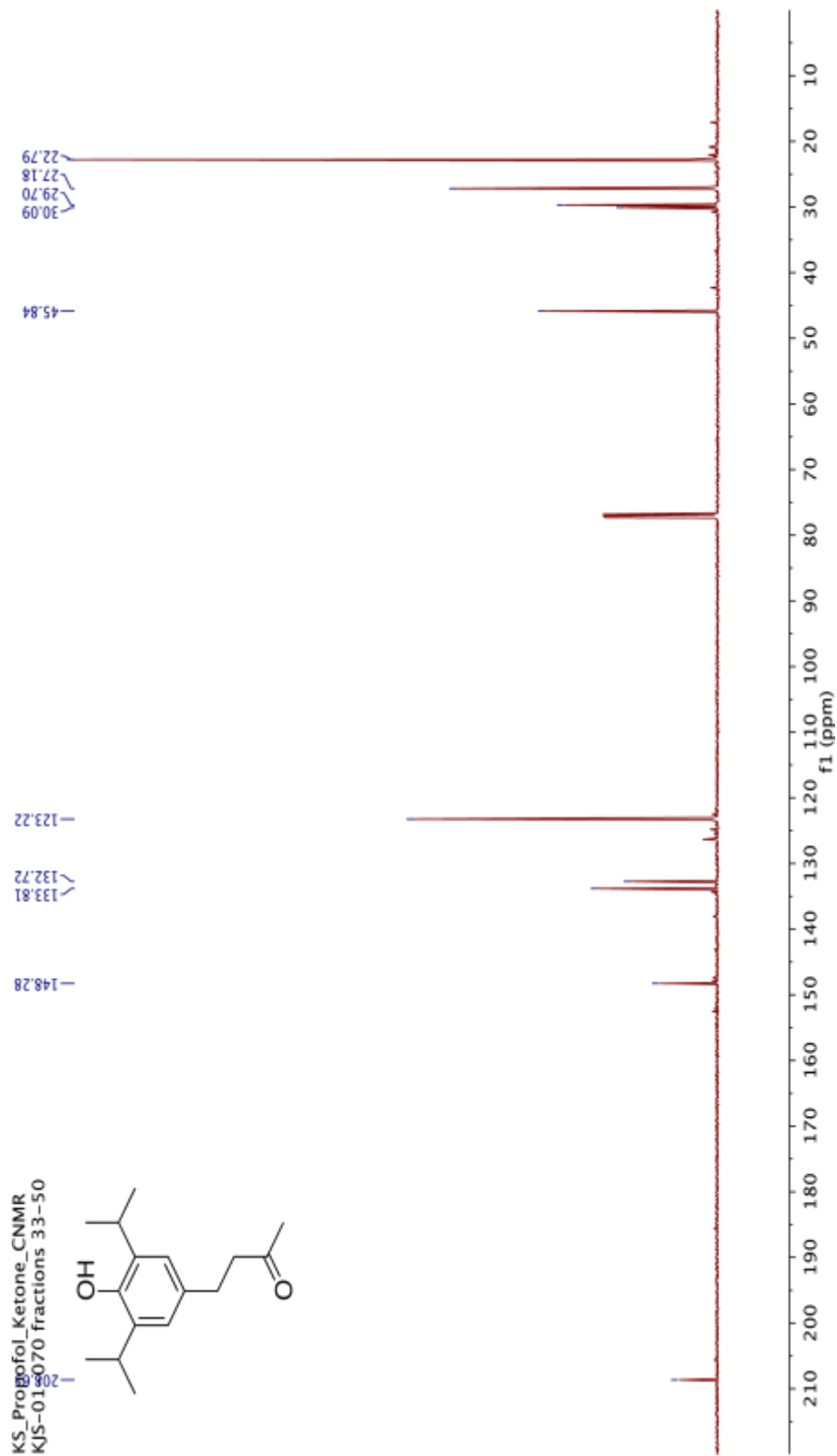
Figure A.2 ^{13}C NMR of 4-(4-Hydroxy-3,5-diisopropylphenyl)butan-2-one

114
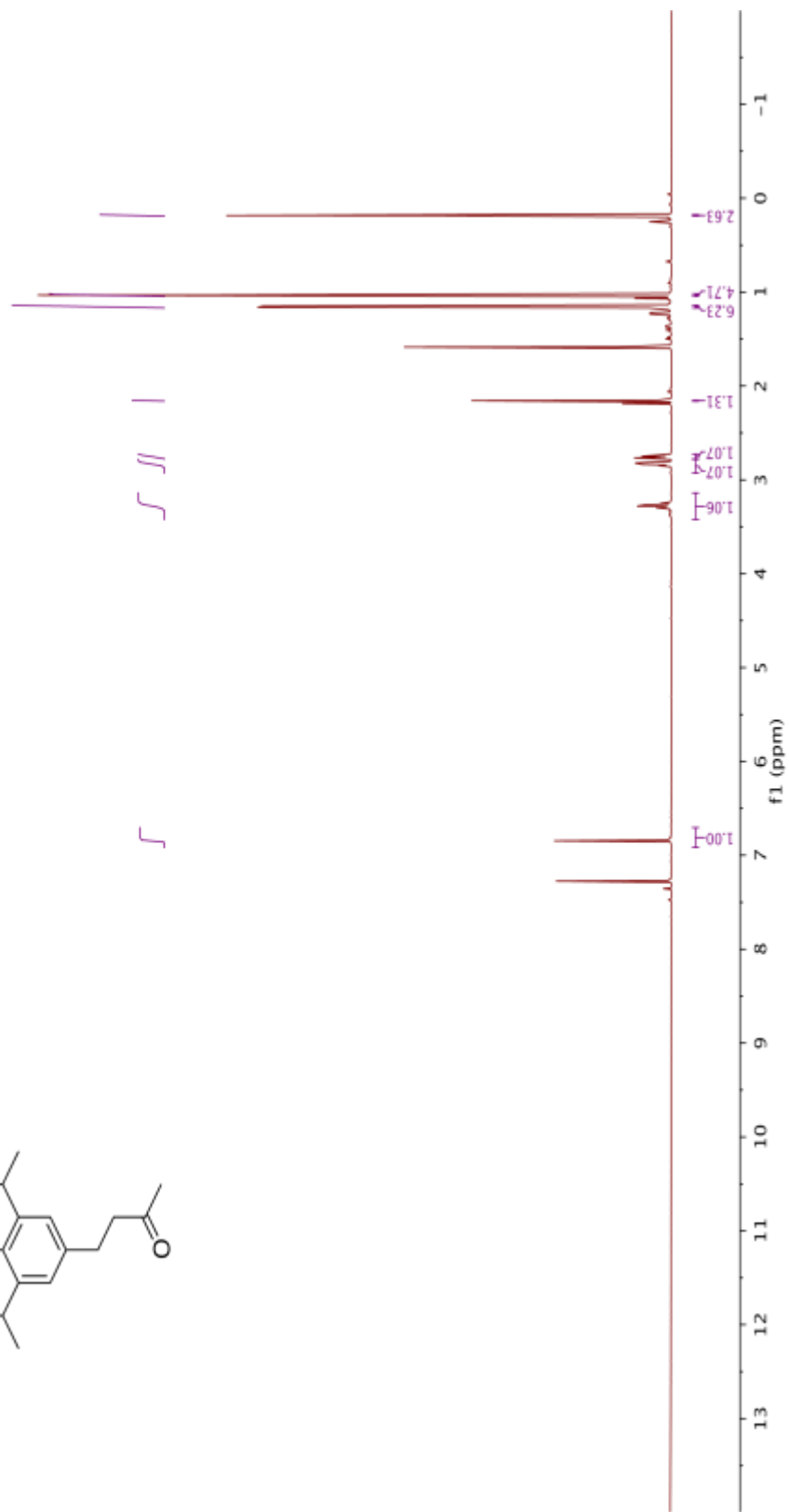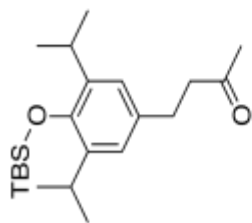
Figure A.3 ¹H NMR of 4-(4-((*tert*-butyldimethylsilyl)oxy)-3,5-diisopropylphenyl)butan-2-one
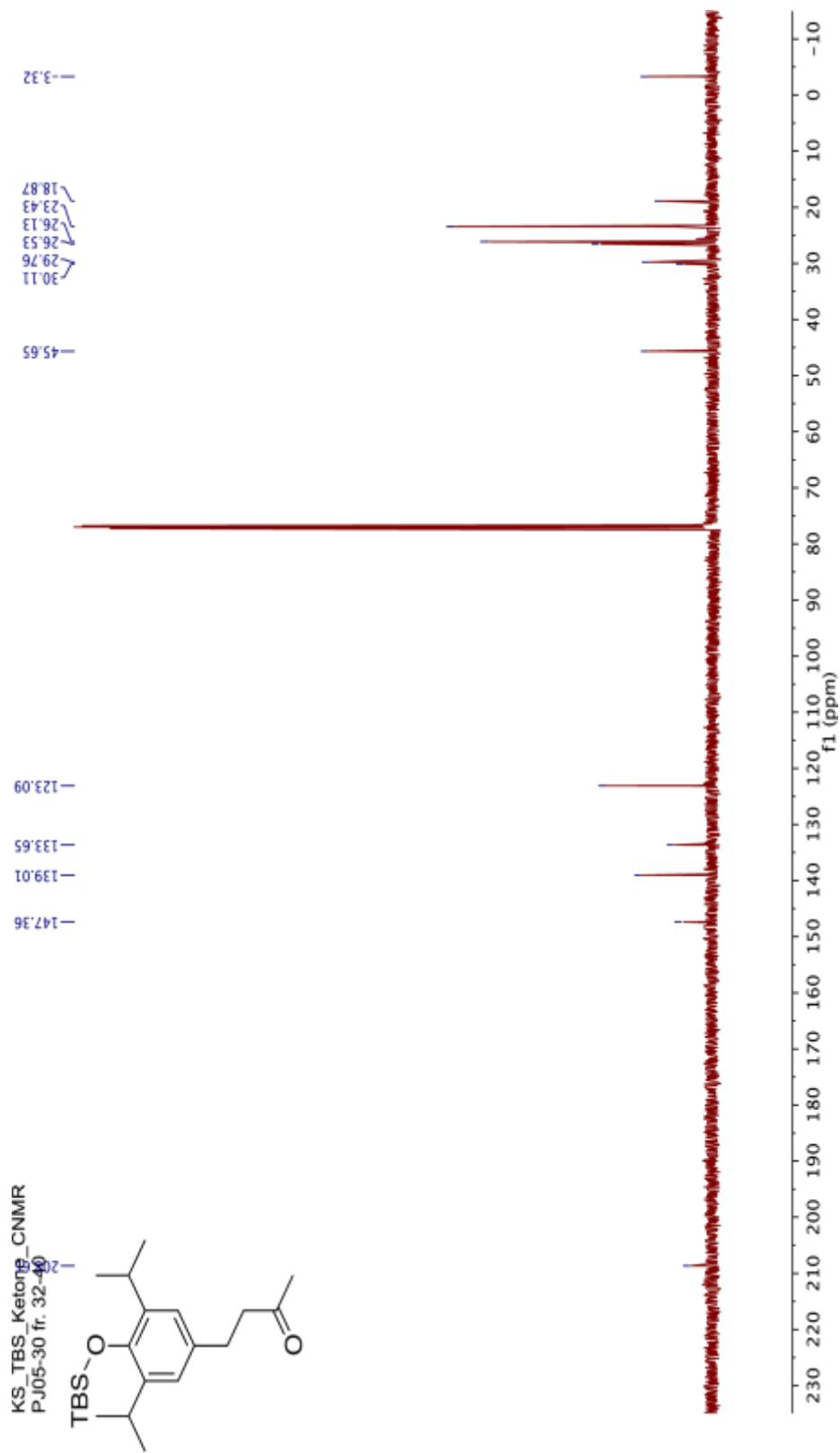
Figure A.4 ^{13}C NMR of 4-(4-((*tert*-butyldimethylsilyl)oxy)-3,5-diisopropylphenyl)butan-2-one

116
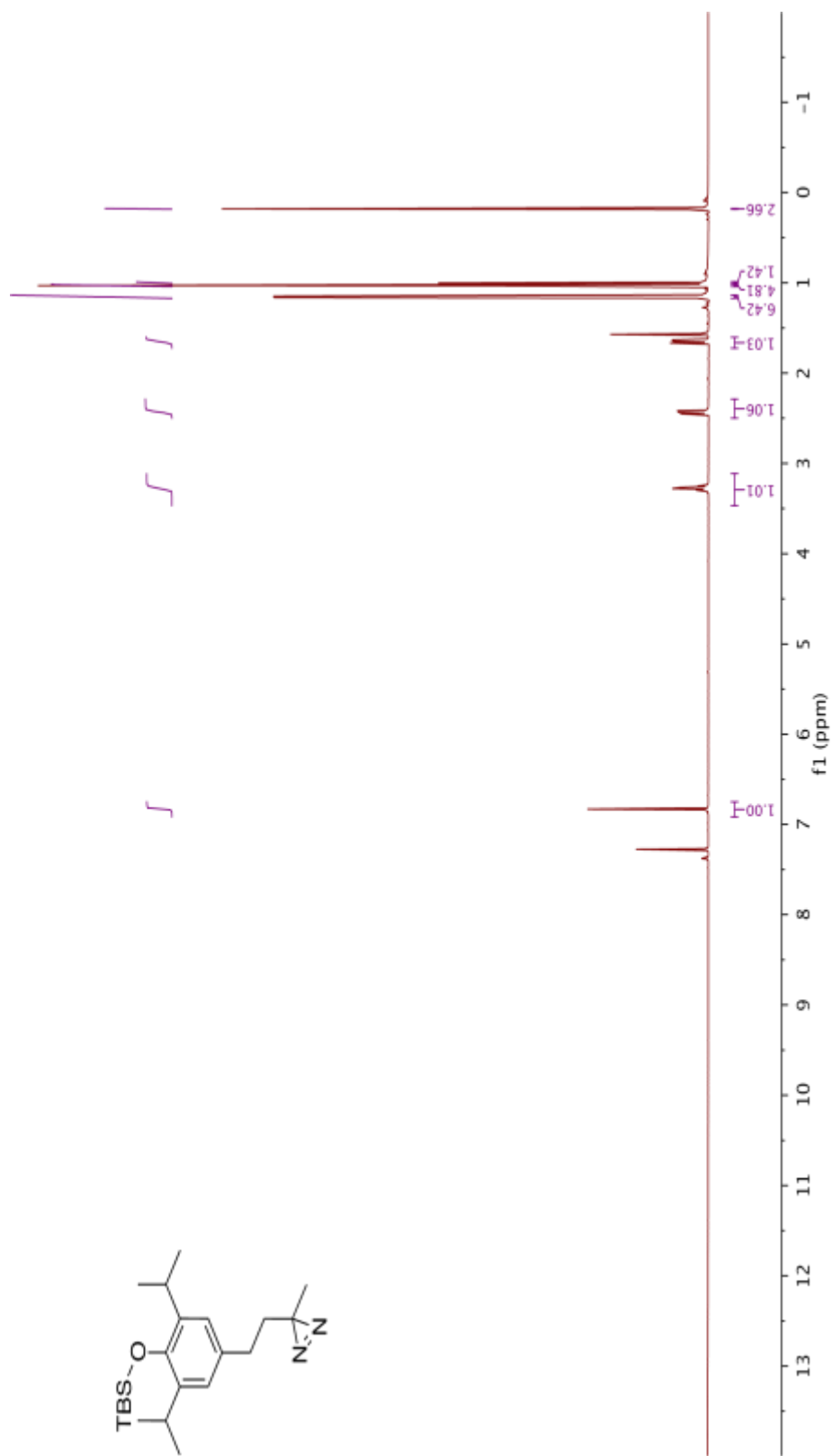
Figure A.5 ^{1}H NMR of 4-(4-((*tert*-butyldimethylsilyl)oxy)-3,5-diisopropylphenyl)-3-methyl-3*H*-diazirine

117
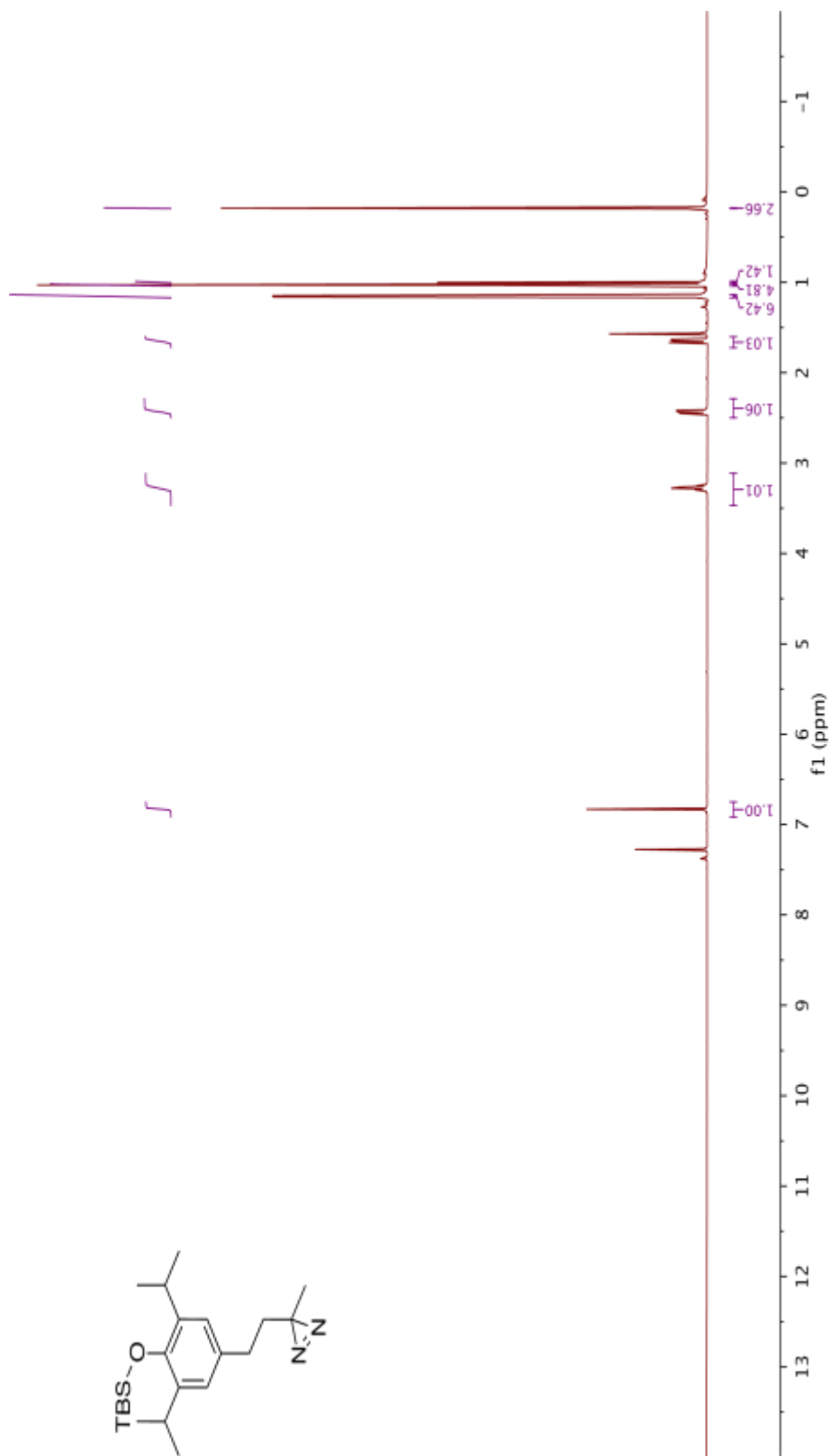
Figure A.6 ^{13}C NMR of 4-(4-((*tert*-butyldimethylsilyl)oxy)-3,5-diisopropylphenyl)-3-methyl-3*H*-diazirine
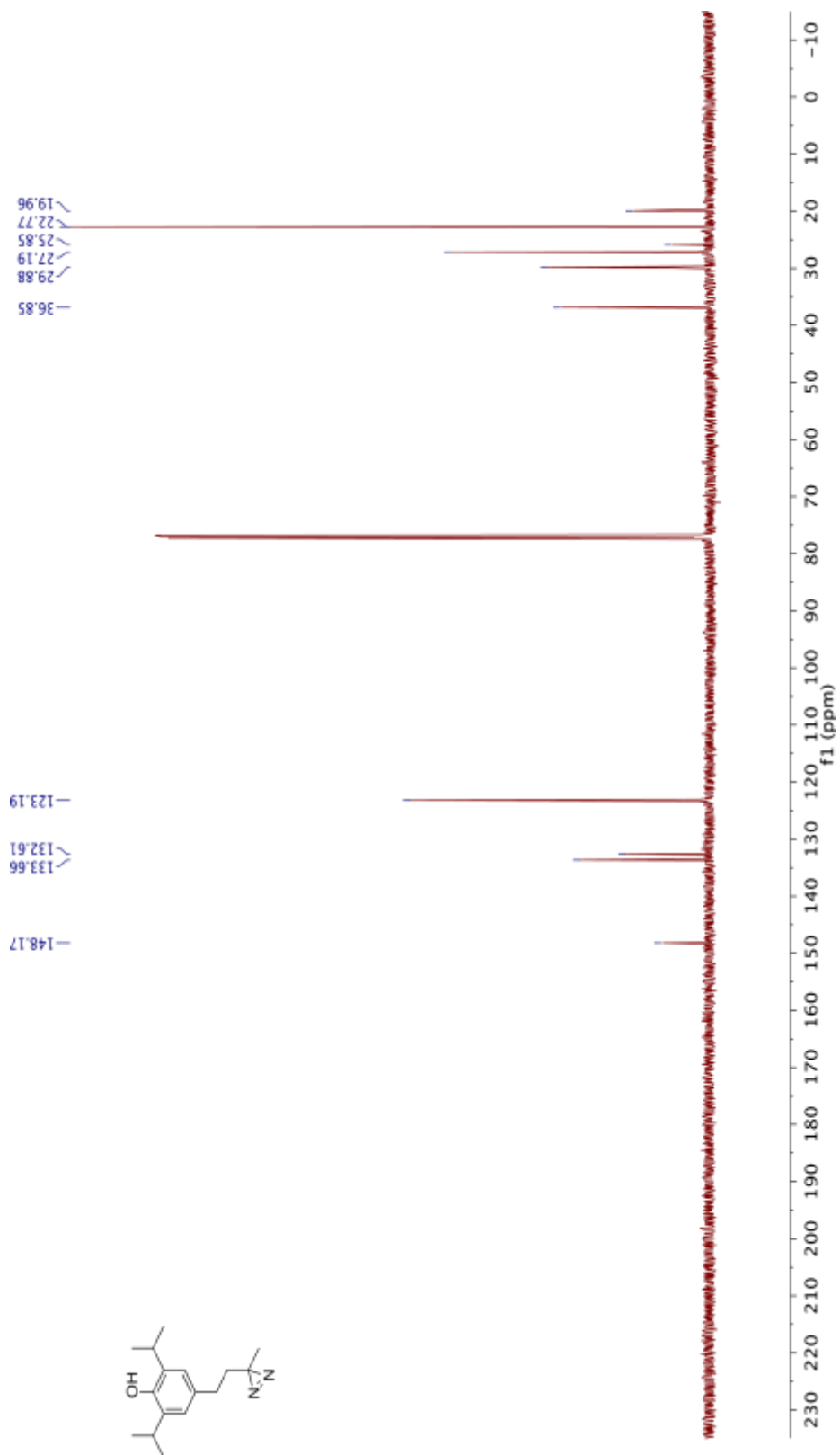
Figure A.7 ^{13}C NMR of 2,6-Diisopropyl-4-(2-(3-methyl-3H-diazirin-3-yl)ethyl)phenol (XPRO)

19.96
22.77
25.85
27.19
29.88
36.85
123.19
132.61
133.66
148.17
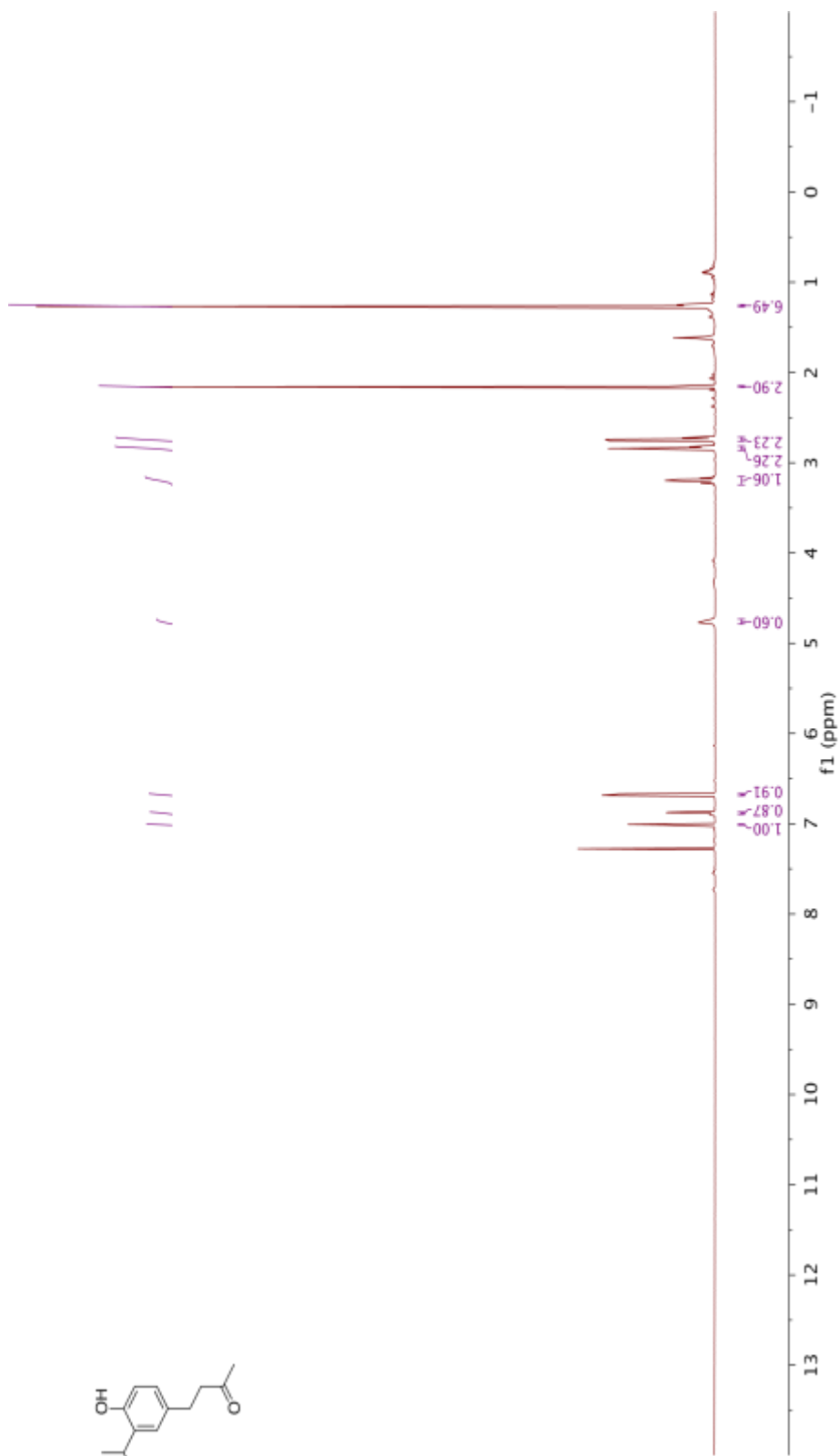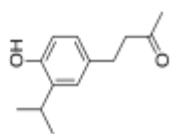
Figure A.8 ^{1}H NMR of 4-(4-hydroxy-3-isopropylphenyl)butan-2-one
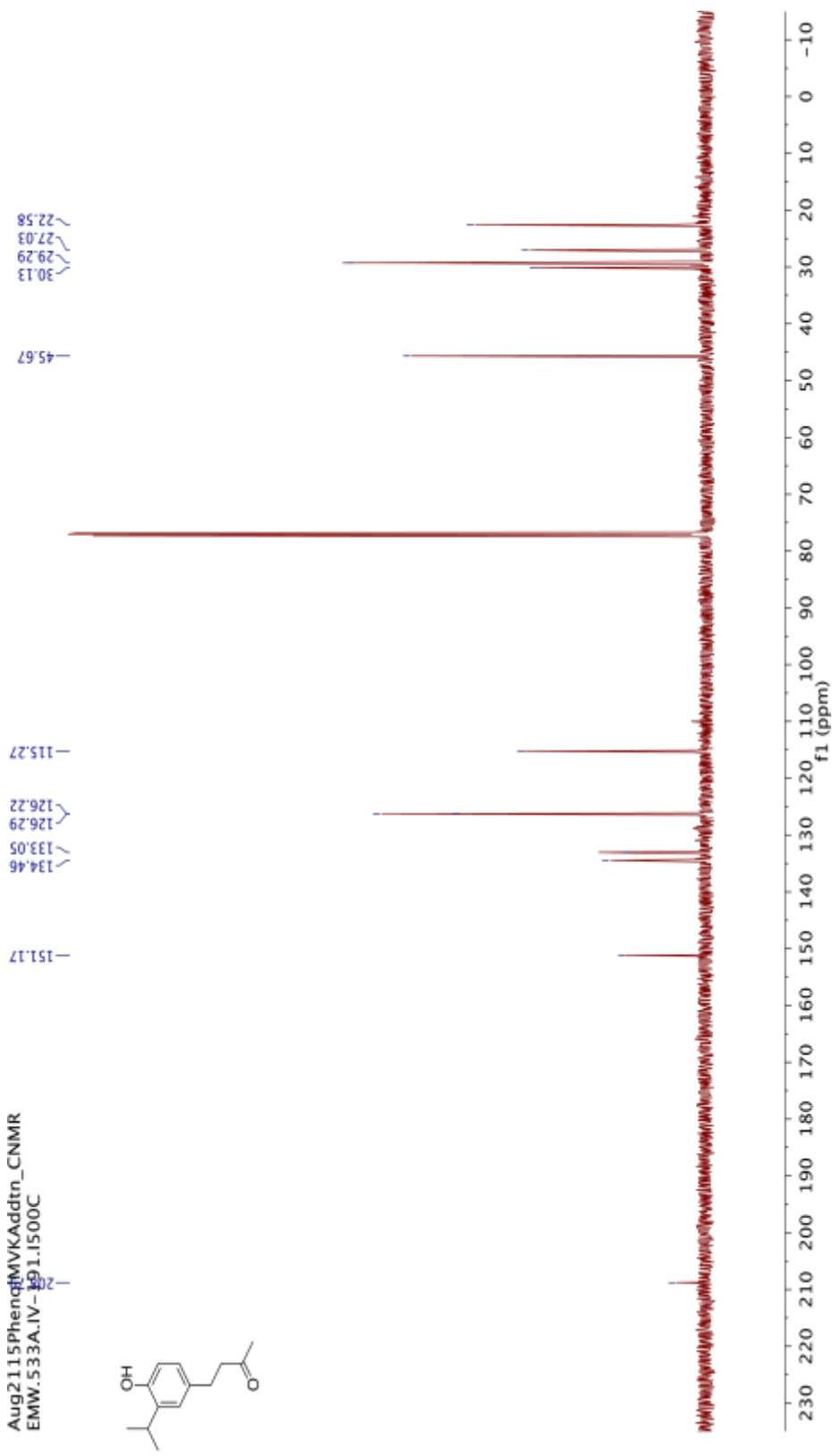
Figure A.9 ^{13}C NMR of 4-(4-hydroxy-3-isopropylphenyl)butan-2-one

121
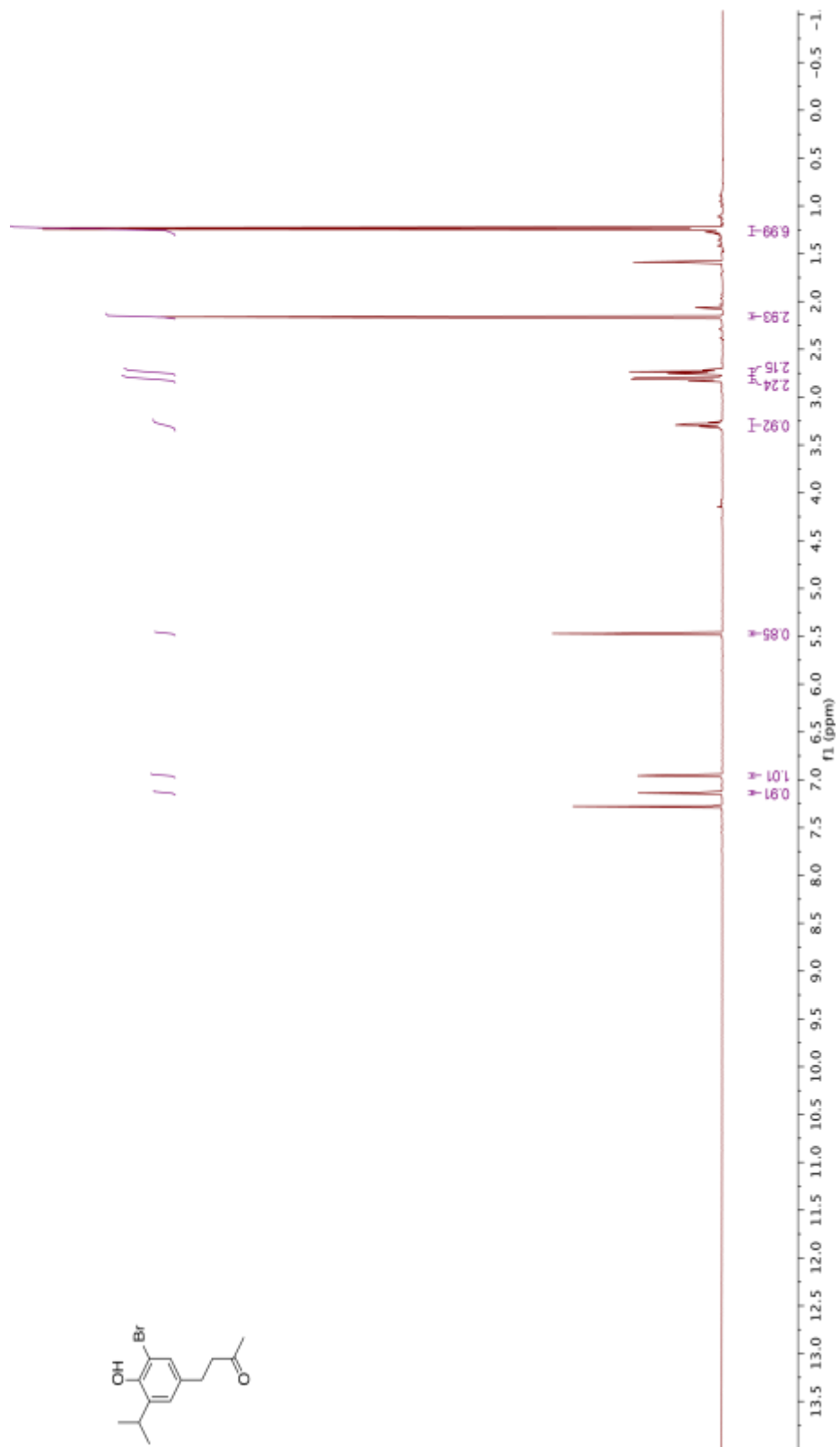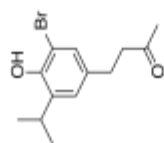
Figure A.10 ^{1}H NMR of 4-(3-bromo-4-hydroxy-5-isopropylphenyl)butan-2-one
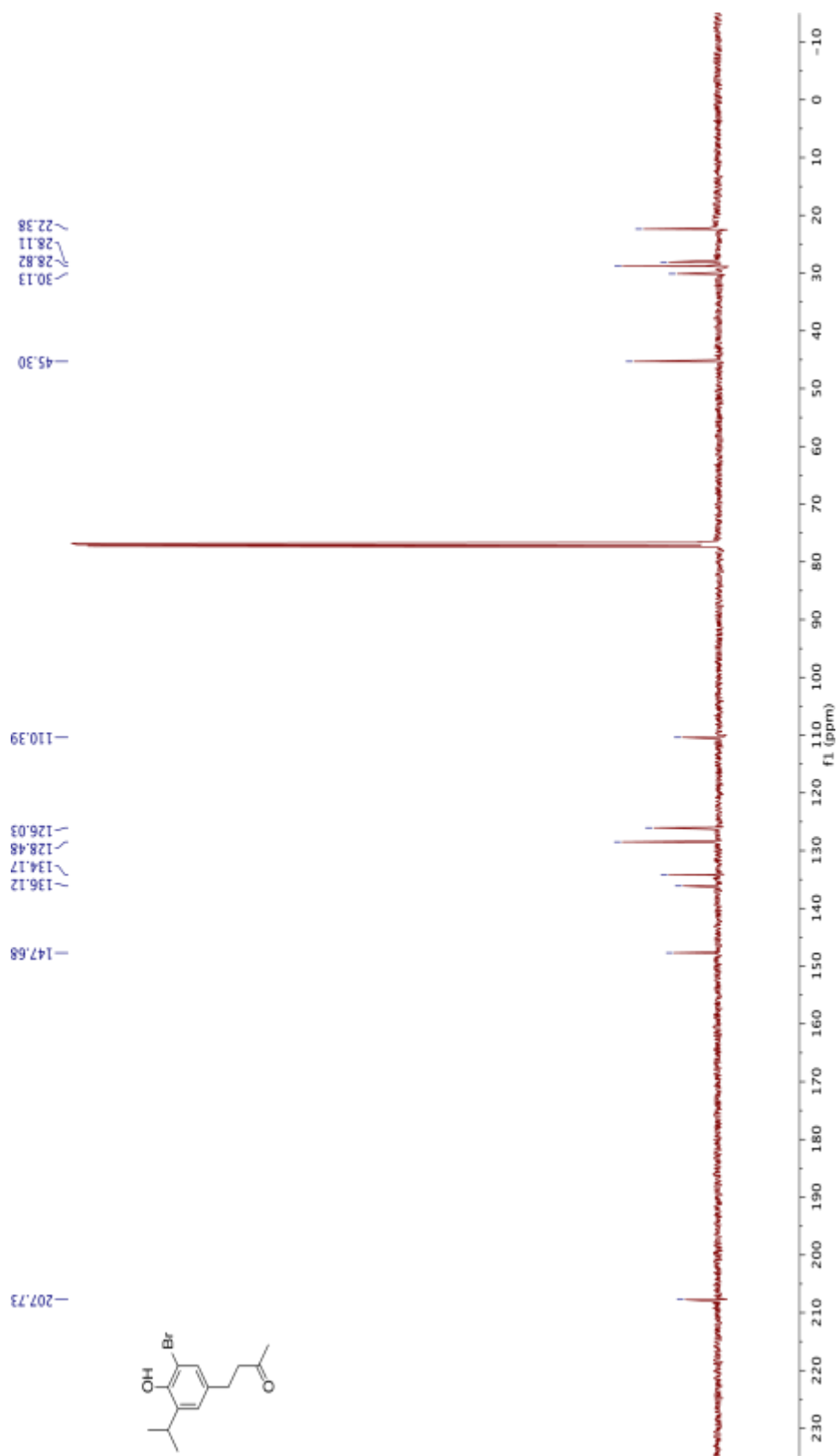
Figure A.11 ^{13}C NMR of 4-(3-bromo-4-hydroxy-5-isopropylphenyl)butan-2-one

207.73

147.68

136.12
134.17
128.48
126.03

110.39

45.30

30.13
28.82
28.11
22.38
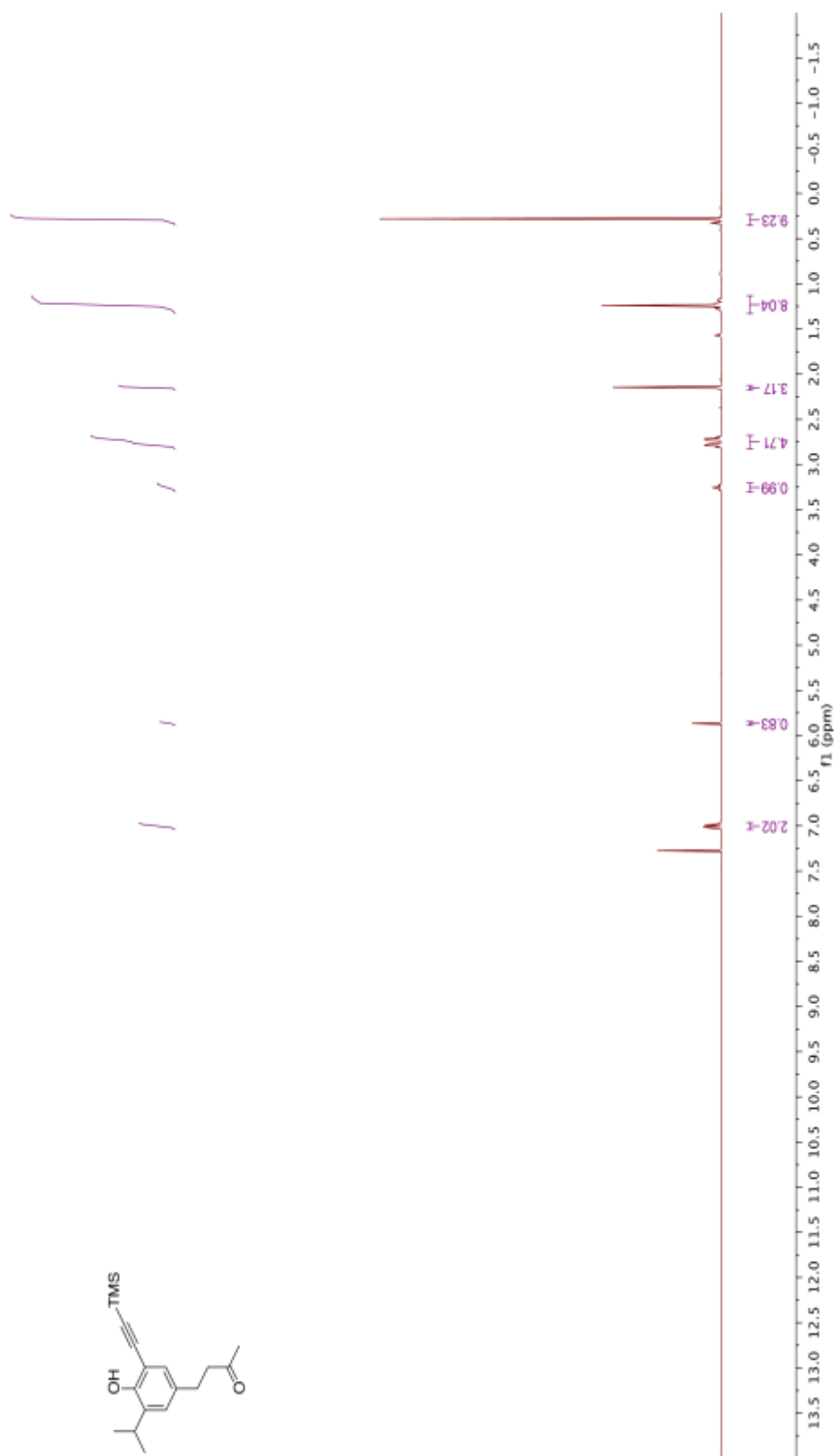
Figure A.12 ^{1}H NMR of 4-(4-hydroxy-3-isopropyl-5-((trimethylsilyl)ethynyl)phenyl)butan-2-one
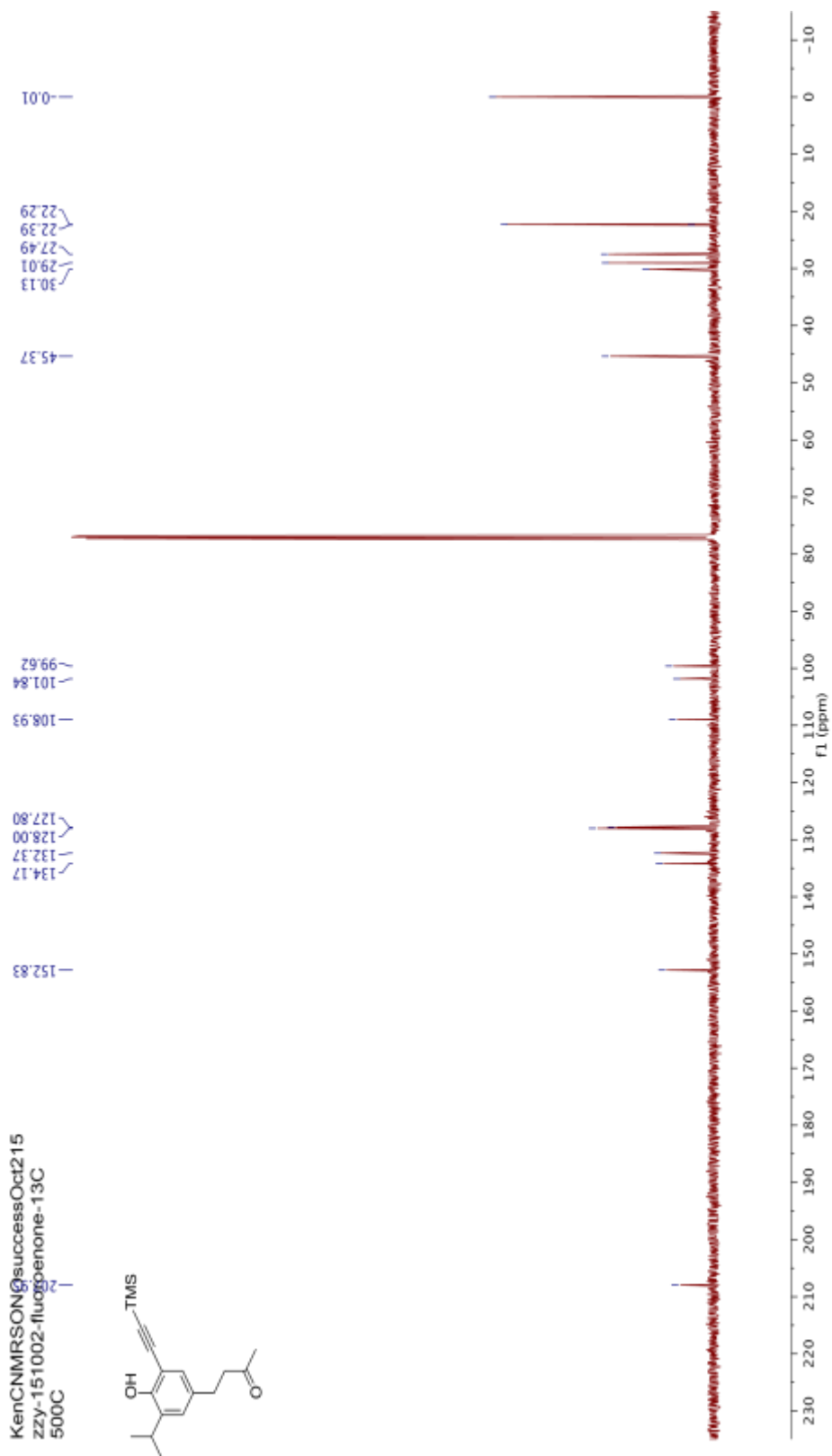
Figure A.13 ^{13}C NMR of 4-(4-hydroxy-3-isopropyl-5-((trimethylsilyl)ethynyl)phenyl)butan-2-one
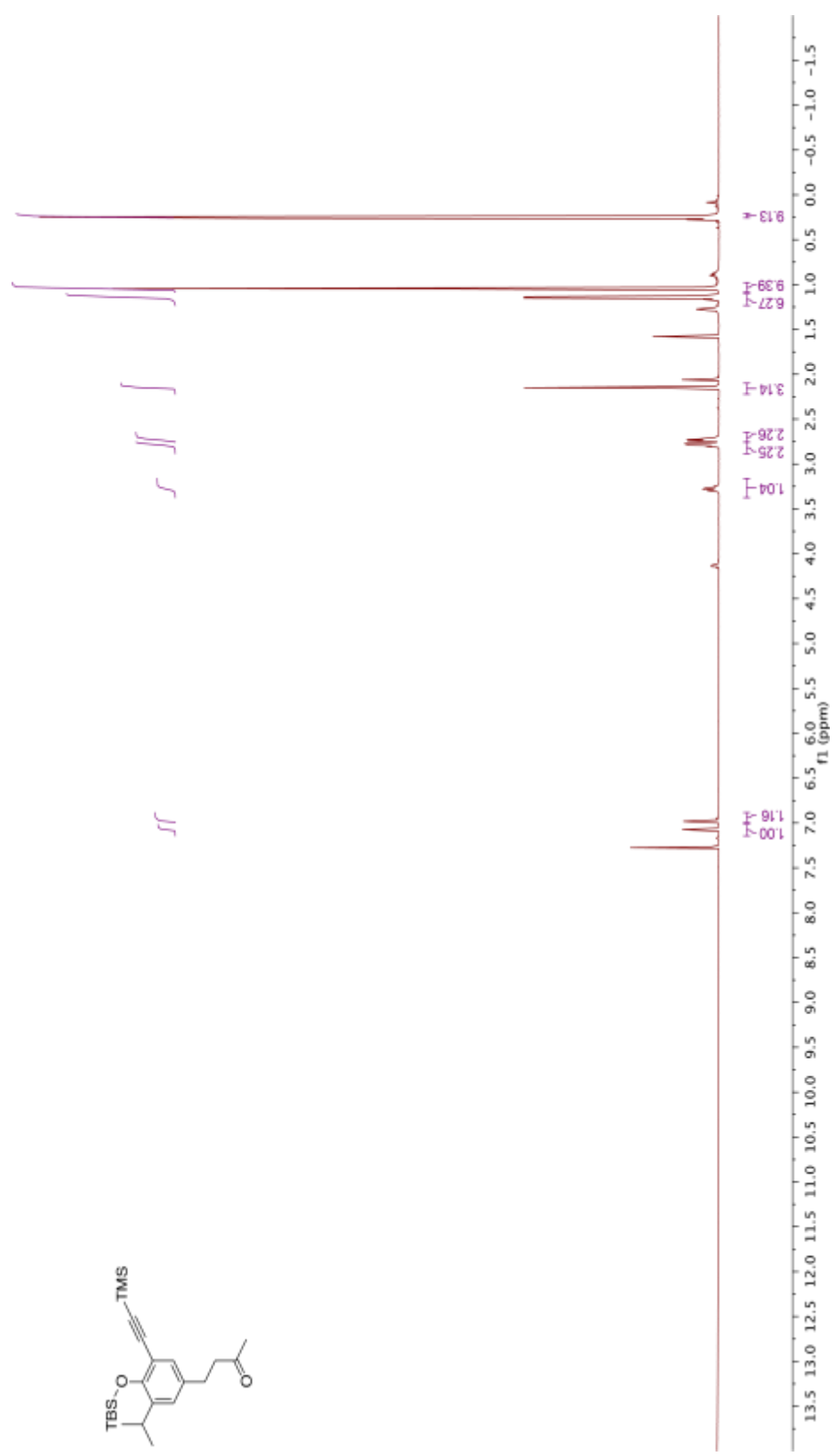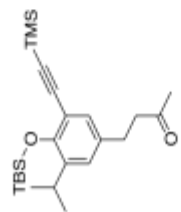
Figure A.14 ^{1}H NMR of 4-(4-((tert-butyldimethylsilyl)oxy)-3-isopropyl-5-((trimethylsilyl)ethynyl)butan-2-one

Figure A.15 ^{13}C NMR of 4-(4-((tert-butyldimethylsilyl)oxy)-3-isopropyl-5-((trimethylsilyl)ethynyl)butan-2-one

127
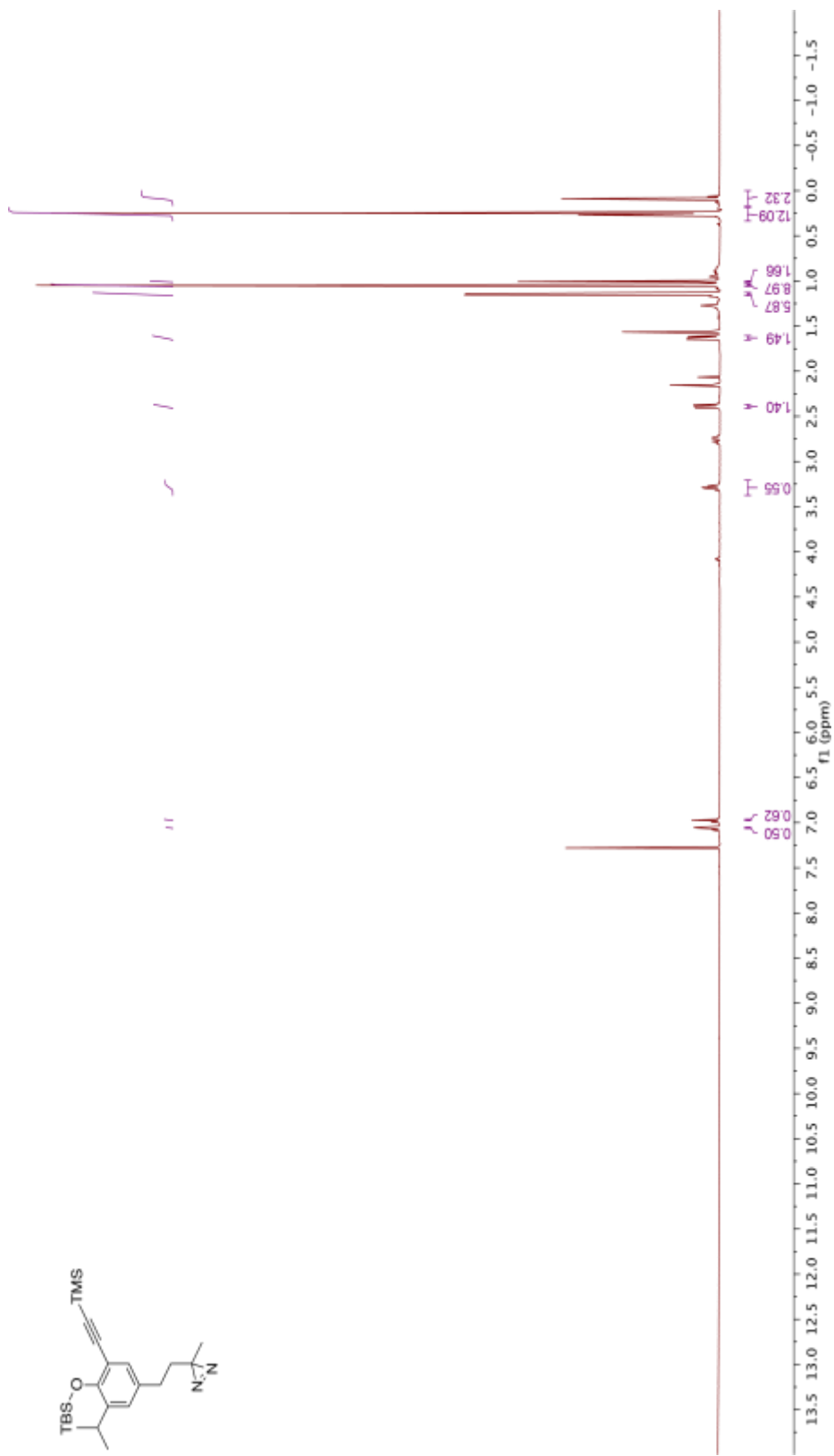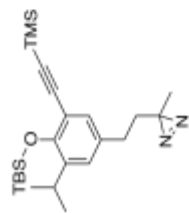
Figure A.16 ^{1}H NMR of 4-(4-((tert-butyldimethylsilyl)oxy)-3-isopropyl-5-((trimethylsilyl)ethynyl)phenethyl)-3-methyl-3*H*-diazirine
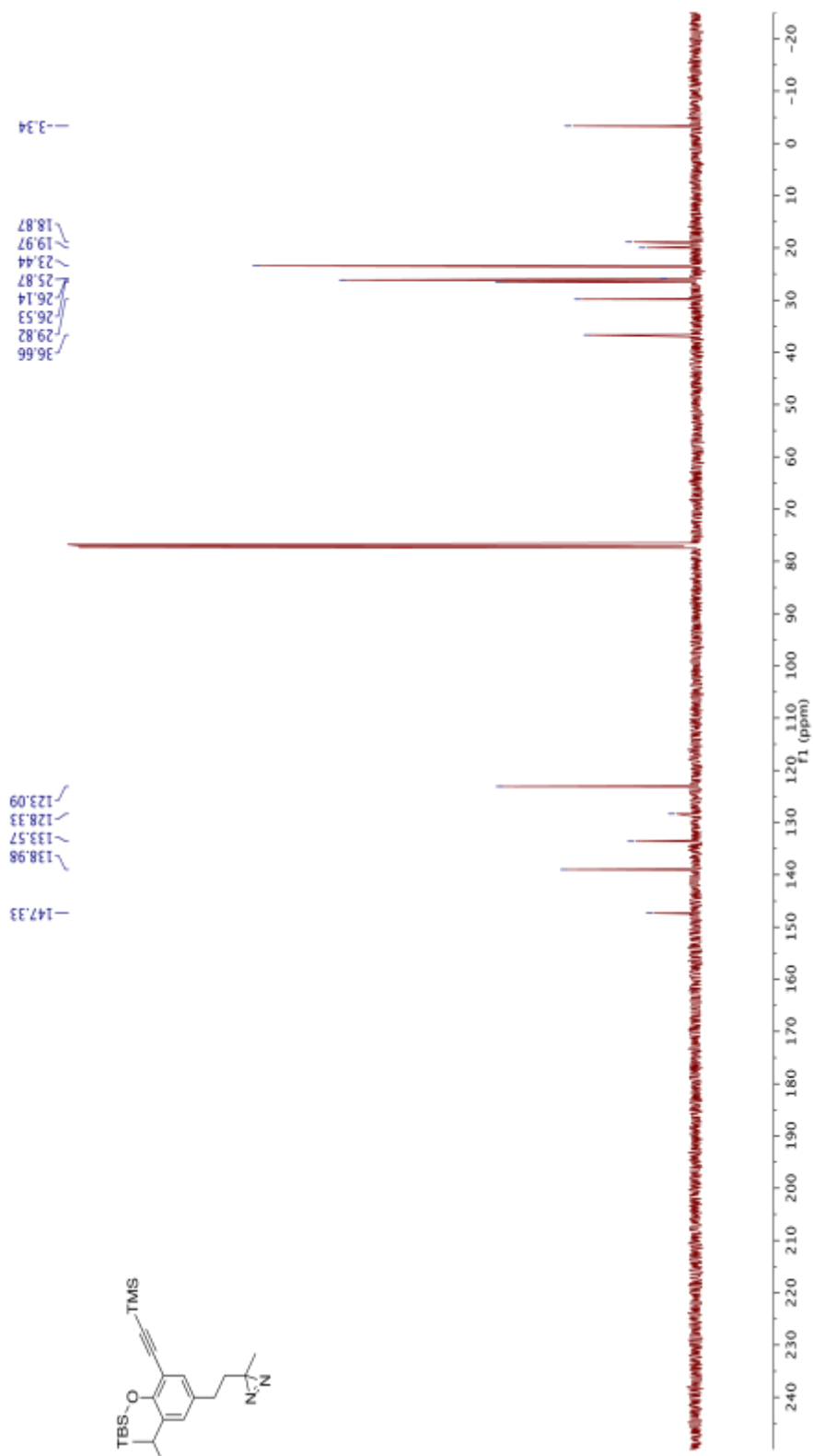
Figure A.17 ^{13}C NMR of 4-(4-((tert-butyldimethylsilyl)oxy)-3-isopropyl-5

-((trimethylsilyl)ethynyl)phenethyl)-3-methyl-3*H*-diazirine
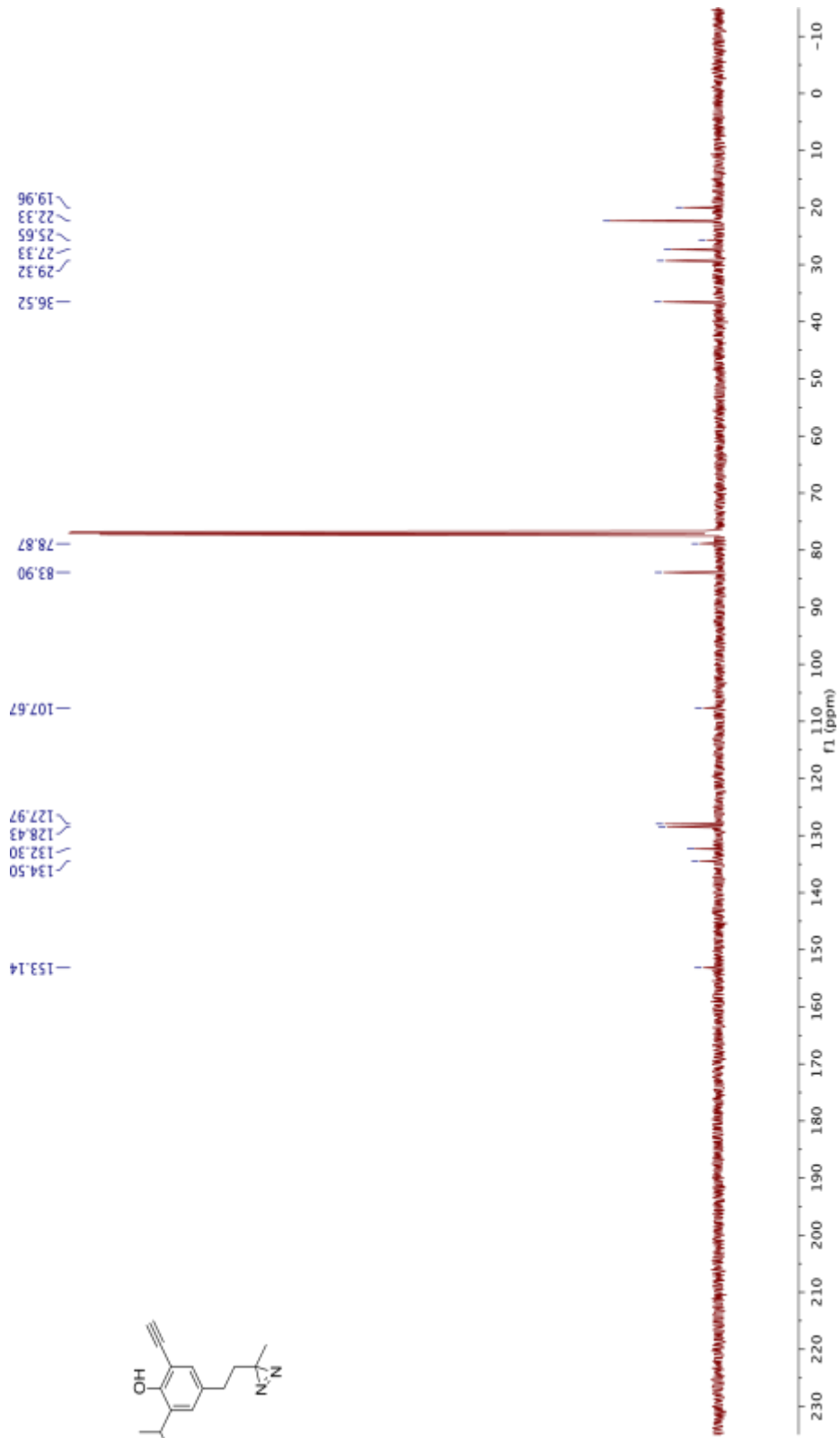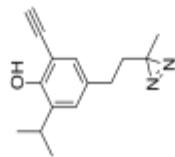
Figure A.18 ¹³C NMR of 2-ethynyl-6-isopropyl-4-(2-(3-methyl-3H-diazirin-3-yl)ethyl)phenol (*o*-XPRO-Click)
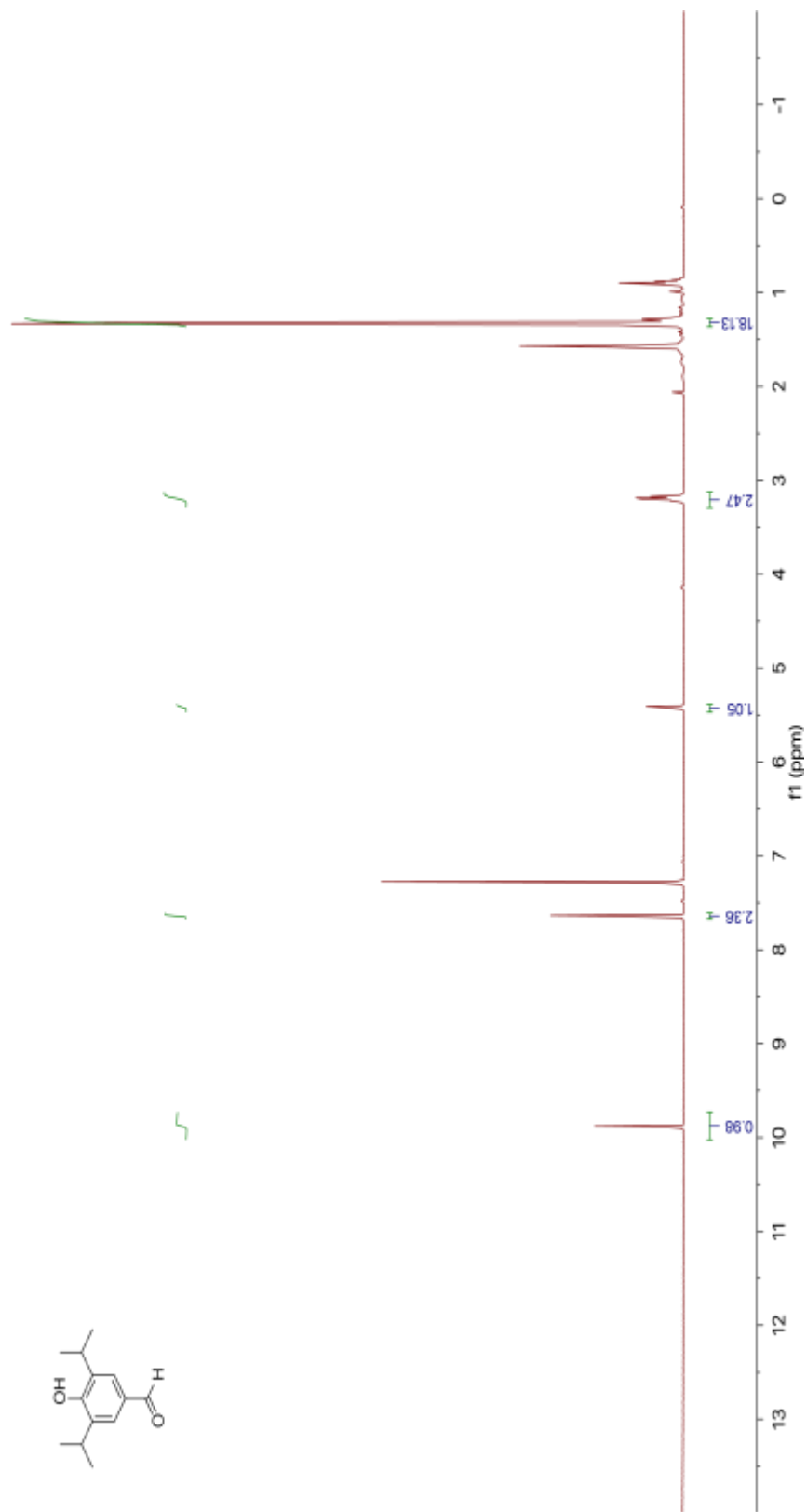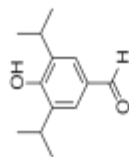
Figure A.19 ^{1}H NMR of 4-hydroxy-3,5-diisopropylbenzaldehyde
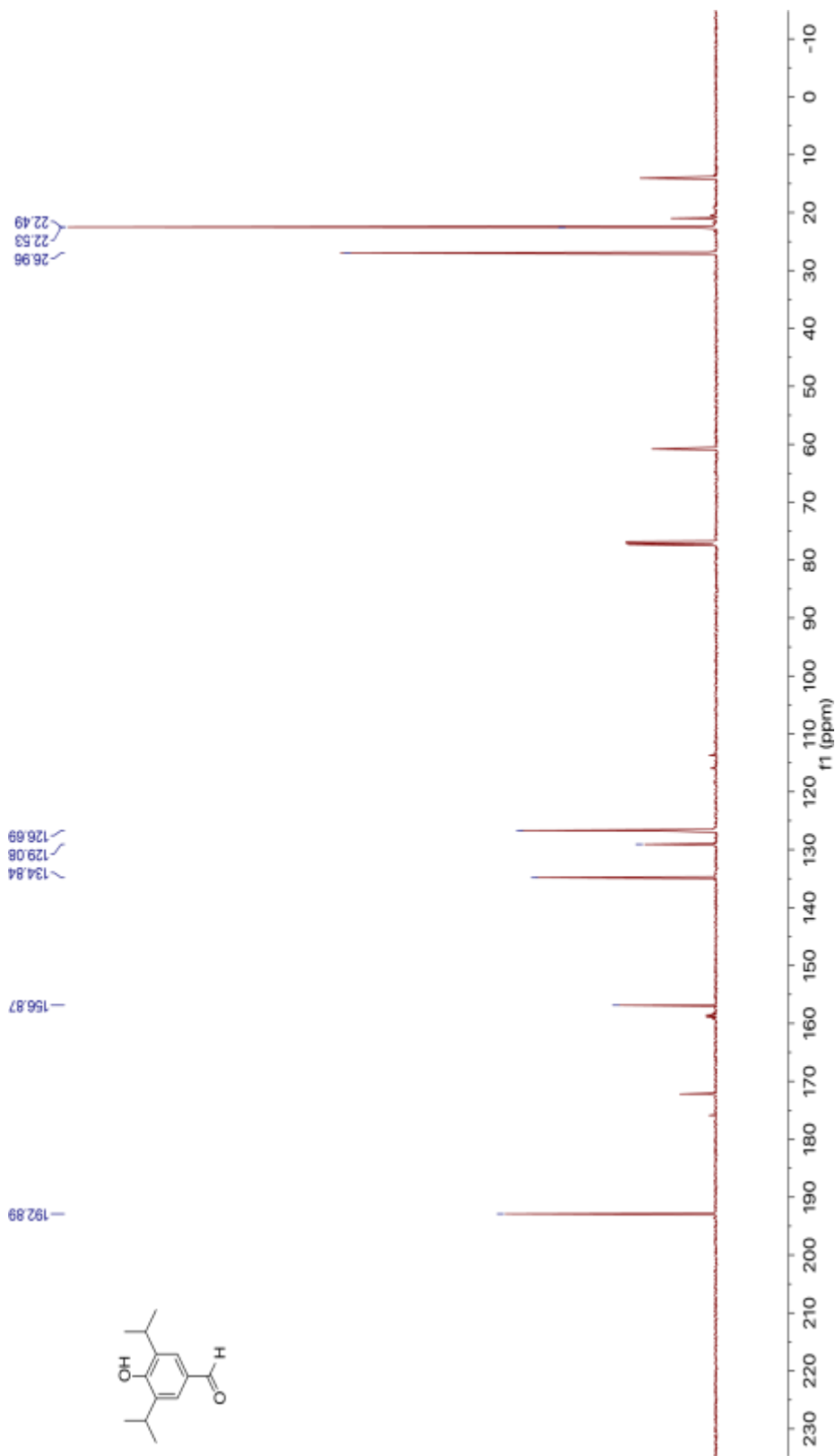
Figure A.20 ¹³C NMR 4-hydroxy-3,5-diisopropylbenzaldehyde

132
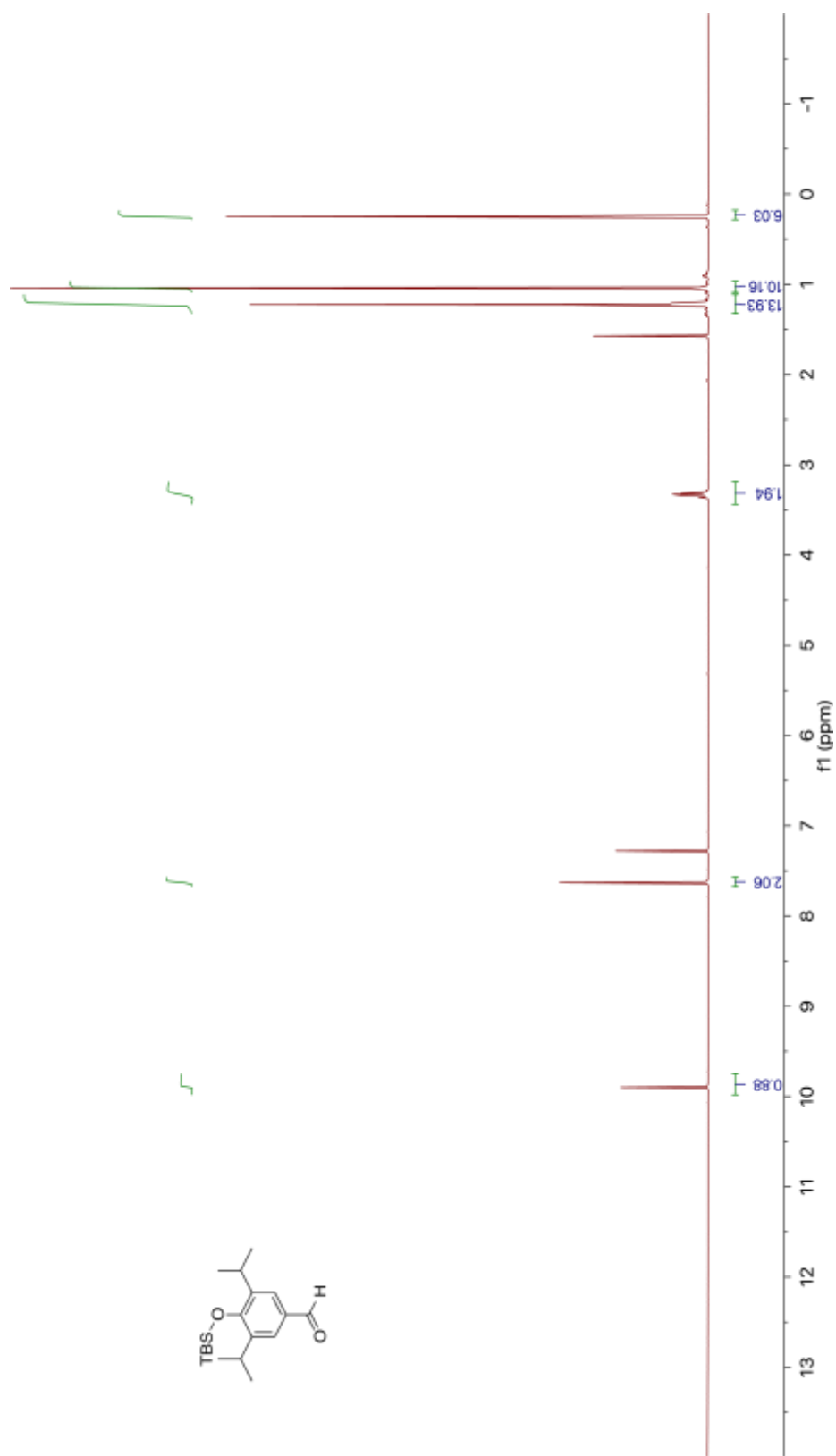
Figure A.21 ^{1}H NMR of 4-(***tert*-butyldimethylsilyl)oxy)-3,5-diisopropylbenzaldehyde**

133
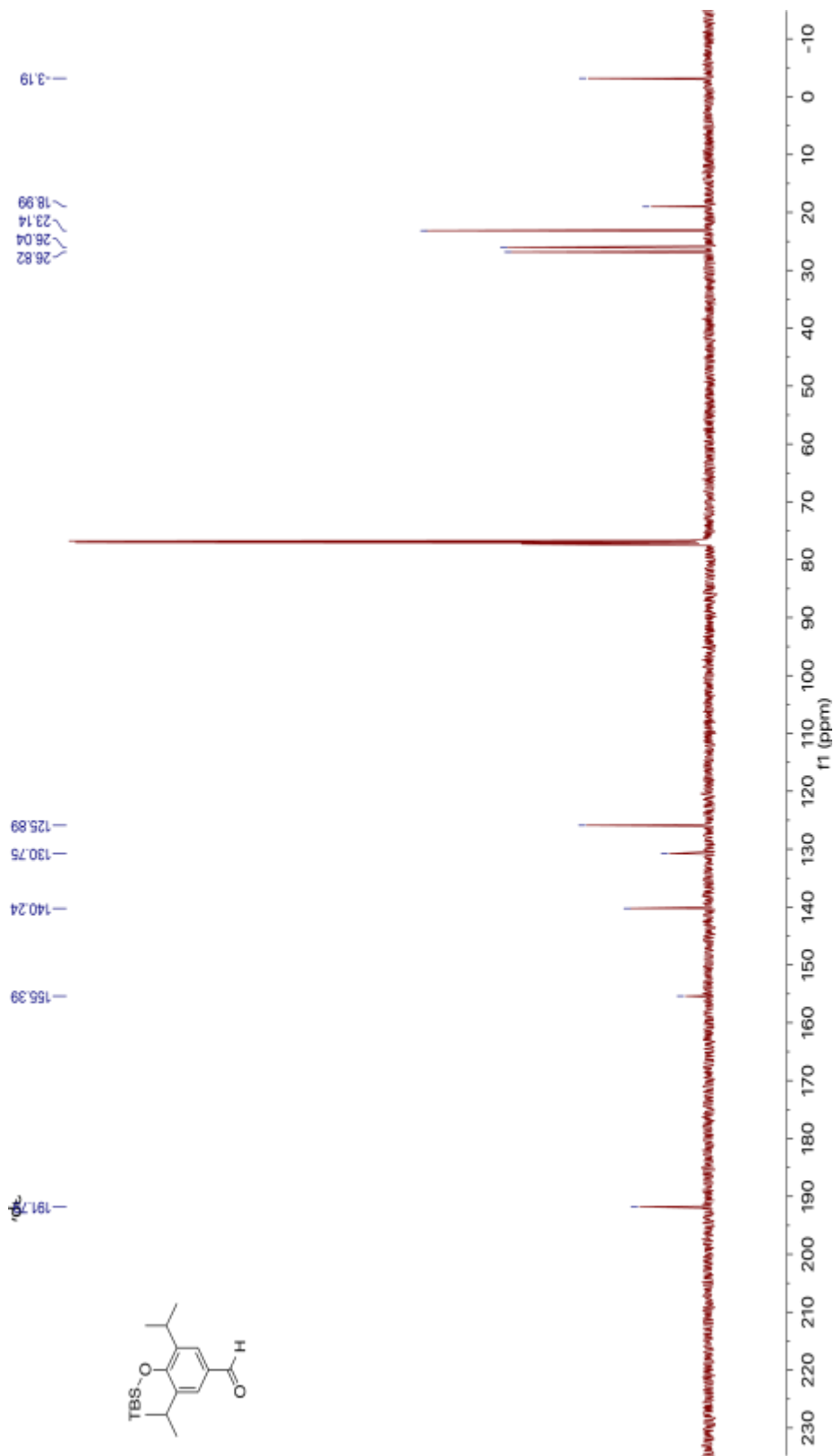
Figure A.22 ^{13}C NMR of 4-(*tert*-butyldimethylsilyl)oxy)-3,5-diisopropylbenzaldehyde
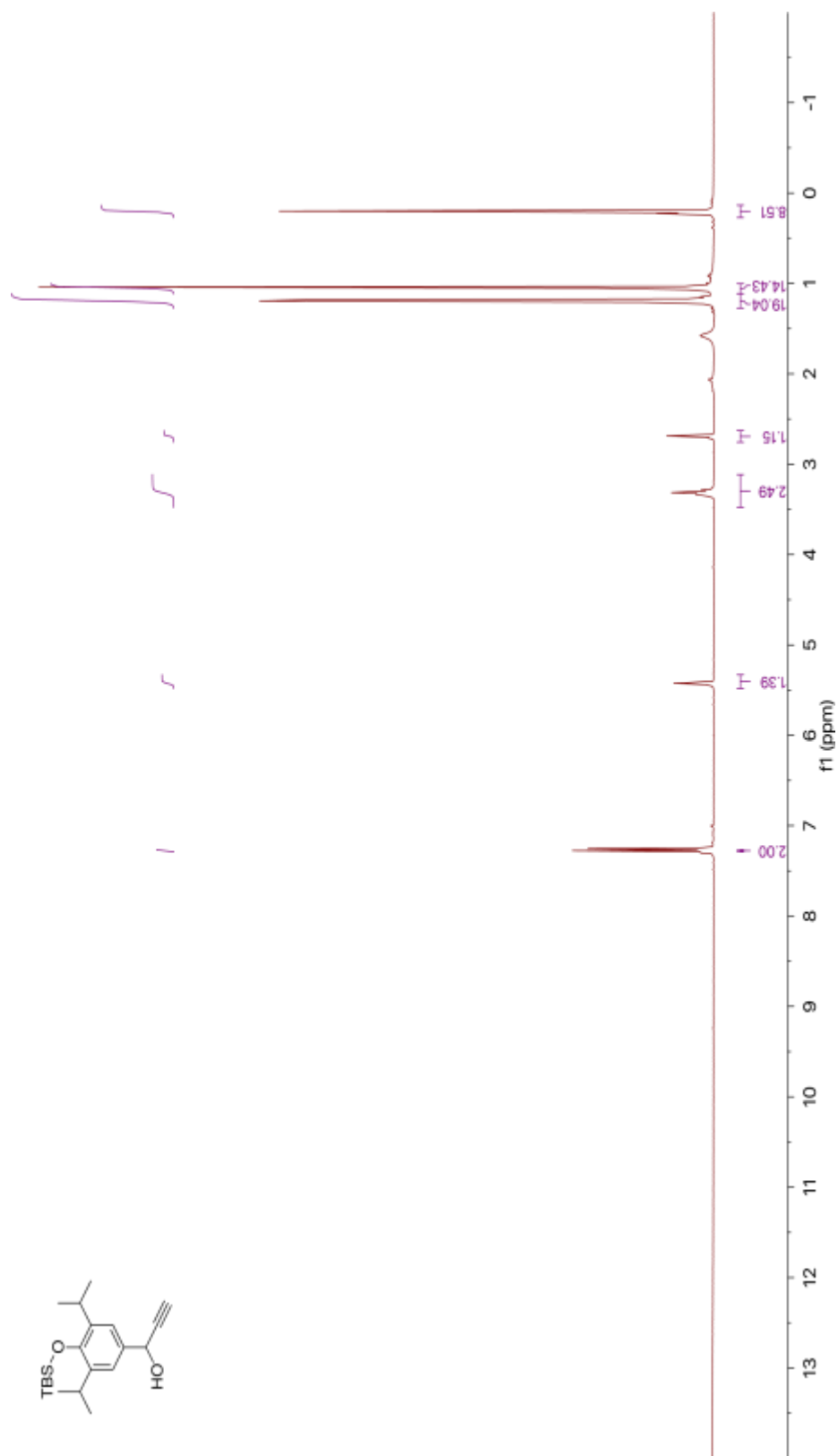
Figure A.23 ^{1}H NMR of 1-4-((*tert*-butyldimethylsilyl)oxy)-3,5-diisopropylphenyl)prop-2-yn-1-ol
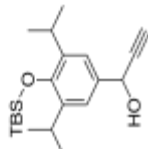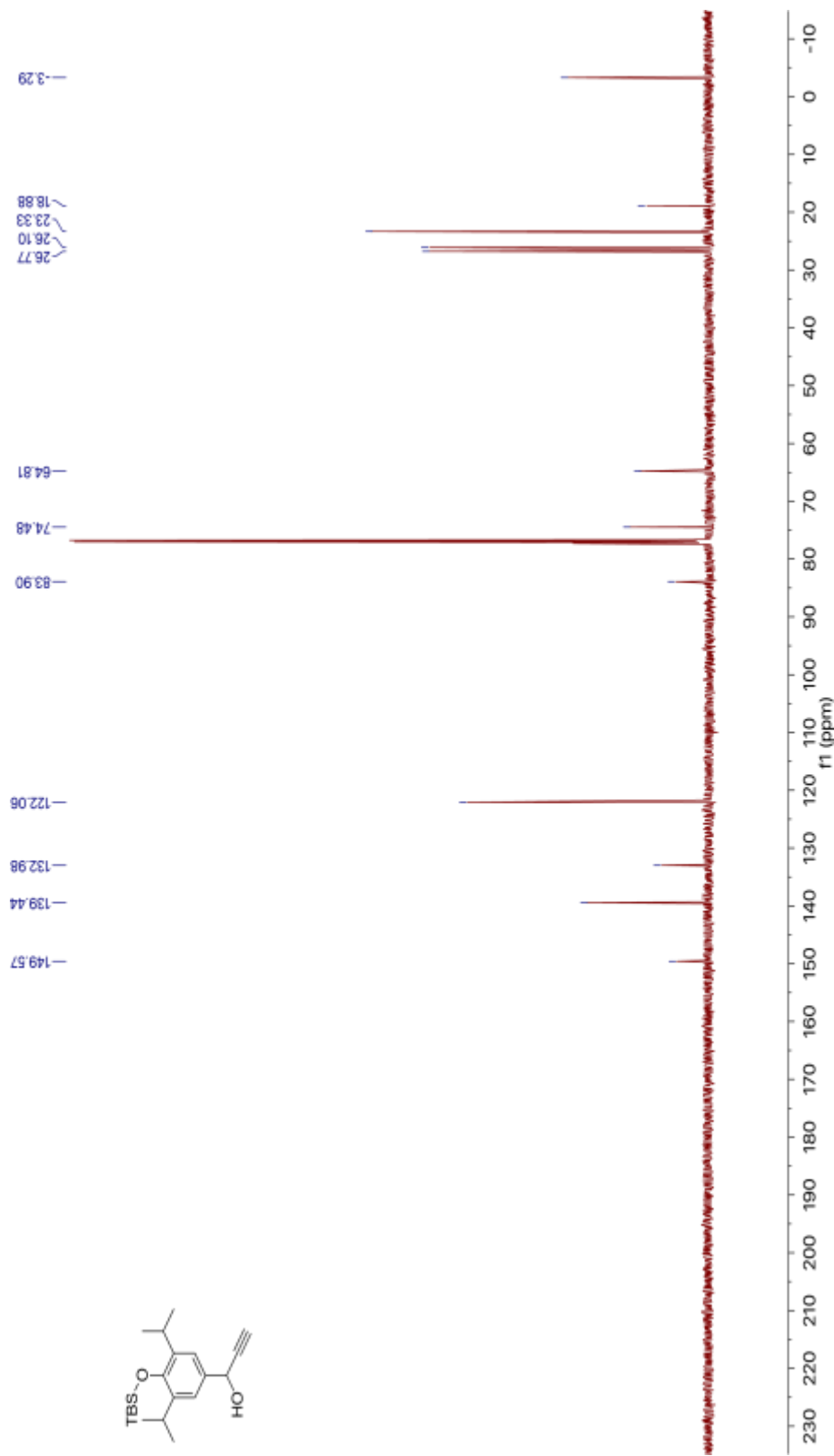
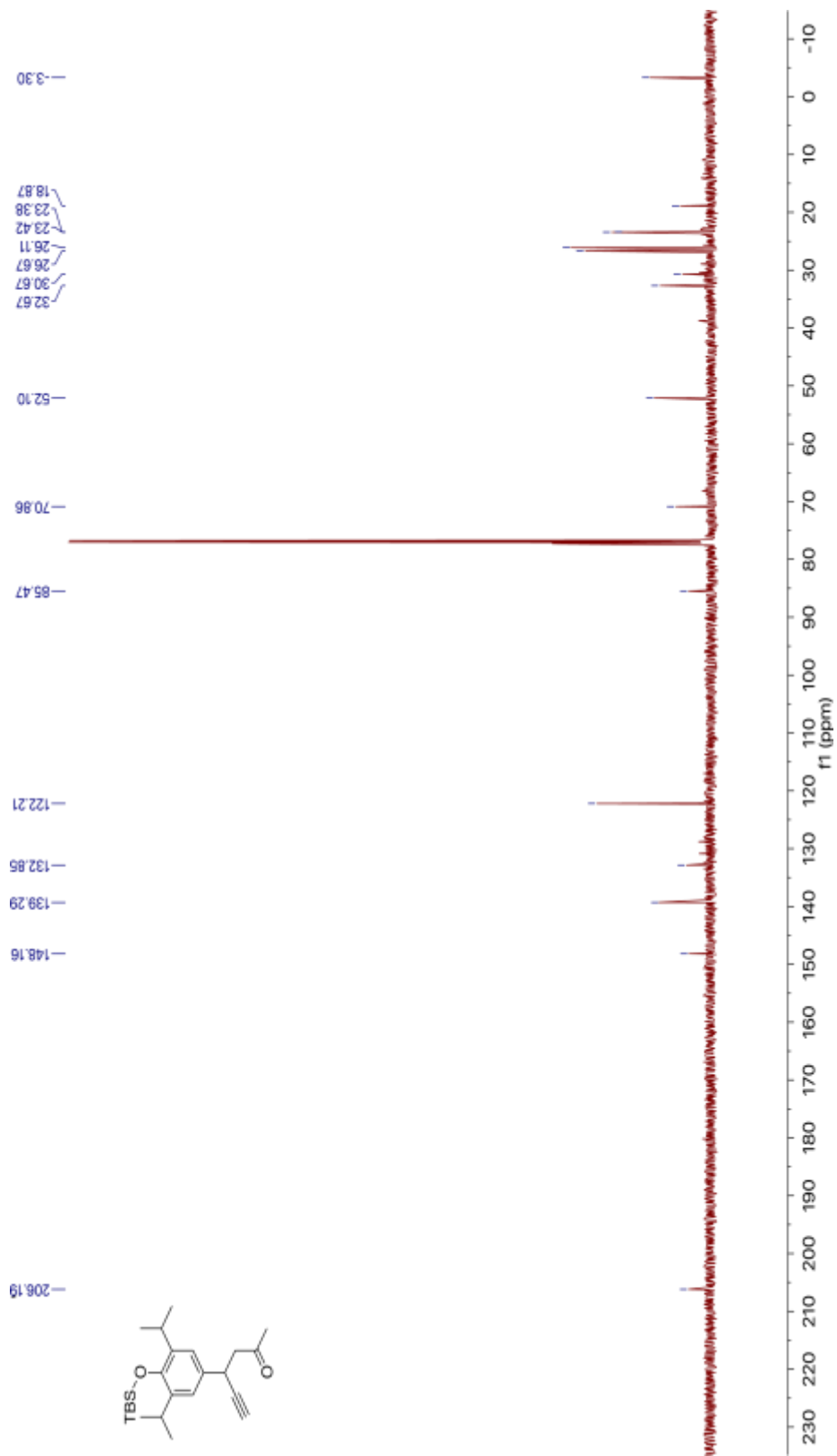Figure A.24 ^{13}C NMR of 1-4-((*tert*-butyldimethylsilyl)oxy)-3,5-diisopropylphenyl)prop-2-yn-1-ol

136
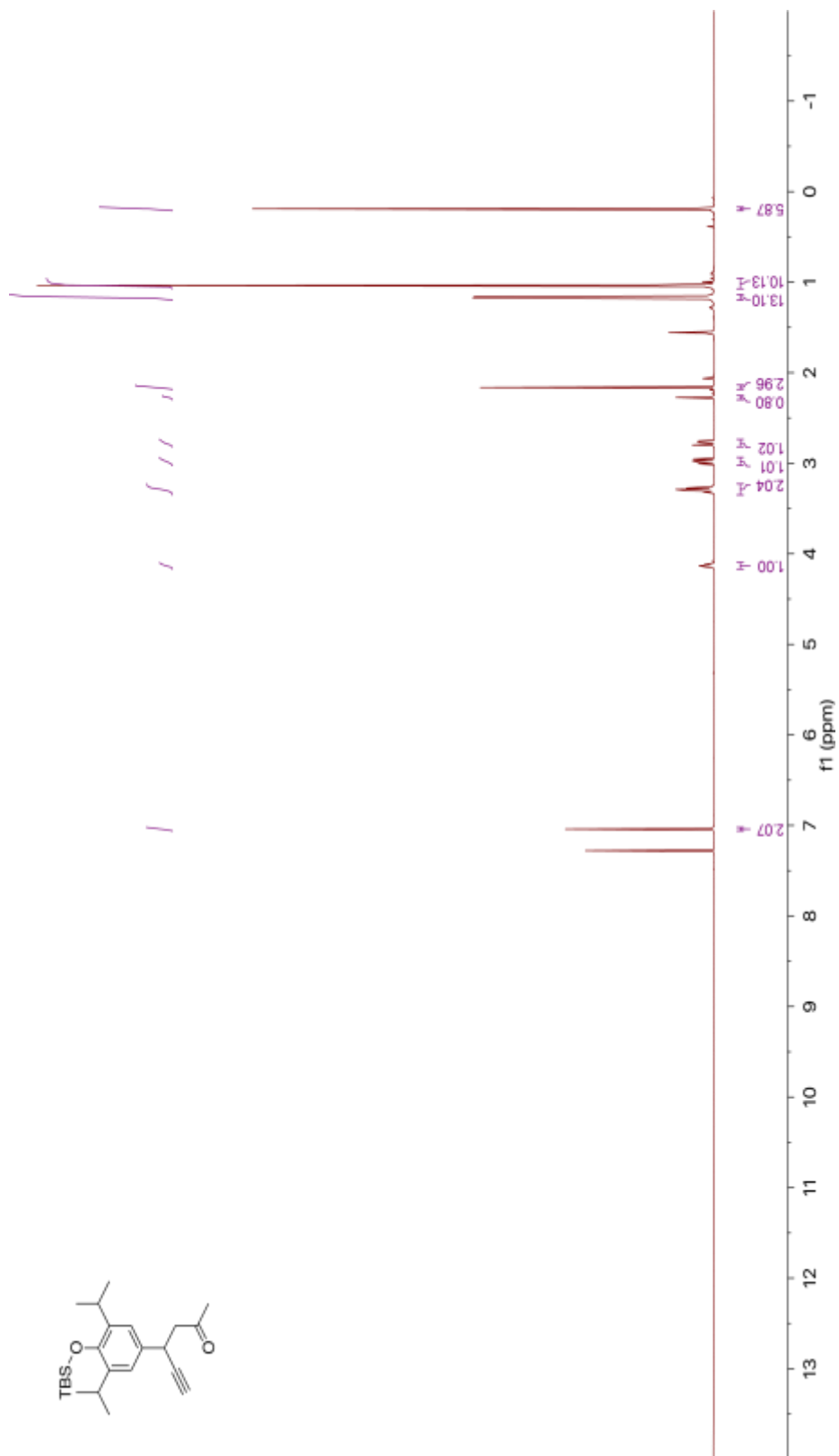
Figure A.25 ^{1}H NMR 4-(4-((*tert*-butyldimethylsilyl)oxy)-3,5-diisopropylphenyl)hex-5-yn-2-one

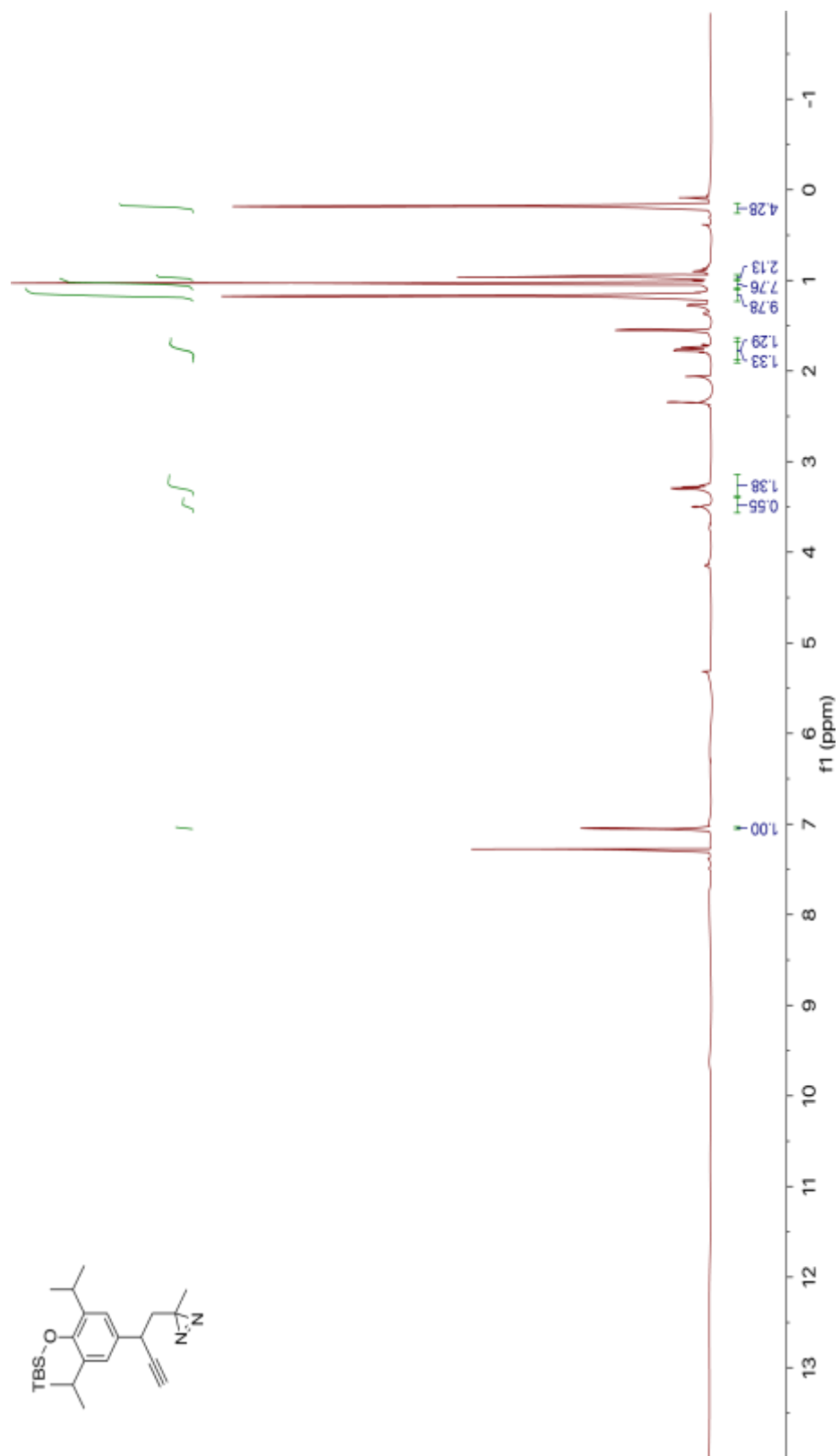**Figure A.26** ^{13}C NMR 4-(4-((*tert*-butyldimethylsilyl)oxy)-3,5-diisopropylphenyl)hex-5-yn-2-one

138

Figure A.27 ^{1}H NMR 3-(2-(4-((*tert*-butyldimethylsilyl)oxy)-3,5-diisopropylphenyl)but-3-yn-1-yl)-3-methyl-3*H*-diazirine
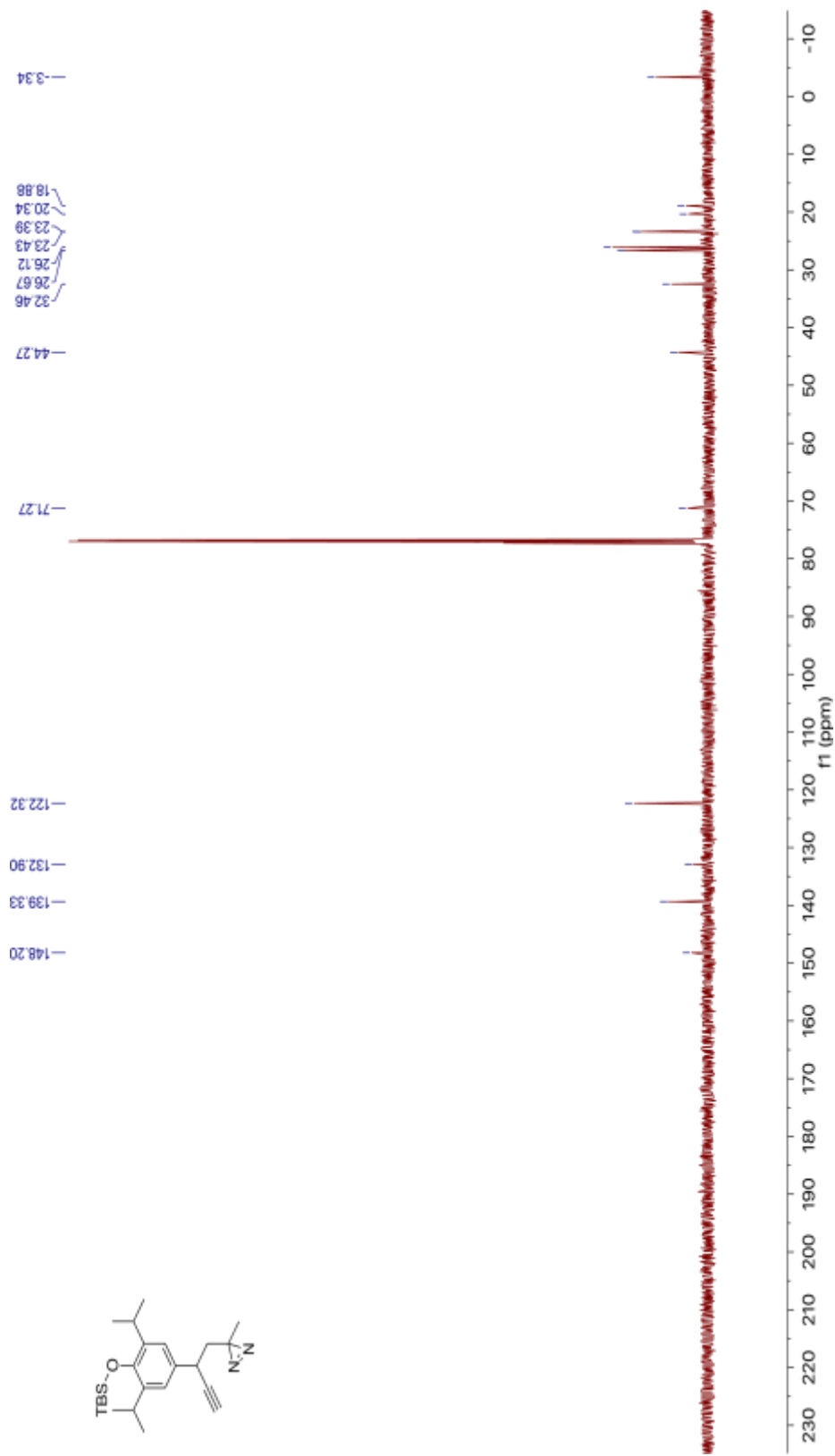
Figure A.28 ^{13}C NMR 3-(2-(4-((*tert*-butyldimethylsilyl)oxy)-3,5-diisopropylphenyl)but-3-yn-1-yl)-3-methyl-3*H*-diazirine

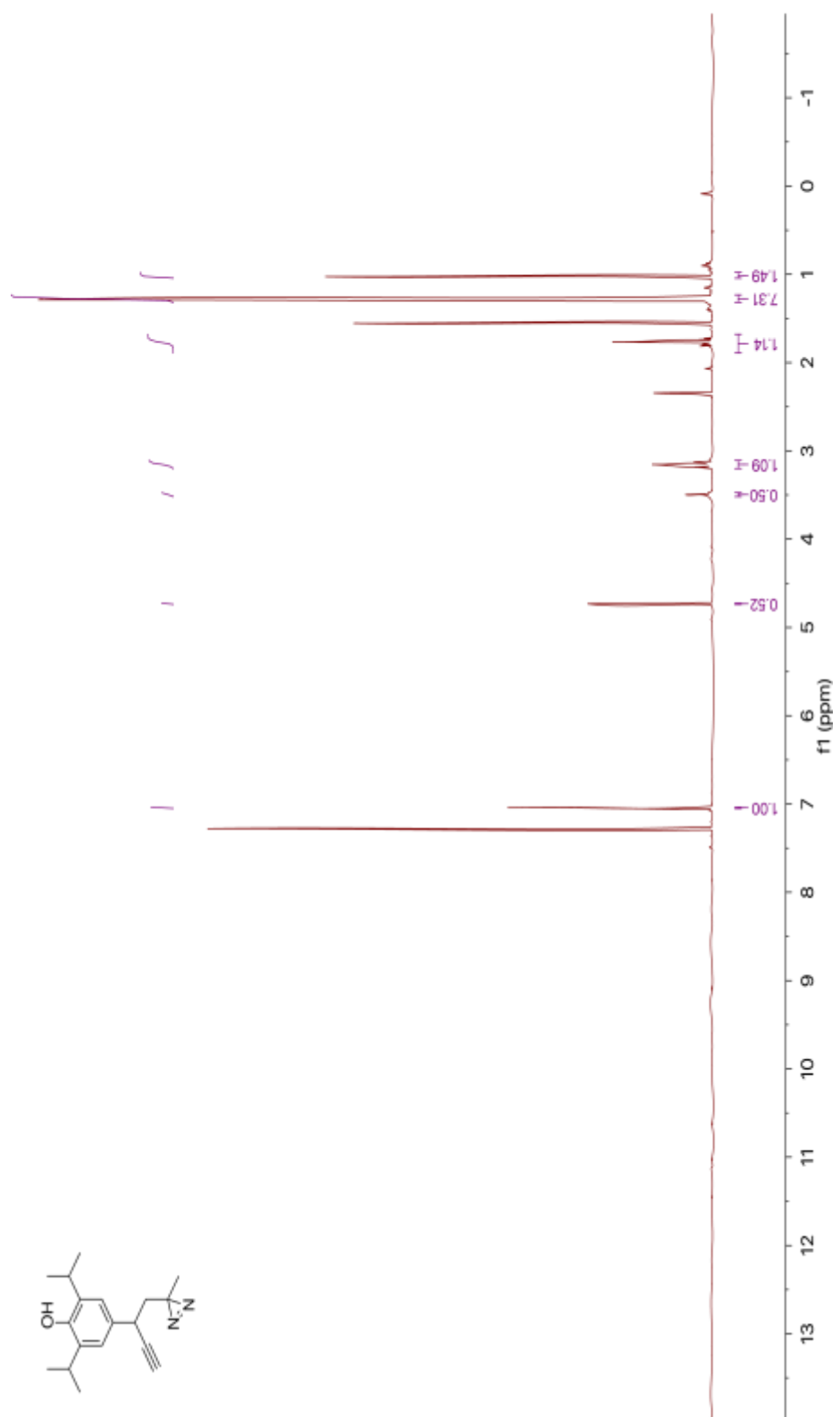**Figure A. 29** 13C NMR of 2,6-diisopropyl-4-(1-(3-methyl-3H-diazirin-3-yl)but-3-yn-2-yl)phenol (*p*-XPRO-Click